This is to certify that the
dissertation entitled

PROTON AND WATER EXIT IN CYTOCHROME *C* OXIDASE

presented by

BRYAN JACOB SCHMIDT

has been accepted towards fulfillment
of the requirements for the

Ph.D. degree in Biochemistry and Molecular Biology and Chemistry

S. Ferguson-Miller
Major Professor's Signature

August 19, 2003
Date

PRO

PROTON AND WATER EXIT IN CYTOCHROME *C* OXIDASE

By

Bryan Jacob Schmidt

A DISSERTATION

Submitted to
Michigan State Unversity
in partial fulfillment of the requirements
for the degree of

DOCTOR OF PHILOSOPHY

Department of Biochemistry and Molecular Biology

Department of Chemistry

2003

P

An

understand

redox activ

outside of

Water mov

Mn of deut

electron sp

access of w

with D_2O

used for w

turn over a

$H_2^{17}O$, wa

Fu

fluorescen

deuterium

fluorescei

was noted

ABSTRACT

PROTON AND WATER EXIT IN CYTOCHROME *C* OXIDASE

By

Bryan Jacob Schmidt

An understanding of proton and water exit is essential for a complete understanding of the mechanism of cytochrome *c* oxidase (CcO). Using the non-redox active Mn site of cytochrome *c* oxidase as a probe, water access from the outside of the enzyme and water escape from the buried active site were studied. Water movement was time-resolved by monitoring the magnetic interaction with Mn of deuterium or the oxygen isotope ^{17}O, by using a rapid freeze-quench – electron spin echo envelope modulation (ESEEM) technique. Rapid millisecond access of water from the bulk phase to the Mn was demonstrated by mixing CcO with D_2O or with $H_2{}^{17}O$. To determine whether a channel involving the Mn was used for water exit from the active site, samples incubated in $^{17}O_2$ were allowed to turn over approximately 5 times before freezing. The ^{17}O, now in the form of $H_2{}^{17}O$, was detected at the Mn.

Further definition of the exit channel was provided by similar analysis of a fluorescently labeled arginine mutant, R234C. This mutant showed unaltered deuterium exchange from the bulk when unlabeled, but after labeling with fluorescein maleimide a substantial decrease in the millisecond exchange of D_2O was noted. Additionally, exchange of bulk deuterium at the Mn site was hindered

while the

that there

solvent al

near R23

Re

suggested

asparagine

proton pur

Inhibition

H93C mut

this residu

enzyme a

W

water exi

pathways

while the wild-type enzyme was actively turning over. These data together suggest that there is a defined water exit channel that leads from the buried Mn to the bulk solvent along a pathway that is composed of the subunit I/II interface and ending near R234.

Regulation of proton and water exit on the external side of the enzyme was suggested by a mutation of an external histidine, H93, to a cysteine and an asparagine. This residue is not the specific site of proton exit, as shown by normal proton pumping stoichiometry of the mutants and a lowered kinetic isotope effect. Inhibition of activity at low pH of these mutants and the specific labeling of the H93C mutant with fluorescein maleimide only when cytochrome *c* was bound show this residue is involved in a conformational change during turnover that regulates enzyme activity.

While the proton exit pathway is not yet defined, we have established a water exit pathway and have evidence for conformational control of the exit pathways.

I w
as a gradu
thank my
provided
independ
advisors i
inspiration
my tenure
Hausinger
yearly mee

Th
endless di
invaluable
the suppor
biology. I
projected.
many hour
I also had
Biochemis
Haymond
Yuejun Zh

ACKNOWLEDGEMENTS

I would like to take this opportunity to thank those who helped make my years as a graduate student both successful and enjoyable. First and foremost I would like to thank my advisor in Biochemistry, Dr. Shelagh Ferguson-Miller. She not only provided some direction and constant knowledge, but also allowed to me to be independent and develop my own ideas. I also have the deepest gratitude for my advisors in Chemistry; the late Dr. Jerry Babcock, who was always a source of inspiration, and Dr. John McCracken, who agreed to be my advisor halfway through my tenure here. I would also like to thank the members of my committee, Dr. Bob Hausinger, Dr. Leslie Kuhn and Dr. Joan Broderick for keeping me on track at at our yearly meetings.

There are also an abundant number of coworkers I would like to thank. The endless discussions I had with Dr. Denise Mills and Dr. Warwick Hillier were invaluable, as was the work done in collaboration with them. Dr. Carrie Hiser provided the support and nurturing required for me to learn the fundamentals of molecular biology. I am deeply indebted to Dr. Laurence Florens, with whom I started this projected. And would also like to thank Dr. Muthukumaran Rajendra-Bose, who spent many hours with me, sharing his theoretical and practical knowledge of EPR with me. I also had many insightful and useful discussions with other lab members in both Biochemistry and Chemistry: Dr. Steve Seibold, Dr. Denis Proshlyakov, Dr. Shannon Haymond, Dr. Jose Cerda, Dr. Eric Saari, Dr. Burak Esat, Dr. Yasmin Hilmi, Dr. Yuejun Zhen, Ling Qin and Namjoon Kim, as well as all the others who I interacted

with s

Slater

Peter B

teachin

with scientifically throughout my time here. I would also like to especially thank Jamie Slater for spending countless days running activity assays for me with no complaint.

I would also like to acknowledge our collaborator in Stockholm, Sweden, Dr. Peter Brzezinski and his student Dr. Magnus Branden, for having me in their lab and teaching me the flash-flow method.

List of

List of

List of

Chapte

TABLE OF CONTENTS

VI. Co

Chapte

R

D

Chapter

Int

Ev

Re

Dis

Chapter 4:

Intr

Exp

Res

Table 3.

Table 3.

LIST OF TABLES

LIST OF FIGURES

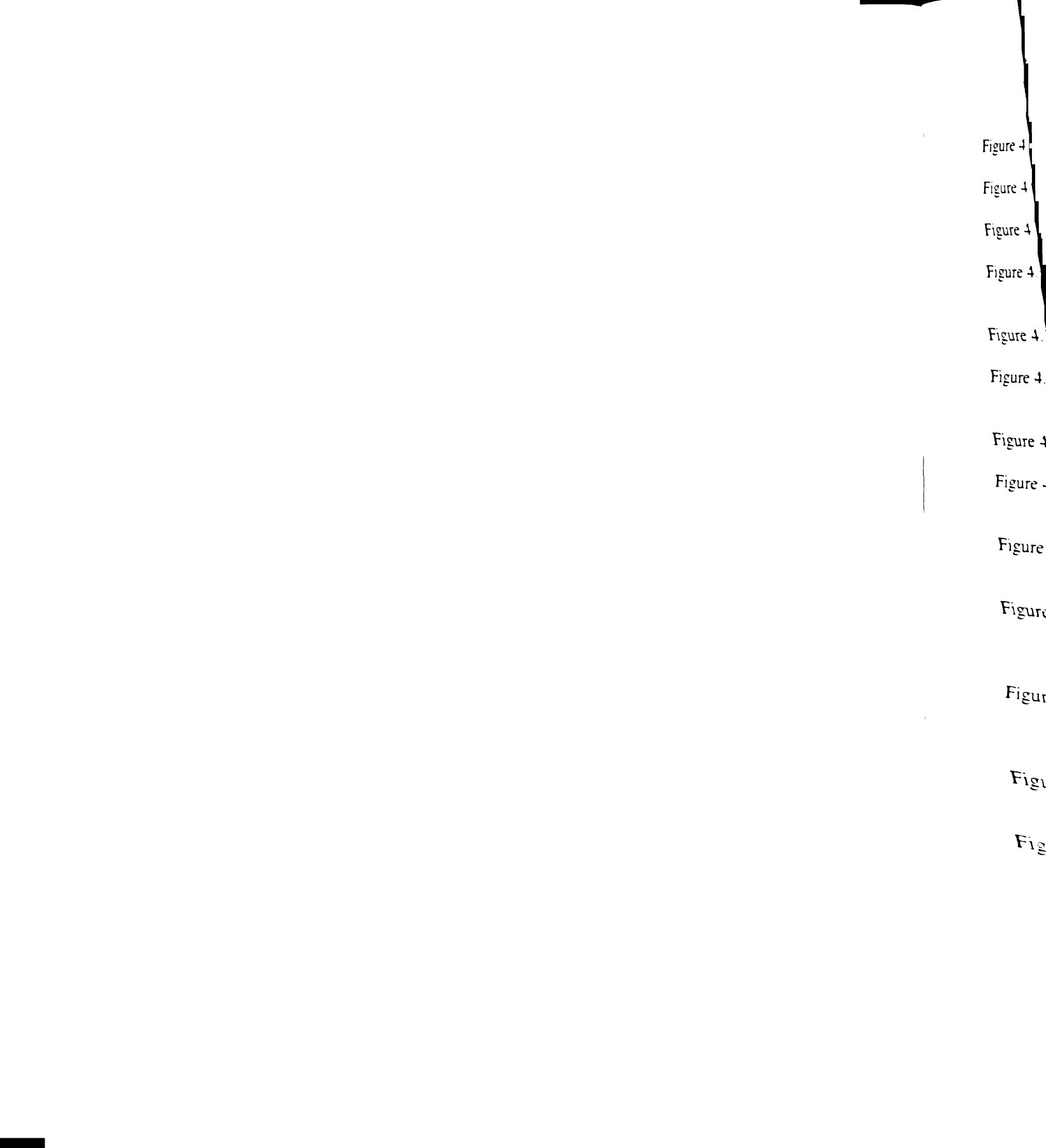

ATP – A

BR – Ba

CcO – C

DEAE –

EDTA –

ENDOR

EPR – E

ESE – E

ESEEM

FADH

FCCP

FM – F

FMN

FPLC

FT –

FTIR

HEP

KIE

MC

ME

M

M

LIST OF ABBREVIATIONS

ATP – Adenine triphosphate

BR – Bacteriorhodopsin

CcO – Cytochrome *c* oxidase

DEAE – Diethylaminoethyl

EDTA – Ethyldiaminetetracetic acid

ENDOR – Electron nuclear double resonance

EPR – Electron paramagnetic resonance

ESE – Electron spin echo

ESEEM – Electron spin echo envelope modulation

FADH – Flavin adenine dinucleotide

FCCP – Carbonylcyanide-*p*-trifluoromethoxy-phenylhydrazone

FM – Fluorescein maleimide

FMN – Flavin mononucleotide

FPLC – Fast protein liquid chromatography

FT – Fourier transform

FTIR – Fourier transform infrared spectroscopy

HEPES – N-(2-hydroxyethyl)piperazine-N'-(2-ethanesulfonic acid)

KIE – Kinetic isotope effect

MCT – Mercury-cadmium-tellurium

MES – 2-(N-morpholino)ethanesulfonic acid

MHz – Megahertz

MRI – Magnetic resonance imaging

NADH -

NAHPH

NMR -

NTA - N

OTTLE

PSI - Ph

PSII - Ph

RC - Ba

RFQ - R

SDS-PA

TMPD -

UV - U

NADH – Nicotinamide adenine dinucleotide

NAHPH - Nicotinamide adenine dinucleotide phosphate

NMR – Nuclear magnetic resonance

NTA – Nitroloacetic acid

OTTLE – Optically transparent thin-layer electrode

PSI – Photosystem I

PSII – Photosystem II

RC – Bacterial photosynthetic reaction center

RFQ – Rapid freeze-quench

SDS-PAGE – sodium dodecylsulfate – polyacrylamide gel electrophoresis

TMPD – N, N, N', N'-tetramethyl-p-phenylenediamine

UV – Ultra-violet

Chapter 1:

Introduction

I. Th

memb

electr

from t

mitoch

The ch

dehydr

(Comp

moiety

two el

out the

four p

transf

conta

succi

reduc

FAD

enou

I. The electron transport chain

The primary electron transport chain, found in the inner mitochondrial membrane of eukaryotes and the plasma membrane of many prokaryotes, transfers electrons from NADH or FADH to molecular oxygen and uses the energy released from this process to create a chemiosmotic gradient by pumping protons across the mitochondrial membrane for eukaryotes, or the plasma membrane for prokaryotes. The chain consists of four separate complexes (see Figure 1.1): NADH dehydrogenase (Complex I), succinate dehydrogenase (Complex II), cytochrome bc_1 (Complex III), and cytochrome *c* oxidase (Complex IV).

Oxidation of NADH occurs through complex I, which contains an FMN moiety, several FeS clusters, and possibly one or more bound ubisemiquinones. The two electrons taken from NADH are transferred through these redox centers to carry out the two-electron reduction of free ubiquinone to ubiquinol. During this transfer, four protons are pumped across the membrane: two protons for each electron that is transferred.

Reduction of ubiquinone also occurs through Complex II, which contains several FeS clusters and a b-type heme, and uses the electrons from succinate oxidation by a tightly bound FAD cofactor to carry out the two-electron reduction of free ubiquinone to ubiquinol. Due to the higher redox potential of FADH compared to NADH, the reaction carried out by complex II does not have enough energy to pump protons across the membrane. However, this provides a point

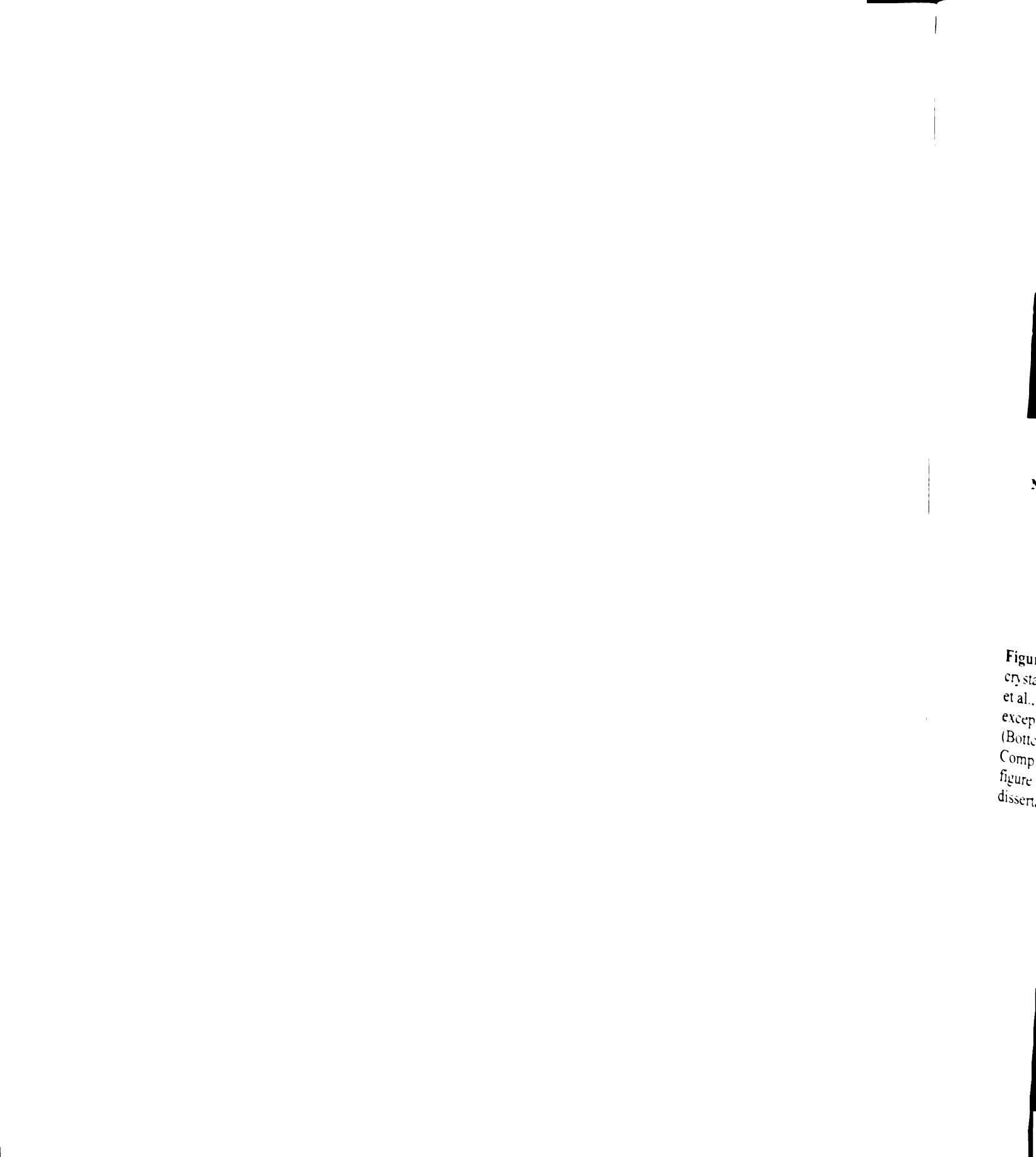

Figur
crysta
et al.,
excep
(Bott
Comp
figure
dissert

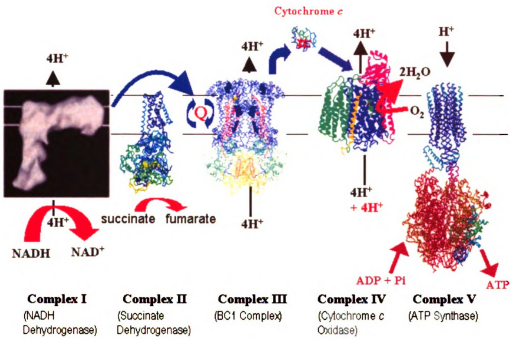

Figure 1.1: The mitochondrial respiratory chain. The structures represent the crystallographically defined structure of each enzyme (Bushnell et al., 1990; Iverson et al., 1999; Iwata et al., 1998; Stock et al., 1999; Svensson-Ek et al., 2002), with the exception of Complex I, which is an electron microscopically defined structure (Bottcher et al., 2002). All structures are of relative size, with the exception of Complex I, which is reduced from its relative size for illustration purposes. This figure is a modification of a figure courtesy of Dr. Denise Mills. Images in this dissertation are presented in color.

for e

(and

III).

as an

electr

b. ulti

donat

forwar

cytoch

oxidize

reproto

across t

where i

(Cu_A) a

a-type H

bindin

utilizin

during t

molecu

for entry into the electron transport chain for relatively high potential electrons.

The reduced quinone pool created by both complex I and complex II (and other flavin-linked dehydrogenases) is oxidized by cytochrome bc_1 (Complex III). The bc_1 complex, as its name implies, contains both b- and c-type hemes, as well as an FeS center. Electron transfer is bifurcated in this complex, with one of the electrons from ubiquinol passing through the low-spin heme *b* to the high-spin heme *b*, ultimately to reduce an internally located ubiquinone. The other electron is donated to the FeS center and on to the membrane bound heme c_1. This is the forward branch of the reaction, with cytochrome c_1 donating its electron to the soluble cytochrome *c*. This process gives rise to the quinone cycle, in which quinol is oxidized and deprotonated on one side of the membrane and rereduced and reprotonated on the other side, giving the overall result of translocation of protons across the membrane.

The soluble cytochrome *c* then diffuses to cytochrome *c* oxidase (CcO), where it donates its electron. Electrons in CcO are passed through a copper center (Cu_A) and an a-type heme (heme *a*), to the binuclear active site composed of another a-type heme (heme a_3) and a copper ion (Cu_B). With four separate cytochrome *c* binding events, the four-electron reduction of molecular oxygen to water is catalyzed, utilizing four protons. In addition, four protons are pumped across the membrane during this cycle, resulting in eight protons taken up by the enzyme for each oxygen molecule that is reduced to two water molecules.

All of the complexes of the electron transport chain, with the exception

of comp

higher r

electroc

other m

stored e

drive th

enzymes

al., 1995

(Figure

reveal th

to the in

inability

resolutio

rearrange

full unde

with thes

biologica

II. The r

oxidase

I. Visible

of complex II, harness the energy released by transferring electrons to a site with higher redox potential to pump protons across the membrane, creating an electrochemical gradient across the membrane. This gradient is then used by the other member of the respiratory chain, ATP synthase (Complex V) which releases the stored energy by transporting protons down their chemical and potential gradient to drive the synthesis of ATP, the main energy source for the cell.

High-resolution crystal structures have been obtained for all of these enzymes (Abrahams et al., 1994; Iverson et al., 1999; Iwata et al., 1995; Tsukihara et al., 1995; Xia et al., 1997), with the exception of complex I (Bottcher et al., 2002) (Figure 1.1). However, the atomic detail provided by these structures has yet to reveal the mechanism of energy transformation by cytochrome *c* oxidase, due in part to the inability to see subatomic particles crystallographically, but also due to the inability to obtain crystal structures of different intermediates of the enzyme at high resolution, which would likely reveal conformational changes and water rearrangement required for protons to move unidirectionally against a pH gradient. A full understanding of the mechanism of the structure/function relationships associated with these processes will further our understanding not only of the energetics of biological systems, but also of bioenergetically related diseases and aging.

II. The role of spectroscopy in the history of understanding cytochrome *c* oxidase

1. Visible and UV spectroscopy

The first mention of the enzyme that would eventually come to be

known as cytochrome *c* oxidase was reported by MacMunn in 1886 (MacMunn, 1886). At that time, he reported on a respiratory pigment, capable of changing its oxidation state, that he called myohaematin (when extracted from muscle cells) or histohaematin (when isolated from other cell types). It was characterized by four absorption bands in the visible spectrum when reduced. MacMunn's discovery was generally discredited, though, as nothing more than hemoglobin at various depths in the tissue or hemoglobin derivatives. This topic was not revisited again until 1925, when studies undertaken by Keilin proved not only that the compound identified by MacMunn was distinct from hemoglobin, but also that it was very widely distributed (Keilin, 1925). Keilin also pointed out that this pigment was in fact composed of three distinct chromophores, though he still believed these three chromophores to reside in the same enzyme.

Keilin renamed the compound *cytochrome*, meaning "cellular pigment", and described its visible spectral characteristics. The three chromophores he detected were differentiated based on how red their absorbance band was: the most red band (furthest from the ultraviolet) being referred to as *a*, the second as *b*, and the third as *c*. He also noted an additional band, to the blue of *c*, but speculated this band had the same origin as band *c*, and hence referred to the primary bands of each chromophore as the α-band, and the second band associated with a chromophore as the β-band. As it was discovered that each of these α-β band pairs was associated with an independent enzyme that could be isolated, they became known as cytochromes *a*, *b* and *c*, based on their characteristic α-band absorbance. Another band was eventually noticed in the extreme violet region (400-450 nm) of the spectrum, and was referred to as the γ-band. However, as suggested in 1899 by Gamgee (Gamgee, 1899), this

even

deve

cytoc

Keilin

direct

(Keilin

oxidase

of anot

that of

was inti

cytochro

cytochro

state, bou

2. Electr

when oxi

most wid

oxidase ((

investigati

spin reson

metals of (

al., 1976; J

eventually became known as the Soret band, in reference to the French scientist who developed quartz oculars that allowed observation in this region (Soret, 1878).

After the rediscovery of cytochromes by Keilin, it was noted that cytochromes were involved in the oxidation of various substances in the cell. It was Keilin again, this time with Hartree, that noted the sole attribute they could ascribe directly to this oxidase was the oxidation of cytochrome *c* and the uptake of O_2 (Keilin, 1938). Hence, they proposed this enzyme be referred to as cytochrome oxidase. The very next year, Hartree and Keilin presented evidence for the existence of another cytochrome (Keilin and Hartree, 1939), whose spectrum was fused with that of cytochrome *a*, which they called cytochrome a_3. They demonstrated that it was intimately linked with cytochrome *a* and was explicitly involved in the activity of cytochrome oxidase. They also noted, based on spectral shifts, that it was cytochrome a_3 that, when in its reduced state, bound CO, and when in its oxidized state, bound various other lethal compounds, such as KCN, sodium azide and H_2S.

2. Electron paramagnetic resonance (EPR) spectroscopy

The characteristic UV-visible spectral signatures of the different hemes when oxidized, reduced, or with an exogenous ligand bound, has proven to be the most widely used method for examining the structure and function of cytochrome *c* oxidase (CcO). But other techniques were also developed that allowed further investigation of the enzyme. Magnetic resonance spectroscopy, in particular electron spin resonance (ESR or EPR), became the next method of choice in examining the metals of CcO. While EPR has also been used to further probe the hemes (Aasa et al., 1976; Hartzell and Beinert, 1974), its most significant use has been in the study of

the copper site, Cu_A. Though the presence of copper was first detected in CcO in 1959 (Sands and Beinert, 1959), the stoichiometry of copper was highly debated. Once it was resolved that CcO had two copper sites (Beinert et al., 1962), one that was detectable by EPR (Cu_A) and another undetectable one, magnetically coupled to the heme a_3 (Cu_B), the focus became the number of copper ions in the Cu_A site. EPR eventually clarified that the Cu_A site was composed of a spin-delocalized dinuclear copper center (Kroneck et al., 1989; Kroneck et al., 1990).

Lately there has been a resurgence of EPR spectroscopy of CcO, this time looking for a catalytically relevant organic radical (Chen et al., 1999; MacMillan et al., 1999; Rich et al., 2002; Rigby et al., 2000) and monitoring changes in the non-catalytic Mg site that can be replaced with the paramagnetic ion Mn. A tyrosine residue cross-linked to a histidine ligand of Cu_B is suggested to be oxidized to a radical during the catalytic cycle of CcO (Proshlyakov et al., 1998). Several groups have tried to produce CcO in an intermediate state in which such a radical would be predicted to exist and to be visible by EPR. Unfortunately, due to the presence at the active site of the heme a_3 and Cu_B, which are paramagnetic and strongly coupled, it is unlikely that any radical formed in the active site would be unaffected by these two other spins and remain visible by EPR. While some groups have detected an EPR-active radical that they propose is catalytically relevant (MacMillan et al., 1999; Rigby et al., 2000), it is most likely an artifact of the highly oxidizing hydrogen peroxide used to generate the sample (Rich et al., 2002). Chemical approaches to this question have also been made with some success (Proshlyakov et al., 2000). Studies on the Mg/Mn site will be discussed in chapters two and three.

3. Re

reason

advan

inform

spectro

Resona

excitati

informa

been us

Proshly

reactio

4. Hig

crystal

(Tsuki

1995)

(Svens

been a

directe

precise

water n

aqueou

been in

3. Resonance Raman spectroscopy

With the general spectral composition and characteristics of CcO reasonably well determined with magnetic and UV-visible spectroscopy, more advanced spectroscopic techniques became prevalent in the 1980s to obtain specific information on the reaction mechanism. Raman spectroscopy is an advanced optical spectroscopy that observes frequency shifts of laser light scattered off a sample. Resonance Raman is a more refined version of this technique that relies on specific excitation of a chromophore by the laser light, enhancing the signal to give detailed information only on the environment of the excited chromophore. This technique has been used extensively (Han et al., 1990a; Han et al., 1990b; Kitagawa, 2000; Proshlyakov et al., 1994; Proshlyakov et al., 1996) to study the intermediates of the reaction cycle (see section III.2)

4. High resolution x-ray crystallography

The next advance in the study of CcO was the atomic resolution x-ray crystal structures that were originally determined in 1995 for CcO from bovine (Tsukihara et al., 1995) and the bacterium *Paraccocus denitrificans* (Iwata et al., 1995) and in 2002 for the CcO from the bacterium *Rhodobacter sphaeroides* (Svensson-Ek et al., 2002). While many of the details of the metal sites had already been accurately determined by UV-visible, EPR and Raman spectroscopies and site-directed mutagenesis, the crystal structure provided much needed verification and precise structural detail, creating a platform for more incisive analysis of proton and water movement in the enzyme. Upon examination of the first crystal structures, two aqueous channels that lead from the bottom of the enzyme to the interior, which had been indicated by mutagenesis (Fetter et al., 1995; Thomas et al., 1993), were clearly

visibl

work.

proton

mamm

sphaer

analys

species

5. Fou

been in

knowle

dipole m

has bee

absorpti

the infor

complex

feasible

large pr

induced

Chance,

introduc

electrod

same FT

Hellwig e

visible (Tsukihara et al., 1996) and later established to be proton channels. Recent work, including the work presented here, has used the structure to propose water and proton exit pathways. The crystal structures of CcO from diverse sources, the mammalian oxidase (from bovine heart) and two bacteria (*P. denitrificans* and *R. sphaeroides*), allows for comparative structural analysis and focusing of functional analysis and mutagenesis to the regions of structure that are conserved between species.

5. Fourier transform infrared (FTIR) spectroscopy

The latest spectroscopy to be used extensively in the analysis of CcO has been infrared spectroscopy. FTIR is an information rich spectroscopy, providing knowledge of all bond vibrations in a molecule that lead to a change in the electronic dipole moment. The extensive amount of information carried in an FTIR spectrum has been the reason for its limited use in large proteins like CcO; there is too much absorption to detect and assign specific bands to specific residues. In order to limit the information obtained, a difference spectrum must be taken. Due to small and complex spectral band changes and difficulty in preparing identical samples, it is not feasible to make a difference spectrum of two different samples. Hence, FTIR on large proteins has been restricted to looking at light-induced changes, such as those induced by photolysis of CO in a CO inhibited enzyme (Alben et al., 1982; Miller and Chance, 1994; Moody et al., 1995). Two new techniques have recently been introduced to alleviate this restriction. The use of optically-transparent, thin-layer electrodes allows one to electrochemically reduce and oxidize a sample kept in the same FTIR cell by means of a potentiostat (Behr et al., 1998; Hellwig et al., 1998; Hellwig et al., 1999). Alternatively, one can use an FTIR spectrometer based on

attenu

penetr

patter

Hence

states

6. Rap

structur

static.

chemic

of prot

process

occurs

Thus, t

introdu

mainly

first, us

examin

1995; K

center a

reduced

The poi

cuvette.

reaction

attenuated total reflection (ATR) in which the IR radiation is reflected back before it penetrates all the way through the sample layer, but still contains the absorption pattern of the sample (Iwaki et al., 2003; Nyquist et al., 2001; Nyquist et al., 2003). Hence, various buffers can be flowed over the sample, resulting in different redox states or liganding states of the enzyme without otherwise affecting the sample.

6. Rapid kinetic spectroscopy

While all the static spectroscopies provide useful information about the structure of the enzyme and its stable intermediates, as with all enzymes CcO is not static. It rapidly transfers protons, electrons, dioxygen and water, carries out a chemical reaction, and drives a thermodynamically unfavorable process (the pumping of protons against a gradient). The challenge in the case of CcO is not just the diverse processes being carried out, but also the speed of the reactions: overall turnover occurs in a millisecond or less and individual steps in the microsecond time frame. Thus, to get information about the catalytic function of CcO, kinetics must be introduced to spectroscopic experiments. The introduction of kinetic resolution has mainly been achieved in UV-visible spectroscopy by two different methods. The first, used extensively to determine the mechanics of the oxygen chemistry and examine unstable intermediates, is called the flow-flash technique (Adelroth et al., 1995; Karpefors et al., 1998). This relies upon binding CO to a reduced binuclear center and the ability to photodissociate the CO with a short laser pulse. The fully reduced CcO is incubated with CO anaerobically, and then the excess CO is removed. The poisoned CcO is then rapidly mixed with oxygenated buffer and pushed into a cuvette. Just after the probe light is started, the CO is flashed off and the entire reaction can be observed, with a resolution of nanoseconds. The other kinetic UV-

visibl

(i.e.,

into a

wavel

can ha

al., 20

method

collecte

measur

Hiser e

III. T

1. Ov

similar

system

Rhodo

thirteen

I is the

binucle

role for

hydropi

the initi

transme

visible spectroscopy used is stopped-flow spectroscopy. In this technique, the sample (i.e., CcO) is rapidly mixed with the reactant (i.e., reduced cytochrome *c*) and pushed into a cuvette, where recording takes place. When observing only a single wavelength or using a sensitive charge-coupled diode (CCD) detector, this technique can have microsecond resolution if very special mixing methods are used (Szundi et al., 2001a; Szundi et al., 2001b; Van Eps et al., 2003). However, most stopped-flow methods involve millisecond mixing times, but allow for an entire spectrum to be collected with millisecond resolution. This technique has been used extensively for measuring proton pumping of CcO in artificial lipid vesicles (Antonini et al., 1993; Hiser et al., 2001).

III. The current understanding of cytochrome *c* oxidase function

1. Overall structure and subunit composition

The cytochrome *c* oxidase from *R. sphaeroides* has a high degree of similarity to its mammalian counterpart but has fewer subunits, making it an ideal system for studying the function of CcO (Figure 1.2) (Hosler et al., 1992). The *Rhodobacter* CcO is now known to be composed of four subunits (compared to thirteen in the mammalian enzyme) and several metal cofactors (Figure 1.3). Subunit I is the largest subunit, with 12 transmembrane helices, and contains heme *a*, the binuclear active site of heme a_3 and Cu_B, as well as a non-redox active calcium. The role for this Ca^{2+} is currently unknown (Lee et al., 2002). Subunit II has the largest hydrophilic domain of the protein and only two transmembrane helices; it contains the initial electron acceptor, the dinuclear Cu_A center. Subunit III consists of seven transmembrane helices and contains no metal centers. The function of this subunit is

Figur
bacte
simil
orang
cofac
Rhod
transf
subur
Warw

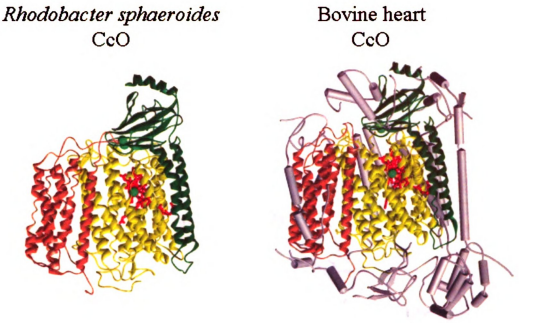

Figure 1.2: Comparison of bacterial and mammalian CcO structures. The bacterial CcO structure from *R. sphaeroides* (left) contains subunits that are highly similar to the core three subunits of bovine CcO (right), shown in yellow, green and orange. They both contain the same spatial alignment of the redox active metal cofactors (hemes *a* and a_3 shown in red, Cu_A and Cu_B shown in bright green). *Rhodobacter* CcO contains an additional subunit consisting of a single transmembrane helix (not seen in this view). Bovine CcO contains an additional 10 subunits, shown in gray. This figure is a modification of a figure courtesy of Dr. Warwick Hillier.

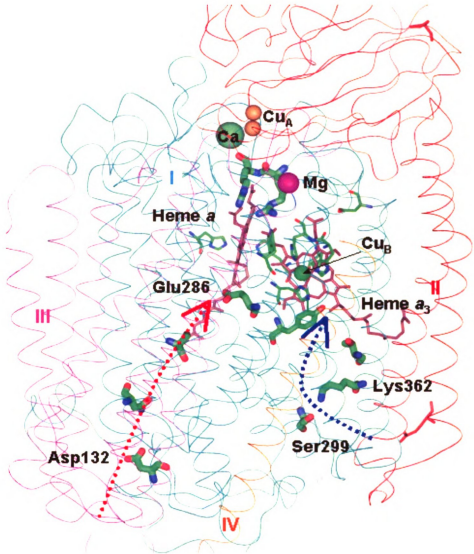

Figure 1.3: Overall structure and composition of *R. sphaeroides* CcO. Diagram of the four subunit structure of *R. sphaeroides* cytochrome *c* oxidase showing two well-defined proton uptake paths, the D (red) and K (blue) paths. The 3 redox active centers are labeled: the binuclear Cu_A center where electrons enter, heme *a*, and the heme a_3/Cu_B active site where oxygen chemistry occurs. The two non-redox metal sites, Ca and Mg, are also shown. The backbone structures of subunit I (cyan), II (red), III (magenta) and IV (orange) are shown. This figure is a reproduction from (Mills and Ferguson-Miller, 2003).

curre

suicid

transi

crysta

throu

one a

II. just

role of

structu

(Floren

suggest

its con

2. The

unders

CeO ca

model

1.4). F

there a

second

the do

rapidly

and on

immed

currently unknown, but its removal affects proton movement in the protein and causes suicide inactivation of the enzyme as it turns over. Subunit IV is a short, one transmembrane helix that was only discovered when the enzyme was first crystallized. Its association with the other subunits appears to be made mainly through embedded lipid molecules, and its function is currently unknown. There is one additional non-redox active metal, a Mg^{2+} that is located between subunits I and II, just above the heme a_3 propionates (Espe et al., 1995; Hosler et al., 1995). The role of this additional metal is unknown, though it has been postulated to serve in a structural role, maintaining the alignment of subunits I and II relative to each other (Florens et al., 1999). Additionally, the proximity of this metal to the active site suggests it may also serve some other, more direct role in proper enzyme function or its control.

2. The oxygen chemistry

The spectroscopies discussed above have been employed to gain a detailed understanding of CcO function, and particularly to elucidate the oxygen chemistry that CcO catalyzes. While there still remain a few details that are in question, a specific model for the oxygen chemistry carried out by CcO is now generally accepted (Figure 1.4). Electrons enter CcO from cytochrome *c* through the dinuclear Cu_A site and from there are transferred to heme *a* and eventually on to Cu_B (intermediate E). When a second electron is injected, the electron is transferred to heme a_3 (intermediate R), and the doubly reduced binuclear center binds oxygen (intermediate A). The oxygen bond is rapidly cleaved at this point, using two electrons from the heme a_3 to form a ferryl-oxo and one electron from Cu_B to form a cuprous hydroxide. If a fourth electron is not immediately available, an electron is taken from a nearby amino acid residue, most likely

Figure
electro
the rel
The se
to allo
Oxyge
sponta
at the
288 (Y
of the
proton
accom
oxidiz
involv
Denis

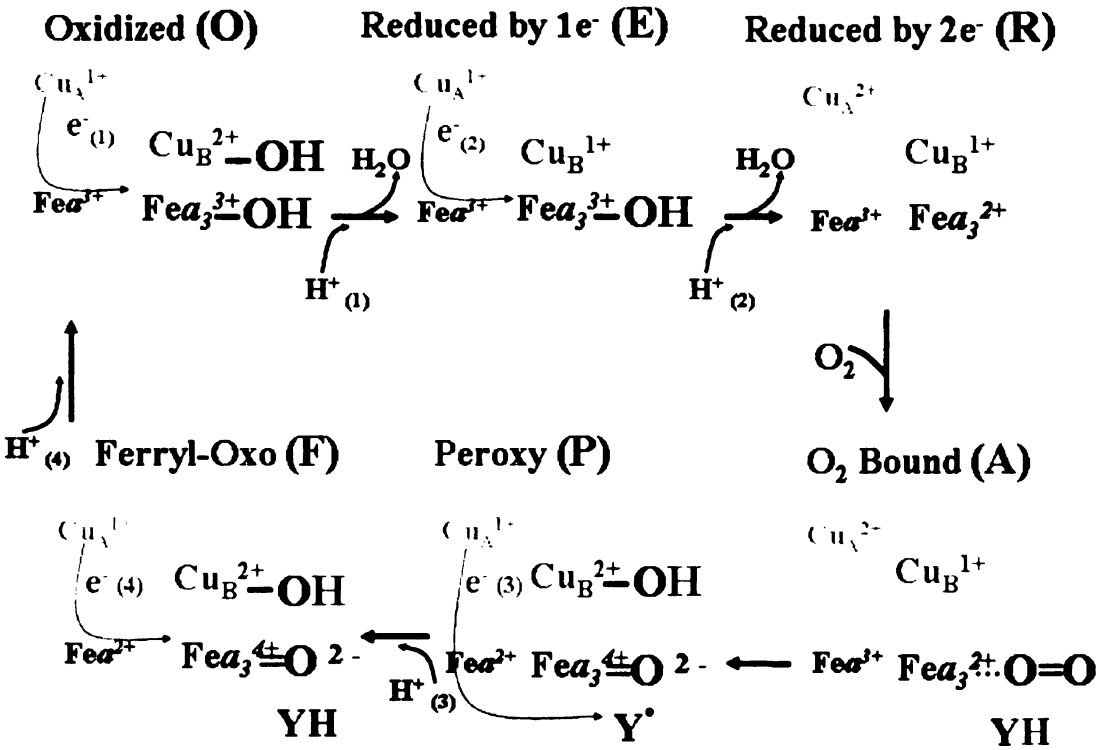

Figure 1.4: The oxygen chemistry catalytic cycle carried out by CcO. The first electron received is delivered to the active site, with the uptake of a proton, allowing the release of a hydroxyl ligand as water and resulting in the unstable intermediate E. The second electron also proceeds to the binuclear center, accompanied by a proton, to allow the second hydroxyl ligand to be released as water and yield intermediate R. Oxygen rapidly binds at this point and forms intermediate A. Intermediate A spontaneously degrades to intermediate P, where electrons from the two metal centers at the binuclear site, as well as a proton and electron donated from the nearby tyrosine 288 (Y), form a ferryl-oxo, a cupric hydroxide and a neutral tyrosyl radical. Injection of the third electron yields intermediate F, with the electron, again accompanied by proton uptake, regenerating the tyrosine. The injection of the fourth electron and accompanying proton reduces the ferryl-oxo to a ferric hydroxide, regenerating the oxidized state O. The four protons that are pumped are not shown since the steps involved are not yet known. This figure is a modification of a figure courtesy of Dr. Denise Mills.

Y25
now
elect
(inter
elect
heme

3. Pro

chemis
mutage
crystal
proton
lysine
termin
unders
al., 19
D-path
channe
embed
betwee
glutam
some s
2001; 2
protons

Y288. This state is referred to as the P (for peroxy) intermediate, even though it is now apparent that there is no actual peroxy state of the oxygen. When a third electron is injected, it reduces the amino acid radical back to its stable state (intermediate F, for ferryl-oxo). Finally, a fourth cytochrome *c* injects the last electron to return the enzyme to its oxidized state, leaving a hydroxyl on both the heme a_3 and Cu_B.

3. Proton pumping

Proton movement in CcO is not as well understood as the oxygen chemistry, as studies have largely been limited to indirect observations based on mutagenesis and pH sensitive dyes in the external medium and analysis of the static crystal structures. However, these techniques have been successful in defining two proton intake channels (Figure 1.5). One, called the K-path because of a conserved lysine (K362) in the channel, leads from the bulk directly to the heme a_3-Cu_B site. Its termination at the site where oxygen chemistry is carried out has led to the understanding that the K-path is used only for substrate proton delivery (Adelroth et al., 1998; Pecoraro et al., 2001; Zaslavsky and Gennis, 1998). The second, called the D-path because of a conserved aspartate (D132) found near the entrance of the channel, leads from the surface, through a series of polar amino acid residues and embedded water molecules, to a conserved glutamate (E286) that is positioned between and slightly below the two hemes. The pathway is not defined past this glutamate. It is proposed to be involved in transferring all pumped protons, as well as some substrate protons (Adelroth et al., 1996; Adelroth et al., 1998; Pecoraro et al., 2001; Zaslavsky and Gennis, 1998). An additional proton pathway for pumped protons, termed the H channel, has also been proposed based on the crystal structure

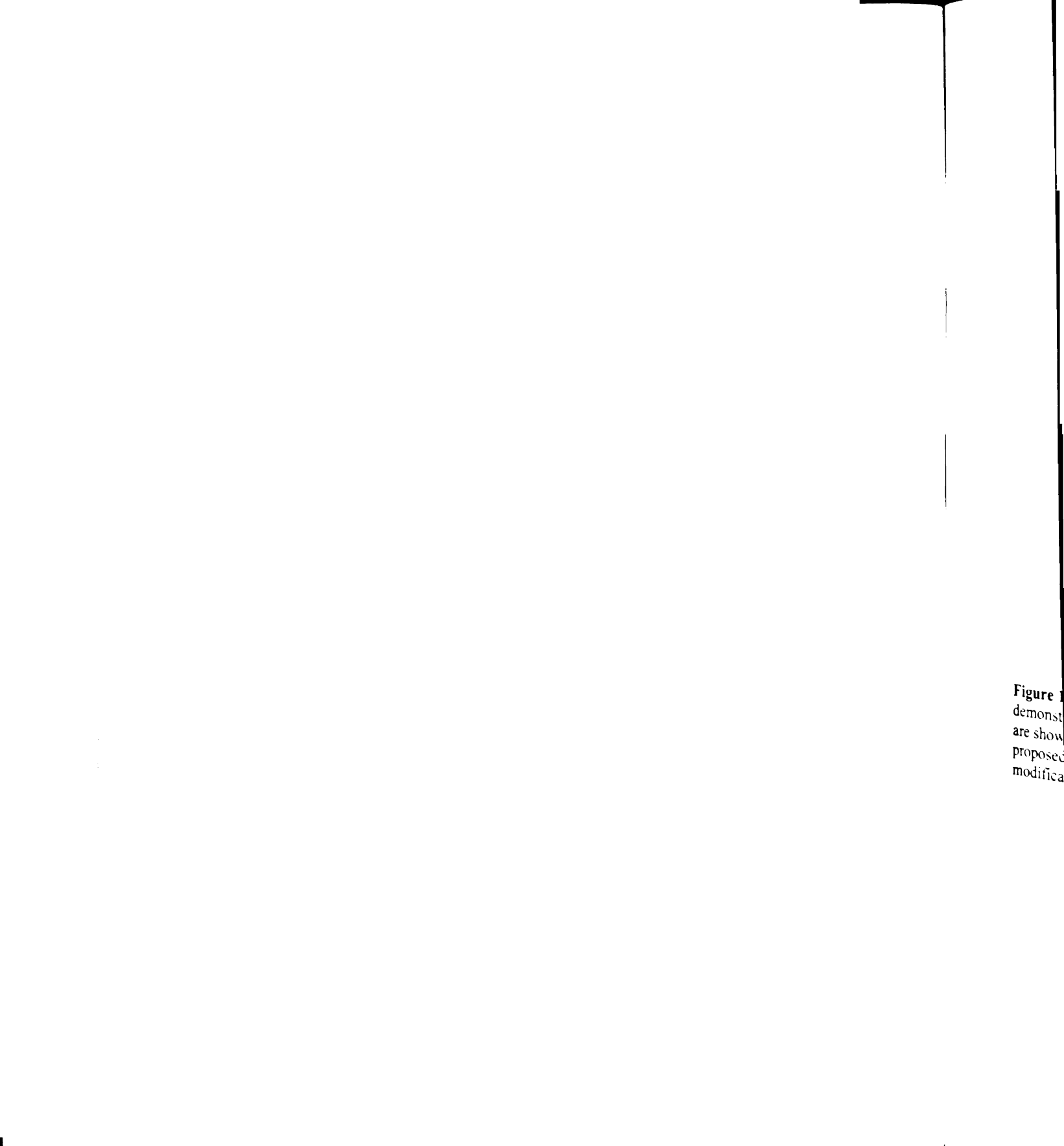

Figure 1
demonst
are show
proposed
modifica

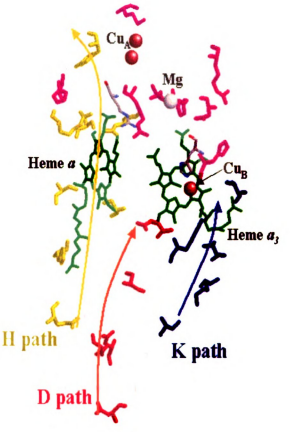

Figure 1.5: Proton uptake pathways. Residues involved in the two channels demonstrated to be used in proton uptake; the D path (in red) and the K path (in blue) are shown, as well as residues from the proposed H path (in yellow). Residues proposed to be important in proton exit are shown in purple. This figure is a modification of a figure in (Mills and Ferguson-Miller, 2002).

of th

2000

studi

and t

pathw

propo

the D

conclu

what p

4. Ex

E286

Puust

Flore

transf

bulk

regio

sugg

route

func

for

Zhe

of the bovine CcO (Tsukihara et al., 1996; Yoshikawa et al., 1998a; Yoshikawa et al., 2000). While there are proponents of the functionality of this pathway, mutagenesis studies of the amino acid residues proposed to define this channel (Lee et al., 2000) and the lack of conservation of essential residues across species, indicate that this pathway is not likely to be a universal proton-pumping channel. While the K path is proposed to deliver only substrate protons, the H channel only pumped protons and the D path is proposed to deliver both pumped and substrate protons, there is no conclusive evidence yet as to how many protons are supplied by each pathway and at what points in the reaction cycle they are used.

4. Exit for pumped protons and product water

There are few proposals for possible routes of pumped protons between E286 and the protein surface (Florens et al., 1999; Michel, 1998; Papa et al., 1998; Puustinen and Wikstrom, 1999), or for exit of product water (Backgren et al., 2000; Florens et al., 1999; Zheng et al., 2003). Several suggest that pumped protons transfer from E286 to the propionates of the hemes, and from there move into the bulk phase through the extensive hydrogen bonded network found in this external region of the protein (Figure 1.6). While zinc inhibition on the outside of the enzyme suggests there is a specific site for proton exit, there is little evidence defining exact routes from the propionates to the protein surface.

Water exit through the enzyme is considered vital for proper enzyme function (Kornblatt, 1998), but there are very few suggestions for specific exit routes for the water produced at the active site to reach the bulk (Backgren et al., 2000; Zheng et al., 2003). Due to the high fluidity of water in proteins (Dwyer et al., 2000;

Figure
hydrog
potenti
no sing
figure i

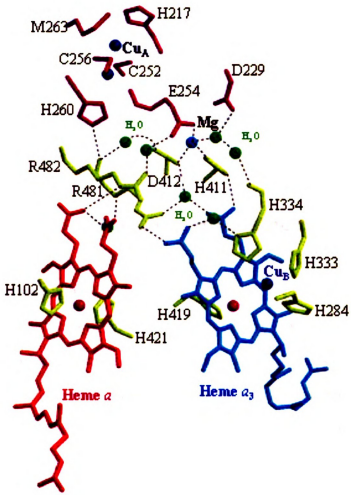

Figure 1.6: Hydrogen-bonded network above the heme propionates. The hydrogen bonding between amino acid residues and water molecules provides a potential pathway for proton exit from the protein. Due to the extent of this network, no single pathway in this region has been verified. This figure is a modification of a figure in (Ostermeier et al., 1997).

Garc

1999

chan

direc

quite

exit c

IV. T

1. Pr

by mu

analy

under

funda

proto

under

uncov

its fu

theor

bioch

of pr

deriv

Garcia and Hummer, 2000; Gottschalk et al., 2001; Schiffer and van Gunsteren, 1999), it is not unreasonable to suggest that there is in fact no specific water exit channel, but that water exits by simple diffusion. However, since strict control of directionality of electron and proton movement is required for proper function, it is quite likely that water flow must also be controlled, hence requiring a specific water exit channel.

IV. Theory and examples from other proton and water translocating proteins

1. Proton transfer theory

While many mechanistic details of CcO function have been elucidated by mutational and spectroscopic interrogation, theory provides another platform for analysis. There are many proteins that catalyze proton transfer reactions, which are understood mechanistically to varying levels. Comparative analysis of the fundamental principles employed by these enzymes has led to generalized theories of proton translocation in nature (Krishtalik, 2000; Silverman, 2000). With an understanding of these principles, more rational experiments can be designed to uncover the specific details of the proton pumping mechanism of CcO.

The abundance of proteins using or catalyzing proton transfer, as well as its fundamental reliance on the principles of quantum mechanics, has led to extensive theoretical research on mechanisms of proton conductance and proton transfer by biochemists, physical chemists and physicists. The first paper to discuss mechanisms of proton movement was almost 200 years ago, long before quantum mechanics was derived and first used to describe protons. Using a galvanic electrode to study the

composition of water, Grotthuss in 1806 first described the polar nature of water and the tendency of oxygen to migrate towards a positive cathode and hydrogen to migrate towards a negative anode (de Grotthuss, 1806). Based on this work, he determined that water was composed of one hydrogen molecule and one oxygen molecule, which had an inherent polarity in them, with the oxygen tending to be more negative and the hydrogen more positive. When attracted to opposite ends of a solution by an electrical current, he proposed water could stack in a linear fashion then dissociate to hydrogen and oxygen, with the hydrogen migrating preferentially to the anode and oxygen preferentially migrating to the cathode. When a hydrogen or an oxygen would dissociate and migrate, there would be a hole left that would rapidly be filled by another hydrogen or oxygen to compensate for the dissociated molecule.

Though Grotthuss' groundbreaking work was developed so long ago, understanding of proton movement could not progress further until quantum mechanics was developed and ions could be described on a more detailed basis. One of the main principles in the modern understanding of proton transfer was originally developed as a general description of ion movement in solutions (Onsager, 1969). The theory consists of moving charges, and protons in particular, through chains of hydrogen bonded molecules.

In Onsager's original treatise, these hydrogen bonded chains consisted of water, particularly when in an ice matrix. The protons move by what is now termed the "hop and turn" mechanism: protons move by hopping from donor to acceptor by making and breaking hydrogen bonds. As the proton hops to the acceptor molecule, the bond between the acceptor atom and its existing hydrogen is weakened, and that

hydrogen can form another hydrogen bond with another acceptor. This sequence continues across the chain until the orientation of the hydrogen bonds along the entire chain is reversed (Figure 1.7). At this point a proton has been transferred, but the elements of the chain now have a hydrogen bonding pattern that is reversed (termed a bonding defect) that does not allow the transport of another proton until they reorient. As the water molecules involved in this defect turn, changing their hydrogen bonded pattern as a result of Brownian motion, the defect is propagated along the chain in the opposite direction of the proton translocation, resulting in a reorientation of the water chain back to its original alignment. Thus, while the net result is the loss of a proton from one side of the chain and the appearance of an extra proton on the other side, this is the result of a series of small movements, and one proton does not traverse the entire distance, as it would have to in a diffusive process. Hence rates of proton movement can be achieved that are above the limit of diffusion.

Onsager's theory for proton movement in water was extended by Nagle and Morowitz by explicitly applying it to proton translocation in proteins, using the hydrogen-bonding capacity of amino acids as the hydrogen bonded chain, or "proton wire" required for efficient proton transfer (Nagle and Morowitz, 1978). Additionally, they also address the possible mechanisms for active pumping of protons against a gradient, not just diffusive flow down a gradient. All that is required to adapt the previous model to account for unidirectional transport is to have a gating mechanism that promotes ion or fault generation preferentially on one side of the chain.

Recently, proton translocation in proteins has been studied in more

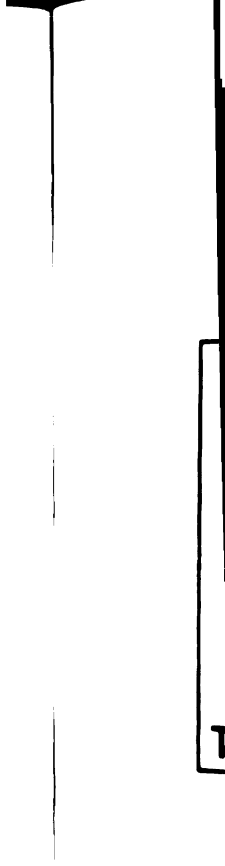

Figur
the h
water
on the
(the h
anothe
turn s

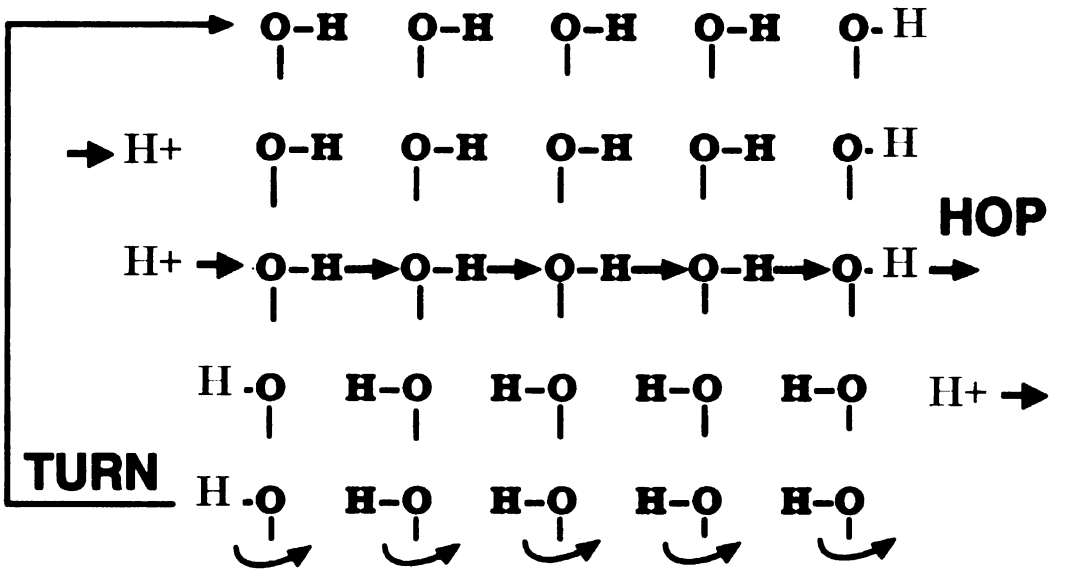

Figure 1.7: Propagation of protons through a hydrogen-bonded water chain by the hop and turn mechanism. Protons approaching an oriented hydrogen-bonded water chain (in blue) can hydrogen bond to the terminal water. The extra charge now on the water chain can be released as the terminal proton (in red) on the other side (the hop step), effectively transferring a charge across the chain. In order to accept another proton from the same side, the orientation of the water chain must flip (the turn step). This figure is a modification of a figure in (Pomes and Roux, 2002).

detail, quantitatively comparing theoretical models with ever more advanced experimental data on model proteins. One of the best-studied proteins that allow for passive proton diffusion is gramicidin A. This is a small molecule that is synthesized and extruded by *Bacillus brevis* as a defense mechanism against Gram-positive bacteria. The cyclic peptide enters the membrane of a potentially invading bacterium, forming a pore for the rapid transit of protons, as well other small cations and water, down their gradients. This leads to the depolarization of the bacterial membrane, killing the invading bacterium. The small nature of this peptide and simplicity of function has led to it being one of the most commonly used models for understanding the principles of proton movement in proteins, particularly with computer simulations (Pomes and Roux, 2002; Roux and Karplus, 1994; Sagnella and Voth, 1996).

Proton translocation in gramicidin occurs through a series of single-file hydrogen bonded waters that permeate the pore in a classical hop and turn mechanism. While it was initially believed that the actual proton transfer is fast and the rate limiting step is propagation of the bond defect by turning (Pomes and Roux, 1998), it is now being recognized that bond defect propagation occurs on the same timescale as proton hopping (Pomes and Roux, 2002). The turn step was originally considered to be the slow step as it requires the breaking of hydrogen bonds and is known to occur in a sequential fashion along the chain. While proton transport has no such limitations, it is now clear that hydrogen bonding patterns of the waters to the protein frame of a channel and dipole arrangement of both the water wire and the protein frame can influence proton translocation across the wire (Pomes and Roux, 2002). Protein vibrations, even on the picosecond to nanosecond timeframe, can influence these factors and hence can control the rate of proton transfer (Smondyrev

and

influ

situa

prote

prote

Hence

faster

limita

bondi

when a

donors

and pr

effect p

these l

and eff

channe

into the

rapid fl

and bre

reorien

channel

and Voth, 2002).

Proton wires that are buried in a hydrophobic environment lack the influence of the dipolar protein surface and hence proton transport is fast, but in this situation reorientation of the water wire is limiting (Dellago et al., 2003). In a real protein environment, however, the environment is necessarily more polar, due to the protein backbone amides and carbonyls, as well as polar amino acid side-chains. Hence, the additional possibilities for hydrogen bonding to the protein allows for faster water reorientation. Conversely, the more polar environment can impose limitations to proton transfer by improperly aligned dipoles or by excessive hydrogen bonding to the water chain (Yu et al., 2003). As water is in its lowest energy state when accepting two hydrogen bonds, a channel with properly aligned hydrogen bond donors and acceptors can fully occupy the hydrogen bonding capacity of the water and prevent additional ligation by a proton. Dipole orientation in the channel can effect proton translocation by creating areas of local minima for proton solvation. If these local minima are too low in energy, the proton can be trapped in this location and effectively limit transport across the hydrogen bonded chain. Alternatively, channels with outwardly directed dipoles create an energy barrier for proton entrance into the channel, which limits proton transfer.

These barriers to transport can be overcome in the protein by the small, rapid fluctuations that occur in the protein backbone. These fluctuations can form and break hydrogen-bonding capability with the water wire, allowing for rapid water reorientation. It can also lead to fluctuations of dipoles to allow proton entry into the channel and prevent trapping of the solvated proton at any given point in the channel.

Thus, the rigidity of a protein and the orientation of its dipoles in the proton channel determine proton translocation rates. This has also been verified by experiment with covalently linked dimers of gramicidin (de Godoy and Cukierman, 2001). Introduction of linkers that limit the conformational flexibility of the channel have notable effects of the transport rates supported by the channel.

2. Proton channels in enzymes

Vectorial transport of protons across lipid membranes is essential for life. As mentioned above, energy metabolism supported by the electron transport chain involves building up a chemiosmotic gradient by pumping protons against their gradient. This gradient can then be diffused, using the energy released to drive ATP synthesis. Since the chemiosmotic gradient is achieved not only by CcO, but also by the respiratory complexes I and III, these are useful to elucidate the general principles of unidirectional proton pumping. Additionally, there are many other proteins that translocate protons, either actively or passively, across part or all of a membrane. These proteins can also provide important clues to the mechanism of proton transport in proteins that can be applied to CcO.

2.1 Enzymes that vectorially pump protons against their gradient

As mentioned above, all of the enzyme complexes in the electron transport chain, with the exception of complex II, vectorially translocate protons across their gradient, providing the chemiosmotic gradient used to drive ATP synthesis. The enzymes of the electron transport chain are not conserved across all species, and other proteins are used to achieve the same function. In addition, enzymes such as ATP synthase, which normally allows protons to flow down their

gradient, can also function in reverse under appropriate conditions, pumping protons against their gradient. Understanding of these proteins can be useful in the understanding of CcO function, as they carry out the same basic function: unidirectionally pumping protons against their gradient.

2.1.1 NADH dehydrogenase

Complex I, being the only respiratory complex for which the structure has not been determined by high-resolution crystallography, offers the fewest functional details of proton channels. Nevertheless it does provide some useful insights. It offers perhaps the best comparison to CcO, as it does not explicitly rely on a quinone cycle to pump protons. While it does contain at least one bound ubisemiquinone that is used in electron transfer (De Jong and Albracht, 1994; Ragan et al., 1974), it has been proposed that this cofactor is not used as the proton pump. Indeed, some bacteria use complex I to pump Na^+ instead of protons (Steuber, 2001), which cannot be transferred by a quinone cycle. Additionally, since complex I pumps two protons for every electron transferred, for a quinone cycle to account for all the protons pumped, several bound quinones would be necessary to achieve the correct stoichiometry. However, inhibitory studies seem to indicate this is not the case (Okun et al., 1999).

It is becoming increasingly accepted that the proton pumping mechanism of complex I is due to large-scale, long-range conformational changes as a result of the redox state of one or more of the electron transfer sites (Friedrich, 2001). The strongest evidence suggests that pumping occurs across a subunit that has a high degree of similarity to a proton-pumping, membrane-bound NiFe hydrogenase

(Friedrich and Scheide, 2000). In this mechanism, the directionality of the pump is dependent upon large-scale conformation changes, which can be seen by electron microscopy. It has been proposed that this conformational change is likely induced by the one FeS cluster (N2) that shows a clear pH dependence of its redox potential.

2.1.2 Cytochrome bc_1 (Complex III) and cytochrome b_6f

The mechanism of proton pumping carried out by complex III is quite different from CcO in that it relies on a quinone cycle. This mechanism was first proposed by Mitchell when proposing the chemiosmotic hypothesis (Mitchell and Moyle, 1965): a quinone is reduced and picks up protons on one side of the membrane, and is oxidized and deprotonates on the opposite side of the membrane.

This clearly solves the issue of unidirectional transport, as the quinone must protonate as it is reduced and deprotonate as it is oxidized. However, to control the sidedness of the proton uptake and release, the quinone must bind to the protein at a specific site and side of the membrane. To ensure appropriate proton translocation, the protein must guide the release of the proton to the outside at the quinone oxidation site and to the inside at the quinone reduction site. In fact, a steered molecular dynamic study suggests that such a pathway does exist in the bc_1 complex for proton exit to the outside bulk, composed mainly of internal water molecules and hydrophilic amino acid side-chains, as well as the propionates of the low spin c_1 heme (Israilev et al., 1999). Indeed, this channel was verified recently by a high-resolution crystal structure, which resolved the internal waters essential for the pathway proposed by the computer simulation when inhibitor was bound at the quinone oxidation site (Palsdottir et al., 2003).

The presence of this exit pathway only when a quinone analogue is bound at the oxidation site may be due to insufficient resolution of crystal structures with nothing in the oxidation site. However, given the large conformational movements, particularly of the iron-sulfur protein, upon binding of quinone to the oxidation site (Zhang et al., 1998), it is quite likely the exit pathway only exists when the oxidation site is occupied.

The protein complex in the photosynthetic reaction that is analogous to the bc_1 complex, cytochrome b_6f, demonstrates a similar motif for proton exit. In the b_6f complex, electrons are donated from reduced plastoquinone, which was reduced during photosynthetic cycle of photosystem II (PSII), and eventually used to reduce plastocyanin instead of cytochrome *c*. Electron transfer to the b_6 hemes is used to rereduce plastoquinone, creating a Q cycle for proton pumping. The other electron donated from plastoquinone to the iron-sulfur protein (ISP) is further transferred through cytochrome *f* to plastocyanin. Early crystal structures of the isolated cytochrome *f* showed a water chain, consisting of five buried waters, stretching from the heme *f* to near the surface (Martinez et al., 1996). Further mutational studies on the amino acid residues that support this water chain (Ponamarev and Cramer, 1998) confirmed that this channel is necessary for proper electron transfer between the ISP and cytochrome *f*, suggesting that this channel is used to transport protons released from plastoquinone when it is oxidized to the bulk. While there have been no reports yet of a possible channel for proton translocation from the plastoquinone binding site to this water chain in cytochrome *f*, studies of Zn and Cu inhibition have shown that the ISP and cytochrome *f* change their orientation based on the occupation of the

plastoquinone binding site (Roberts et al., 2002). Hence, in both the bc_1 complex and cytochrome b_6f, it appears that binding of the quinone donor causes a conformational change that allows for electron and proton transfer through the ISP and cytochrome *f* or c_1, and allows the proton to be released to the appropriate side of the membrane.

2.1.3 ATP synthase and ATPase

The last enzyme in the respiratory chain, ATP synthase, does not normally pump protons. Instead, it uses the proton gradient created by the other members of the respiratory chain to drive the phosphorylation of ADP to ATP. However, controlled regulation of proton flow through a proton channel is also essential for proper functioning of this enzyme. Additionally, there are several other enzymes closely related to the F-type ATP synthase that use the energy released from ATP hydrolysis to drive pumping of various ions. One of these, V-type ATPase, uses ATP hydrolysis to pump protons into vacuoles, acidifying them.

Both enzymes are structurally and functionally homologous, and both are capable of catalyzing the reverse reaction. They consist of two main domains: the F_1 or V_1, which is composed of several soluble subunits and contains the ATP synthesis/hydrolysis site and the F_0 or V_0, which is composed of multiple copies of one transmembrane subunit as well as a several other hydrophobic subunits (Figure 1.8). The multiple copies of the transmembrane subunit, subunit c, contain the proton channel and are arrayed in a ring structure.

While there are a plethora of high-resolution structures of the F_1 and V_1 domains, there are few high-resolution structures containing the F_0 or V_0 domains.

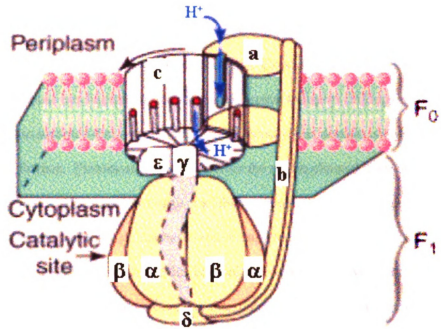

Figure 1.8: Composition of the F_1F_0 ATPase and the location of the proton channels. Rotation of the F_0 subunit due to proton translocation causes rotation of the F_1 subunit through the movement of the γ subunit. The rotation step is necessary to allow protons taken up on the periplasmic side of the membrane to exit on the cytoplasmic side. This rotation causes the γ subunit, which connects the F_0 to F_1 domains. This causes a conformational change of the α and β subunits of the F_1 domain, resulting in changes in the nucleotide-binding site that stimulates the conversion of ADP to ATP. This figure is a modification of a figure in (Fillingame et al., 2002).

Site-directed mutagenesis (Zhang and Fillingame, 1995) and cysteine cross-linking studies and NMR spectroscopic investigation of isolated c subunits of the F_0 domains (Girvin et al., 1998; Jones and Fillingame, 1998; Moody et al., 1987) have identified several critical residues for proton translocation. Cross-linking studies have been used to propose mechanisms of unidirectional proton transport (Fillingame et al., 2002). It is accepted that proton translocation through this domain occurs in a stepwise fashion. Protons are allowed to enter the proton channel from one side of the membrane and proceed to a critical acidic residue in the middle of a transmembrane helix, but do not have continuous access across the entire membrane. Once a proton has been loaded to this internal site, rotational movements (Noji et al., 1997) occur that result in the proton translocation to the other side of the membrane. The rotation of F_0 (or V_0) is transduced to the ATP active site via the central stalk of the enzyme, connected to F_1 (or V_1). This helical rotation results in a rotation of the hydrophobic ring made up of c subunits, driving the rotation of the stalk connecting F_1 and F_0 (Figure 1.8). The stalk rotation in turn drives the conformational changes of the F_1 that result in ATP synthesis or hydrolysis. This rotary mechanism has been observed by single molecule spectroscopy of fluorescently labeled protein immobilized on glass slides (Panke et al., 2000).

2.1.4 Bacteriorhodopsin

One of the most extensively studied proton pumping enzymes, is bacteriorhodopsin (BR), found in halobacteria. The detailed spectroscopic and structural information obtained for this enzyme has been instrumental in developing an understanding of how unidirectional pumping is achieved. In BR, light absorption drives the isomerization of the retinal cofactor, changing from all-*trans* to 13-*cis*.

This isomerization initiates a cascade of movements of amino acid residues and water molecules that results in pumping of a proton across the membrane. Specifically, the isomerization of the retinal causes a rearrangement of local amino acids, due to steric constraints, which results in the transfer of a proton from the protonated Schiff base of the retinal to an aspartic acid, D85 (Butt et al., 1989; Mogi et al., 1988). D85 is connected, via internal waters and an arginine, to a glutamic acid near the surface, E204 (Richter et al., 1996a; Richter et al., 1996b; Sampogna and Honig, 1996). This connectivity results in cooperative pK_a changes of these two acids, so that when D85 is protonated, E204 looses its proton to the extracellular bulk.

To reprotonate the Schiff base, a conformational change of the enzyme is required to create a hydrogen-bonded pathway from the cytoplasmic side (Luecke et al., 1999; Unger et al., 1997). With the formation of this pathway, the environment of another aspartic acid, D96, becomes more hydrophilic, resulting in a lowering of its pKa, causing it to donate its proton to the Schiff base. The reprotonation of the Schiff base allows the thermal isomerization of the retinal back to its resting all-*trans* state. This reisomerization is linked to the reprotonation of D96 and the disappearance of the water pathway from the cytoplasmic surface. From this state, the enzyme returns to its resting state as D85 deprotonates and reprotonates E204.

Thus, the entire cycle consists not of one proton moving across the entire membrane, but rather by a series of small proton movements that have the overall effect of one proton entering from the cytoplasmic side of the membrane and another released to the extracellular side. These small movements are directed by conformational changes that affect the pK_a values of various groups and give rise to

the unidirectional transport that is observed.

2.1.5 Half channels

All of the previously mentioned proteins translocate protons completely across a membrane. There are even more proteins, however, which transfer protons only halfway across the membrane, using the proton as a substrate at the protein interior or as redox-Bohr effectors, allowing electron transfer to or from a buried redox center. While such enzymes do not provide useful information on unidirectional proton translocation, they do provide information on proton transfer pathways in proteins. In fact, due to the plethora of high-resolution crystal structures and the ability to tightly control the catalytic cycle by light flashes, the bacterial photosynthetic reaction center (RC) has possibly the most well defined proton channel.

2.1.5.1 Photosynthetic complexes

Proton pumping is also essential to energy metabolism in photosynthetic organisms. In higher plants, light energy is captured by the chloroplasts to be used as the primary energy source for ATP synthesis, as well as to provide of reducing equivalents that are otherwise obtained from catabolism of ingested foodstuffs in animals. Photons of light are initially absorbed by the pigments of the light harvesting complexes. These complexes convert the light to photons with wavelengths of 700 nm and 680 nm, to be absorbed by either photosystem I (PSI) or photosystem II (PSII). Both PSI and PSII use the absorbed photons to drive charge separation, dissociating an electron from the initial pigment, and rapidly transferring it through a series of other pigments to a final acceptor on one side of the membrane,

with a replacement electron coming from the other side of the membrane. In PSI, the electron donated by the light absorption is transferred to ferredoxin and is rereduced by plastocyanin. In PSII, the final electron donor is water bound to the tetramanganese oxygen-evolving cluster, which, through four cycles of electron donation to a redox active tyrosine (Y_Z), oxidizes two water molecules to a dioxygen molecule. The protons released during the water splitting are released on the same side of membrane as the metal cluster and opposite to the side where the electron is released, again creating a proton gradient used to drive ATP synthesis.

Exact proton exit routes accompanying water splitting cannot be explored, due to the lack of a sufficiently high resolution crystal structure of PSII, so most of the investigation of proton transfer in these photosynthetic complexes has dealt with its coupling to electron transfer in the quinone reduction reaction. This focus has resulted in numerous advances in coupled proton/electron theory, or how electron movement can direct proton movement.

2.1.5.2 Bacterial reaction center

The bacterial reaction center (RC) is the equivalent to photosystem I that is found in photosynthetic bacteria. The absorption of light at a special chlorophyll pair results in a charge separation, donating an electron through a pheophytin and a tightly bound ubiquinone to another, weakly bound ubiquinone on the cytoplasmic side of the membrane. The electron donated from the special chlorophyll pair is eventually replaced by accepting an electron from cytochrome *c* on the extracellular side of the membrane. In this reaction, transfer of electrons from the first quinone acceptor (Q_A) to the final quinone acceptor (Q_B) is coupled to proton transfer,

resulting in the reduction of Q_B from a quinone to a quinol. A combination of structural, mutational and metal inhibition studies have allowed the pathway for proton uptake to Q_B to be clearly defined.

The first proposal for a proton path was based on the first high resolution crystal structure that showed a long chain of hydrogen bonded water molecules leading from the protein surface to the proximity of the quinone binding site (Ermler et al., 1994). When this pathway was tested by mutation of a residue along the water chain (Baciou and Michel, 1995), the results were somewhat ambiguous. The rate-limiting step in the reduction of Q_B is electron transfer. Hence, any change in the proton pathway will not be clearly detected unless it is significant enough to make proton transfer so slow as to become the rate-limiting step. Such a disruption of the proton channel was first achieved with inhibition by the divalent metal ions, Zn, Cd and Ni (Paddock et al., 1999). The inhibition sites of these metals were determined by crystallography (Axelrod et al., 2000) and defined the beginning of the proton channel at a cluster of two histidine and one aspartic acid residues (Figure 1.9).

Additional mutational studies demonstrated three additional residues to be important for proton transfer. A serine (S223 of the L subunit) near the quinone was found to be necessary for delivery of the first proton (Paddock et al., 1990), a glutamate (E212 of the L subunit) was determined to be necessary for delivery of the second proton (Paddock et al., 1989), and an aspartate (D213 of the L subunit) slightly further away from the active site was found to be important in the delivery of both protons (Paddock et al., 1994; Takahashi and Wraight, 1990). The intervening pathway between the surface histidine cluster and the critical D213 residue of subunit

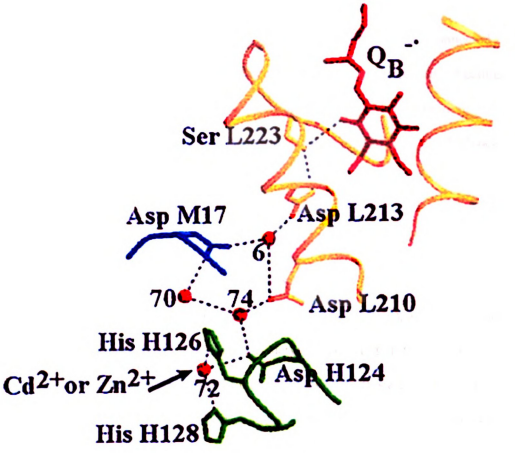

Figure 1.9: The proton uptake pathway in the bacterial reaction center. Crystallographic definition of the Zn and Cd binding site allowed for the identification of the proton uptake pathway as beginning at the surface-exposed histidine residues 126 and 128 of subunit H. Upon entry, protons are transferred via buried water molecules and a pair of asparate residues (210 of the L subunit and 17 of the M subunit) to the termination of the chain at the serine 223 or the aspartate 210 of the L subunit. This figure is from (Axelrod et al., 2000).

L was finally determined to pass two more acidic residues, D210 of subunit L and D17 of subunit M (Paddock et al., 2000; Paddock et al., 2001). Hence the entire proton channel can now be defined as a series of buried acidic residues connected via hydrogen bonds and intervening water molecules that connect the proton collecting histidine antenna to the Q_B binding site. This pathway is capable of providing protons at a rate of $\sim 10^4$ s^{-1} so that electron transfer between Q_A and Q_B, which occurs at rates of $\sim 10^3$ s^{-1}, is always rate limiting.

2.2 Non-energy transducing proton channels

While proton pumping enzymes provide the best comparative analysis for the understanding of CcO function, non-energy transducing proton channels can also further the understanding of CcO function. These enzymes allow protons to cross a membrane, moving down their gradient. While such proteins do not require a gating step to ensure unidirectionality like energy transducing proton channels do, the opening of these channels is often gated, only allowing proton transfer when desired by the cell. Thus, non-energy transducing proton channels can provide a framework for understanding the internal proton translocation steps in CcO as well as further the general understanding of how to gate proton movement.

2.2.1 The M2 viral channel

The role of proton channels is not limited to energy production; they are also important in pathogenesis. The M2 protein is small proton channel-forming protein, essential for infection and maturation of the influenza A virus. The virus is incorporated into the host cell by endocytosis. Once the virus is encapsulated in the

endosome and the endosome begins to acidify, the M2 opens. This serves two purposes for the virus: it induces the fusion of the virus and endosome membranes and stimulates the release of the viral genome. M2 also is used during viral maturation to raise the pH of the *trans* Golgi network, equilibrating it with the cytoplasm. This neutralization of the Golgi is essential to prevent the pH dependent aggregation of hemagglutinin, which prevents viral release from the cell when in the aggregated form.

The M2 channel is a homotetramer of small peptides, each containing a single transmembrane helix. There are two residues on each helix that have been shown to be essential for proper specificity and gating. A histidine near the middle of the transmembrane helix, H37, is important in the selectivity of protons and has also been suggested to provide the gating mechanism (Wang et al., 1995a). The histidine gate works by physically occluding the channel, preventing a continuous hydrogen bonded chain across the membrane. As the pH drops with the acidification of the endosome, however, the histidines become protonated, causing an electrostatic repulsion from one another. This allows for water to come between the histidines, creating a continuous hydrogen bonded chain across the membrane for the protons to travel down.

A nearby tryptophan, W41, has also been suggested to provide the gating mechanism, based on mutagenesis and NMR structural studies (Nishimura et al., 2002; Tang et al., 2002). In this mechanism the protonation of H37 is still essential. At low pH, the probability of the histidine to be doubly protonated increases. The positive charge on the doubly protonated histidine can then interact

with the nearby tryptophan, presumably via a pi-cation interaction (Tang et al., 2002). This interaction would reposition the tryptophan from its neutral position, in which it physically occludes the proton channel, to an open position where water can penetrate between the tryptophans and connect both sides of the membrane via a hydrogen bonded chain.

2.2.2 Voltage-gated proton channels

Proton channels also have an indirect role in some cells preventing infection by an invading pathogen. Voltage-gated proton channels are found in the plasma membrane of phagocytes and extrude protons from the cell when stimulated by an outward electrochemical gradient. This function is a compensatory mechanism for the NADPH oxidase. NADPH oxidase uses electron transfer to produce reactive oxygen species outside of the cell, killing potentially invasive organisms. This transfer of electrons across the membrane results in a net acidification of the cell interior and depolarization of the plasma membrane. The outward electrochemical gradient caused by this depolarization changes the voltage-gated proton channel into its open conformation and protons are allowed to flow outward, resulting in reequilibration of the cytoplasmic pH and repolarization of the membrane.

There are no structural data on these proteins and no high-resolution crystal structures, but they are assumed to act in a manner similar to the viral M2 channel. However, instead of channel opening being regulated by a proton gradient, an outward voltage gradient stimulates the conformational change necessary to open the channel. The specificity of this channel for protons and not any general cation was determined by zinc inhibition studies (Cherny and DeCoursey, 1999). These

experiments demonstrated that zinc binding to the enzyme prevents channel function in a pH dependent manner, with the Zn effectively competing with protons for a particular binding site.

2.2.3 Transhydrogenase

Proton translocation has also been proposed to have a regulatory function. In the H^+ translocating transhydrogenase found in the inner mitochondrial membrane, the catalytic function carried out is to transfer a hydrogen atom from NADH to $NADP^+$. However, since this process can occur in the absence of any catalytic agent at reasonable rates (up to 500 s^{-1}), there is no need to use proton translocation to drive the process. Instead, it has been proposed that the coupling to proton translocation is a regulatory mechanism, keeping the NADH and $NADP^+$ substrates from reacting until there is an abundance of NADH, signaled to the protein as a proton gradient across the mitochondrial membrane (Jackson, 2003).

The intake of the proton channel is assumed to be conformationally closed until the binding of substrate (Rodrigues and Jackson, 2002). Once substrate is bound, the channel is opened and a previously buried residue is available for protonation. This protonation causes a long-range conformational change (down a helix, through a loop and across a β-sheet) that results in bringing the substrates together in the "occluded state" of the enzyme. At this point, a pathway to the other side of the membrane becomes available for the proton, which exits as the hydride is transferred at the active site. As the proton leaves, the enzyme returns to its resting state, allowing the dissociation of the products.

3. Water channels in enzymes

The ubiquitous nature of water in living systems could lead one to propose that water channels are unnecessary in proteins. Indeed, both experimental evidence and computer simulations indicate that even the buried hydrophobic core of proteins is readily accessible to water penetration (Garcia and Hummer, 2000; Gottschalk et al., 2001). This gives credence to the idea that water channels are unnecessary. However, there are situations in nature where control of water movement is desired. In particular, water transport across the lipid bilayer of organelles and the cell itself needs to be regulated.

While there is an abundance of proteins that carry out proton transfer, there is a more limited number of proteins that act as water pores, termed aquaporins. What makes these proteins particularly interesting is that many of them exclude cations, including protons, from moving across them while sustaining water transfer rates near the diffusion limit. Having seen in the previous section how readily protons can be transferred along a hydrogen-bonded chain, in particular in ordered water chains, it is useful to understand how aquaporins can prevent such movement. The most abundant aquaporin, AQP-1, is found in erythrocyte membranes. However, the best understood member of this family is Glp-F, which preferentially transfers glycerol, but also water, while effectively excluding all cations.

Crystal structures of AQP-1 (Murata et al., 2000) and Glp-F (Fu et al., 2000) have proved indispensable in the understanding of the selectivity of these

proteins. Both proteins are found as homotetramers in vivo, and it had been speculated that conductance occurs through a pore at the interface of the monomers. However, it can be seen from the crystal structure that each monomer contains its own channel. The differences in the amino acids composing these channels provide the first indication of selectivity for water in AQP-1 and glycerol in Glp-F. In AQP-1, the channel is lined with hydrophilic residues that will ligate water, whereas the Glp-F channel is amphipathic, with one side being polar to bind the hydroxy sidechains of glycerol and the other side being hydrophobic to accommodate the carbon backbone of glycerol. Both AQP-1 and Glp-F share a common motif that provides resistance to ion flow: a hydrophobic narrowing in the middle of the channel with an asparagine on one side, giving rise to the H-bond isolation mechanism. There are two critical functions of this narrowing (de Groot and Grabmuller, 2001; Zhu et al., 2001). First, the side of the channel narrows to approximately three angstroms, just large enough to allow water flow, but to exclude any large ions. Second, the placement of the asparagine on one side of the narrowing provides a hydrogen bond for the oxygen of a water molecule, while orienting the hydrogens of the water towards the hydrophobic side of the channel. This orientation of the hydrogens into the hydrophobic area prevents them from H-bonding to another water molecule, and thus breaks the H-bond chain required for rapid proton translocation.

This theory is also consistent with the measured activation energy of approximately 3 kcal/mol, which is roughly the energy required to break one hydrogen bond. In the case of CcO, both protons and water are moved, but these two functions may have to be separated in order to maintain the directionality of the proton pump. If they are indeed separated, the same principles that allow selectively

rapid transport of water in the aquaporins should also apply to the water channel in CcO.

As in the case of proton channels, water channels are not necessarily static. The cytochrome P450 family of enzymes carries out the monooxidation of a wide variety of hydrophobic substrates. The substrates are usually toxic and the oxidation results in a more hydrophilic product that can more easily be excreted. In the reaction, one proton and one oxygen molecule are consumed, leaving the hydroxylated substrate compound and a water as the biproducts. While it is possible that the product water is used to form the hydrogen bonded channel necessary for proton translocation to the active site, it has been proposed, based on crystal structures of the enzyme, that protons access the active site by a different route and the water seen in the structure constitutes an exclusive water exit channel (Oprea et al., 1997). As this chain of waters only appears to reach the protein surface in one trapped intermediate state, it was proposed that this channel is only open during that state so that water can exit as required, but the rapid closing prevents the channel from being used to translocate protons to the active site.

V. Magnetic resonance theory

Magnetic resonance spectroscopy is a physical technique which uses the application of a strong magnetic field to induce a splitting of degenerate energy levels of unpaired nuclear or electron spins, which can then be probed with radio- or microwave frequency radiation. The application of magnetic resonance spectroscopies to proteins can yield valuable information regarding the specific local

environment of the nuclear or electron spin center(s) in the protein. Examples of centers that have unpaired electron spins are organic radicals and transition metals in appropriate redox states, such as copper and manganese and high spin heme, all found in CcO. Due to the relatively low abundance of these unpaired spins in biological systems, EPR can effectively study the local environment and report back local structure. The application of this technique to CcO is a major emphasis of this thesis, and therefore the underlying theory is discussed to illustrate how it can yield important information.

There are two general categories of magnetic resonance spectroscopy; EPR, which traditionally uses magnetic fields of in the range of 0.3 Tesla and probes unpaired electron spins with microwaves, and the more commonly known nuclear magnetic resonance (NMR, or its medical equivalent MRI), which uses much larger fields and radiowave frequency radiation to probe nuclear spin states. Both of these techniques are based on the same fundamental quantum mechanical principles.

The solving of the time-dependent equation of state with the inclusion of relativistic terms (the Dirac equation) led to the defining of a fourth quantum number. Unlike the other quantum numbers (the principle quantum number n, the angular quantum number l, and magnetic angular quantum number m_l), spin (m_s) has no classical counterpart and hence is hard to describe in a physical sense. It can be modeled as an intrinsic angular momentum with each electron taking on one of two equal and opposite values, denoted by $m_s = ½$ and $m_s = -½$. The Pauli Exclusion Principle then allows for two electrons to occupy an energy level with the same n, l and m_l. As spin does not contribute to the overall energy of an unperturbed system,

this results in a degeneracy of energy levels. Because this "spin" of a charged particle yields an intrinsic magnetic moment, this degeneracy can be broken by application of a magnetic field. When a paramagnet (with one or more unpaired spins) is placed in a strong field, those spins whose magnetic moment aligns with the laboratory field will be of lower energy and those aligned opposed to the field will be of higher energy (Figure 1.8). However, diamagnets (with each energy level filled with one spin up and one spin down) will not be perturbed by the field and will maintain their original value. As with other spectroscopies (which probe energy level splittings due to the other quantum numbers) these energy level differences can be probed by electromagnetic radiation of an appropriate frequency with an energy equivalent to the splitting and structural characteristics of the center and its local surroundings can be determined by the absorption pattern.

The study of unpaired electron spins by EPR is useful in identifying and studying the local environment of the paramagnet. The classical form of EPR uses continuous-wave microwaves of approximately 9 GHz and a magnetic field of up to 1 T. The local environment can be further explored by perturbation of the nuclear spins (with an additional radiowave irradiation) while probing the electron spin. Due to the interaction of two magnets, changes in the alignment of a nearby magnet (a nuclear spin, such as a proton or nitrogen, in close proximity) will alter the energy level splitting of the electron spin magnet, resulting in the absorbance of a slightly different frequency (Figure 1.8). An even more advanced method is to use short, hard pulses (high power and broad frequency) of microwave radiation. Due to the lifetime broadening of the pulse frequency, there will be appropriate energy to excite all transitions, both allowed and semi-forbidden, and the resulting free-induction decay

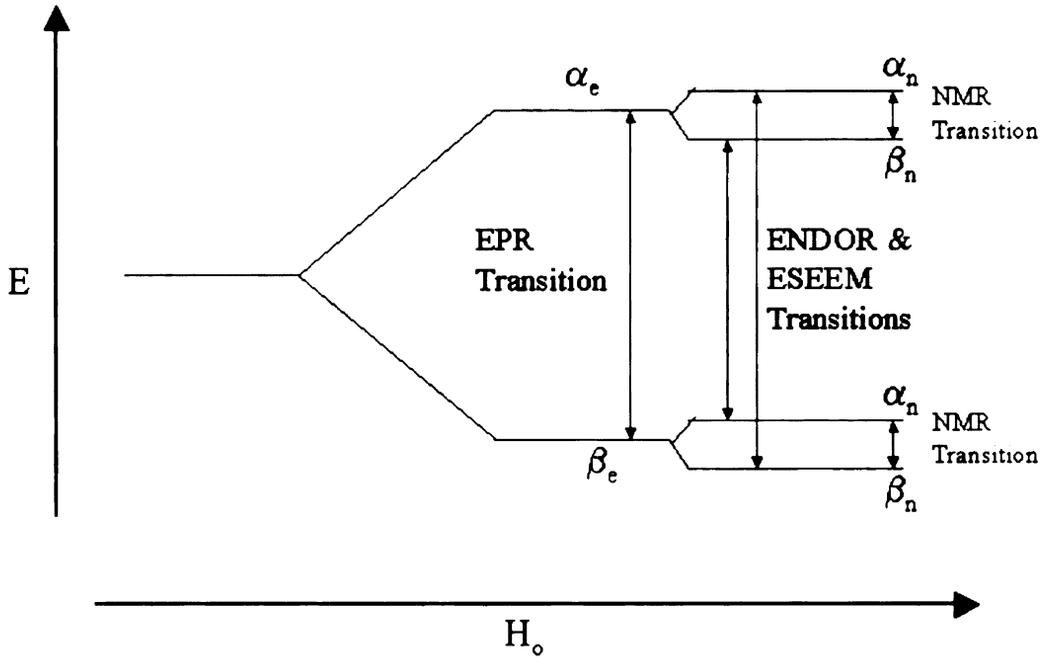

Figure 1.10: Energy splitting levels probed by EPR spectroscopy. As the applied magnetic field (H_o) is increased, degenerate energy levels are split into α and β spin manifolds. These splittings can be probed with electromagnetic radiation of the appropriate wavelength. In addition to removing the degeneracy of the electron spin levels, the magnetic field also removes the degeneracy of nuclear spin states, which can be probed individually (by NMR), or by measuring their effect on the electron energy of the electron spin manifolds (by ENDOR or ESEEM).

provides information not only of nuclear spins in the immediate vicinity of the electron spin, but also of nuclear spins several angstroms away.

Electron spin echo envelope modulation (ESEEM) is an advanced EPR technique that takes advantage of the ability to stimulate both allowed and semi-forbidden transitions by means of short, hard microwave pulses. The simplest form of this technique uses two pulses. The first pulse rotates the spin packets (which are aligned with the applied laboratory field) 90 degrees, from the z-axis into the xy plane. In the rotating frame convention, the spin packets dephase due to changes in oscillation frequency induced by nearby weak (nuclear) spins. The second pulse, which is twice as long as the original turning pulse, rotates the spin packets 180 degrees, leaving them in the xy plane but inverted. The spin packets refocus in a length of time equivalent to the time between the two pulses, resulting in an echo. The area of this echo can be integrated as a function of time between the pulses and will modulate over time. This time-domain spectrum can then be subjected to a Fourier transform which gives the frequencies of this modulation. These frequencies result from the Larmour frequencies of the nuclei near the paramagnetic center being probed (as well as sums and differences of these frequencies). Thus, the nuclear environment of the paramagnetic species can be explored. Additionally, since the depth of the modulations is a product function of the interacting nuclei, it can be used to determine the number of a given nuclei that are interacting with the center.

A more robust form of ESEEM uses three pulses, each with a 90 degree turning angle. The first pulse turns the packet into the xy plane, where they begin to defocus. The second pulse returns the packets to the z-axis, this time in the negative

direction, storing the dephasing information as projections along the lab field where they will be preserved for a time, T_{1e}. After a second free precession period, the third pulse is applied, turning the spin packets back in to the xy plane, inverted, where they refocus. Again, the intensity of the echo can be integrated as a function of the separation time between pulses and transformed into a frequency spectrum that contains information about the nuclei interacting with the spin center.

More information regarding a paramagnetic center can also be ascertained by using higher magnetic fields and higher microwave frequencies. At these higher fields and frequencies, the separation of energy levels is increased. This allows for deconvolution of transitions that overlap at lower fields. Additionally, these conditions can also prevent semi-forbidden transitions from occurring, simplifying the spectrum. This allows for a more rigorous determination of the energy level splittings, thereby giving a more defined description of the structure of a given paramagnet.

VI. Conclusions

With the increased understanding of the specific mechanisms of proton translocation in different proteins, there are a few common principles that appear to apply to proton translocation. Rapid proton transport can occur at rates above the diffusion limit in hydrogen-bonded chains by a hop and turn mechanism. This is allowed by breaking the translocation step into small, discrete transfers across a hydrogen bond in a concerted fashion by multiple atoms. Thus, the net result is the loss of a proton on one side of the chain and the appearance of a proton on the other

side of the chain, though no one proton crossed the entire distance. The probability of translocation to occur and the rate at which it will occur is affected by rapid protein fluctuations and the charge state of the redox active components of the enzyme. The electronic distribution can directly affect proton translocation by determining the orientation of the dipoles along the proton wire or by inducing long range, large scale conformational changes in the protein that can open or close the channel. The large scale conformational changes induced by the electronic distribution seem to be of particular importance in enzymes that actively pump protons unidirectionally against their electrochemical gradient (Mulkidjanian, 1999), preventing a continuous pathway for proton translocation across the entire protein at any given time.

While buried water molecules are often used as components of the proton wire, they need not necessarily be the major components. Protons can also be transported via chains composed mainly of amino acid side-chains instead of crystallographically visible water, as is the case in the bacterial reaction center. In addition, they may be excluded altogether from translocation through a water chain, as in aquaporin.

The four redox active centers in CcO offer several locations for redox-induced conformational regulation of proton transport. While there is only one long-range conformational change that has been documented in the CcO crystal structures (Yoshikawa et al., 1998a), based on the totally reduced versus the totally oxidized redox state, it is quite likely that conformation changes occur during the different intermediates of the reaction cycle (Das et al., 2001; Wang et al., 1995b). Changes have been seen in the isolated soluble domain of subunit II based on the reduction

state of Cu_A (Gupta et al., 2001). Regulation of CcO is complex in the mammalian enzyme and is likely due to conformational changes induced by binding of other molecules, such as ATP, to the extra subunits that are found in mammalian CcO (Follman et al., 1998; Ludwig et al., 2001; Yoshikawa et al., 1998b).

Proton translocation in CcO is coupled to electron transfer. Electron transfer from heme *a* to the active site shows clear dependence on protons and appears to be limited by proton transfer (Branden et al., 2001; Karpefors et al., 1998; Konstantinov et al., 1997; Moody and Rich, 1990; Pecoraro et al., 2001). Additionally, evidence shows that electron transfer from Cu_A to heme *a* is also coupled to proton transfer (Babcock and Callahan, 1983; Capitanio et al., 1996; Capitanio et al., 2000; Papa et al., 1998). The dependence on a proton transfer in this step is not as clear as for electron transfer to the active site, which has led some to suggest there is no direct coupling. However, if the proton transfer rate is faster than electron transfer, as is the case in the RC, a full dependence of proton transfer would not be seen until proton transfer becomes rate limiting.

Finally, the proton exit channel may not be evident in CcO crystal structures as it forms only transiently when needed. The aqueous nature of the top of CcO provides a good candidate for a proton exit pathway but it may not provide the correct dipole orientation to be suitable for proton transfer. In fact, one or more of the water channels in this area seen by crystallography (Figure 1.10) may instead be analogous to the pore in aquaporin, providing a pathway for the exit of product water but excluding protons.

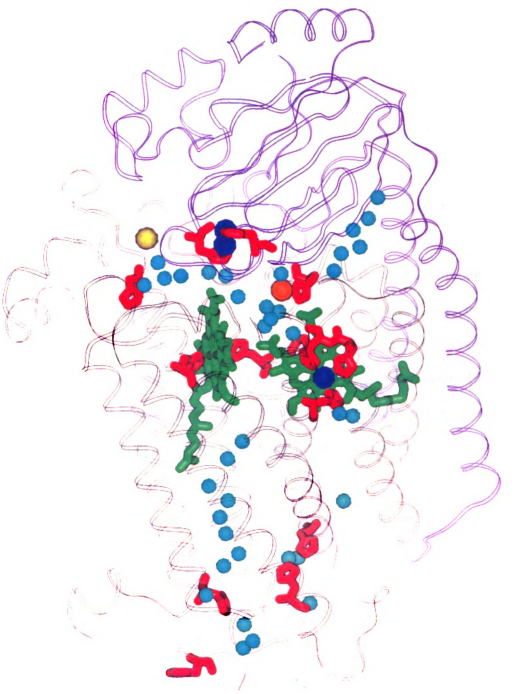

Figure 1.10: Water channels in CcO identified by crystallography. There are four redox active metal centers: the dinuclear copper center Cu_A (blue spheres), hemes *a* and a_3 (both in green) and the mononuclear copper Cu_B (blue sphere). Additionally there are two other non-redox active metal centers with unknown function: calcium (grey sphere) and magnesium (orange sphere). Important crystallographically defined water molecules are shown (cyan spheres), including the waters that define the D channel, the waters found in the K channel and two potential water exit channels at the top of the molecule that pass the Mg site.

In the search for the proton and product water exit channel(s) in CcO, hydrogen bonded chains of amino acid side-chains, peptide backbone and buried water molecule are necessary, but the channel may not be evident in the crystal structures as it may not form until an intermediate state with the correct distribution of electrons induces a conformational change.

Since the small, transient changes that are likely to ensure proton pumping in CcO do not lend themselves to investigation by crystallography, spectroscopic methods with time resolution are necessary to determine the proton and water exit channels. EPR spectroscopy allows for examination of local structure around an unpaired electron spin, and can be used to detect changes in environment. When combined with isotope exchange, on a millisecond timescale, advanced EPR investigations of the Mg/Mn site in CcO allow for interrogation of water and proton movement on the exterior side of the protein, and may be useful in determining proton or water exit pathways in the region.

Chapter 2:

Accessibility of the Mn Site to the Bulk

Most portions of this chapter are based on data published in (Florens et al., 2001) and (Schmidt et al., 2003a).

Introduction

High resolution crystal structures of bacterial (Iwata et al., 1995; Svensson-Ek et al., 2002) and bovine (Tsukihara et al., 1995) cytochrome *c* oxidases (CcO) specify a common spatial organization of the metal centers (Figure 1.11) and define some possible routes for proton translocation within the molecule via hydrogen-bonded paths. Several pathways for protons and water are expected in CcO: on the inside of the membrane, entry pathways for protons to be pumped and for substrate protons required for oxygen reduction; on the outside of the membrane, an exit route for pumped protons and water. Candidates for the entry pathways have been identified by mutational (Fetter et al., 1995; Thomas et al., 1993; Zaslavsky and Gennis, 2000) and structural (Tsukihara et al., 1996) analysis (Figure 1.4), but the exit path remains unclear. A possible water channel which could serve this function was noted in the original bovine oxidase X-ray structure (Figure 2.1) immediately above the active site, at the interface of subunits I and II. It has been proposed that this aqueous region could provide a proton and/or water exit pathway, and that control of its directionality could regulate the rate and the efficiency of coupling of CcO (Ferguson-Miller and Babcock, 1996). However, increasingly high resolution structures indicate that water in this region is highly ordered, as indicated by low R-values and visibility at high and low temperature, and not likely to exchange readily or conduct protons (S. Yoshikawa, personal communication). Further, it is clear that unrestricted proton exchange between the outside and the active site would short-circuit the proton pumping mechanism of the enzyme. Thus the boundary defining the 'outside' (or region of free access to solvent) in CcO needs to be defined (Mills et al., 2000).

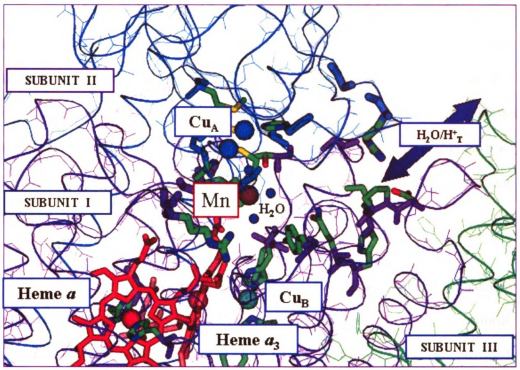

Figure 2.1: Metal centers and proposed water channel at the subunit I and II interface in beef heart CcO. Blue ribbons on the top are from subunit II and contain the dinuclear Cu_A site (larger blue spheres). To the far right, in green ribbons, is subunit III, which contains no metal centers and does not directly contribute to the proposed channel. The purple ribbons represent subunit I, the largest subunit, which contains the two hemes (in red) and Cu_B (light green sphere). The proposed water channel is shown as the gap between subunits I and II, beginning near the heme a_3 propionates and the Mg/Mn site (brown sphere), with residues lining the channel in stick form. The three small blue spheres near the Mn indicate crystallographically defined waters.

A non-redox active Mg ion lies at the bottom of the proposed water channel, 12 Å from the surface of the protein (Figure 2.1). It bridges subunits I and II, shares a ligand with the binuclear Cu_A center, and is bonded through a histidine ligand and a water to the D-ring propionate of heme a_3. The role of the Mg site is not known, however its proximity to the apparent water channel suggests it may have a function in determining the structure and the regulation of a proton and/or water exit pathway.

EPR studies on *Rhodobacter sphaeroides* CcO showed that manganese can be substituted for magnesium during growth of the bacterium with no functional effect (Hosler et al., 1995). Three out of six ligands for the Mg/Mn ion are provided by crystallographically well-defined water molecules (Figure 2.2). The paramagnetic nature of Mn^{2+} allows the use of the advanced EPR methods of electron nuclear double resonance spectroscopy (ENDOR) and ESEEM to detect its ligation structure, and changes in structure, through the measurement of ligand hyperfine coupling.

In the present study, we have combined spectral (ESEEM) and kinetic (rapid freeze-quench) methods to measure the time-scale and extent of proton exchange (by observing ^2H_2O) and water exchange (by observing $H_2{}^{17}O$) at the Mg/Mn site of CcO. The studies provide evidence of rapid water and/or proton exchange at least to the depth of the Mg/Mn site.

Experimental procedures

Protein production and purification

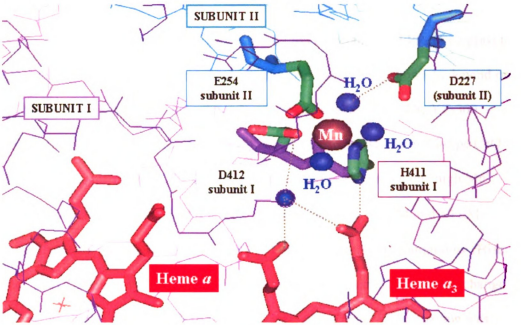

Figure 2.2: Local environment of the Mn site. Mg or Mn can selectively occupy a non-redox active metal site based on levels of each metal in the growth medium. The metal is situated at the subunit I/II interface and is octahedrally coordinated with one histidine (H411) and one aspartate (D412) from subunit I, and one glutamate (E254) from subunit II. The remaining three ligands are crystallographically defined water molecules.

The amount of Mn^{2+} (paramagnetic ion detectable by EPR, in contrast to Mg^{2+} which is EPR silent) incorporated into the protein has been shown to depend on the [Mg] to [Mn] ratio in the growth medium (Hosler et al., 1995). The YZ-300 strain of *R. sphaeroides* (Zhen et al., 1998), which overexpresses the wild-type CcO with a histidine tag added to the C-terminus of subunit I, was grown on "high Mn" medium (with $MnSO_4$ and $MgSO_4$ at final concentrations of 700 μM and 50 μM, respectively). The protein was purified by Ni^{2+}-NTA affinity chromatography (Hiser et al., 2001; Mitchell and Gennis, 1995) and further purified by DEAE ion-exchange chromatography (Hiser et al., 2001) to remove excess subunit I. The enzyme was concentrated and washed into buffer containing 50 mM KH_2PO_4-KOH, pH 7.4, 0.1 mM EDTA and 0.1% (w/v) lauryl maltoside, using a centrifugal filter (Millipore). The visible spectral characteristics of the Mn- and Mg-substituted wild-type enzymes were identical and oxygen consumption activities were unaltered.

Rapid-mix freeze-quench ^2H_2O and $H_2{}^{17}O$ exchange

The samples were prepared using an Update Instruments System 1000 Chemical/Freeze Quench apparatus (model 715 Ram Controller and model 1019 Syringe Ram). Two syringes of equal volume containing 60 μM CcO in buffer A (50 mM KH_2PO_4-KOH, pH 7.6, 0.1 mM EDTA, 0.1% (w/v) lauryl maltoside) and varying concentrations of deuterium oxide (99.9 atom % D, Aldrich), respectively, were maintained at either room temperature or in a water bath at 4°C. The syringe contents were combined in a Wiskind Grid Mixer (model 1155) at a ram velocity of 1.25 $cm \cdot s^{-1}$. Different fast incubation times were achieved by varying the length of the tubing (aging hose) connecting the mixer to the spray nozzle. For incubation

times longer than 500 milliseconds, a two-push method was used to minimize the sample volume used while maintaining experimental variables. An aging hose of constant length (with the hose volume corresponding to the volume to be collected) was filled by an initial push after which the sample incubation times were determined by a delay setting separating the two pushes. The samples were then ejected by a second push of equal volume.

The reaction mix was ultimately sprayed from a 0.008 inch diameter spray nozzle into a 4.5-inch long fused quartz EPR tube equipped with a funnel filled with cold isopentane (HPLC grade, Sigma), which quenches the reaction in approximately 5 milliseconds (A.-L. Tsai, personal communication). The EPR tube and funnel were filled with isopentane and equilibrated for at least 5 min in an 8L isopentane bath maintained at -140°C ± 2 with a LakeShore model 340 temperature controller equipped with a copper-constant thermocouple by an external liquid nitrogen bath. The frozen crystals of CcO were packed into the bottom of the EPR tube by using a pre-cooled packing rod until a densely packed sample with a height of at least one cm was obtained. The final concentration of CcO in the EPR tube was measured by EPR spin quantitation, using aqueous $CuSO_4$ as a reference, to be approximately 10 μM. The rapid freeze-quenched (RFQ) samples were stored in liquid nitrogen until analyzed by ESEEM. More recent studies were carried out using a starting enzyme concentration of approximately 100 μM, giving a final concentration in the EPR tube of approximately 30 μM, as indicated in figure legends, to increase the signal to noise ratio. Funnels and EPR tubes were also modified to use N_2 pressure to aid in the consistency of packing density, as described by Tsai *et al* (Tsai et al., 1998).

Paramagnetic resonance spectroscopy

Electron spin echo (ESE)-detected EPR and two- and three-pulse ESEEM spectra were recorded at 1.8 K by using a liquid helium immersion dewar under reduced (~10 mbar) pressure, on a pulsed spectrometer constructed at Michigan State University (McCracken et al., 1992). Processing of experimental ESEEM data and Fourier transformations (FTs) were performed using Matlab software from Matworks Inc. (Natick, MA). The final ten points of each time-domain data set were acquired with the integration window positioned 200 ns off of the echo to define the background. Spectra were normalized from zero (background) to one (maximum amplitude) before processing. Since the ESEEM of a discrete paramagnetic center is the product of echo modulations arising from each nucleus coupled to it (Dikanov et al., 1981; Rowan et al., 1965), the ^2H modulations were isolated by dividing data obtained for CcO diluted in deuterated buffer by data obtained in a parallel fashion using CcO in a non-deuterated buffer (Mims et al., 1984). Frequency spectra of ESEEM data were obtained using the dead-time reconstruction technique as described by Mims (Mims, 1984). Imperfections in dead-time reconstruction led to baseline roll, or distortions, seen in the FTs. To gauge how the reconstruction procedure influenced the ^2H modulation peak amplitudes, power spectra of each time-domain data set were taken without dead-time reconstruction and used to calculate error bars.

Continuous-wave X-band EPR spectra were measured on a Bruker ESP300E equipped with a TE_{112} cavity resonator. Temperature was maintained at 10 K using an Oxford ESR900 helium cryostat. All spectra were measured using 2.0 milliwatts of microwave power and 8 G of modulation amplitude.

$H_2{}^{17}O$ with a ^{17}O enrichment of 45% was obtained from the Stable Isotope Resource at Los Alamos National Labs. Lauryl maltoside was Anagrade from Anatrace, Inc. All other chemicals were from Sigma.

Results

Observation of exchange exclusively at the Mn site

The ESE-detected EPR spectrum of wild-type CcO purified from *R. sphaeroides* grown in high Mn medium (Figure 2.3B) is a composite of contributions from the Cu_A center (peak near 3120 G) and the Mn ion (broad absorption spanning from 2800 to 3800 G). Figure 2.3A shows an ESE-detected EPR absorption spectrum of a sample of oxidase from *R. sphaeroides* grown in high Mg medium, which contains only EPR-silent Mg, that was taken under identical conditions. This control shows that at the microwave frequency used in our studies, the absorption from Cu_A was characterized by a sharp decrease at magnetic field strengths above 3150 G. Additionally, the longer T_1 value of Cu, in relation to Mn, results in a diminished Cu absorption at temperatures below 2 K, due to saturation, without effect to the Mn absorption. Thus, the Mn ESEEM signal was studied at 3400 G and a temperature of 1.8 K, where there is still significant Mn absorption but no interference from the Cu_A signal.

Rate of deuterium exchange

For CcO in non-deuterated buffer, the Fourier transform (FT) of three-pulse ESEEM experiments performed at 3400 G (Figure 2.4, 0 ms spectrum) shows a

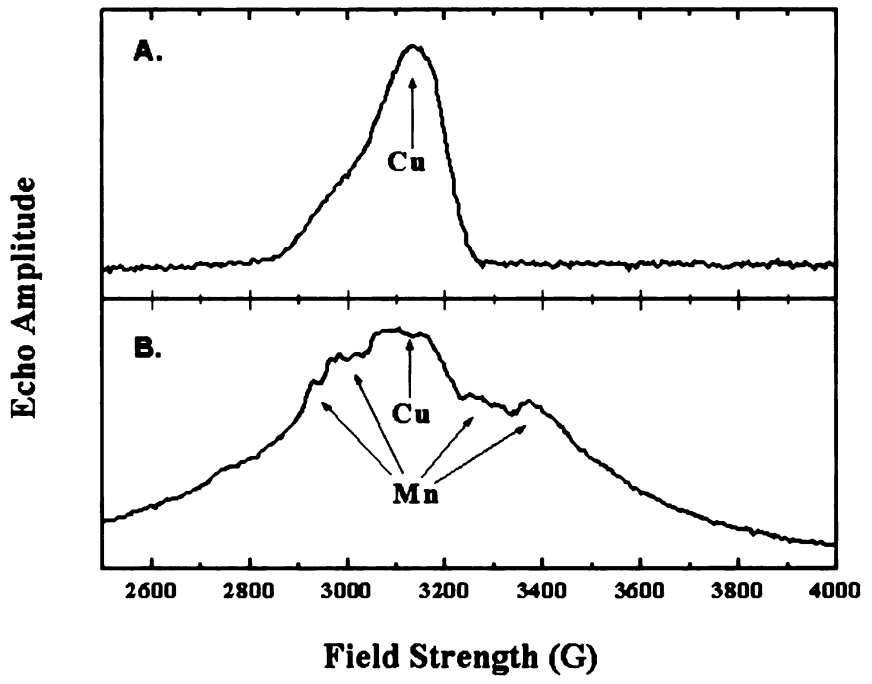

Figure 2.3: ESE-detected EPR spectra of CcO with Mg (A) or Mn (B) incorporated into the metal site. Samples grown in high Mg (A) show a loss of the signal from Cu after 3150 G, whereas CcO grown in high Mn (B) has significant absorption from Mn out to 3400 G.

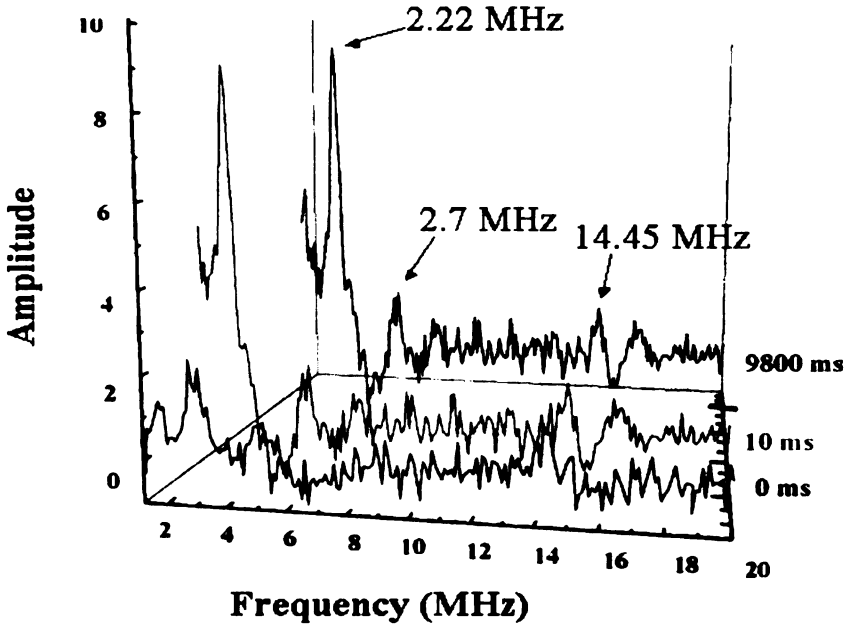

Figure 2.4: Fourier transforms of three-pulse ESEEM of CcO showing the saturation from deuterium exchange into the Mn binding site within 10 milliseconds. CcO (~60 μM) was rapidly mixed with ^2H_2O (1:1 volume ratio) at room temperature by using a freeze quench apparatus. The samples were completely frozen within 10 milliseconds. Time points were taken after 10 milliseconds (red trace) or 9.8 seconds (blue trace) of incubation. For the zero-time reference point (black trace), a CcO sample was frozen in an EPR tube by immersion in liquid nitrogen. The 14.45 MHz peak arises from protons coupled to the Mn and the 2.7 MHz peak is due to coupled nitrogen. Both the 10 millisecond and the 9.8 second samples show a 2.22 MHz peak indicative of deuterons. The amplitudes of these peaks are equal, indicating the presence of an equal amount of deuterons at the Mn site for both time points.

weak signal centered at the proton Larmor frequency typical of ambient water molecules (14.5 MHz). Peaks are also resolved at 1.9, 2.7, and 5 MHz. These low frequency modulations were previously assigned to nitrogen modulation from the histidine ligand (H411) of the Mn (Espe et al., 1995). No deuterium ESEEM, as characterized by modulation at 2.2 MHz, was detected for the control sample. However, in parallel experiments performed on CcO samples rapidly mixed and incubated with ^2H_2O for 10 milliseconds using the RFQ apparatus, an intense signal at the deuteron Larmor frequency (2.2 MHz), showing that within 10 milliseconds protons magnetically coupled to the metal are exchanged for deuterons (Figure 2.4). When the sample was mixed in a 1:1 ratio with 100% ^2H_2O to give a final concentration of 50% ^2H_2O, the 2.2 MHz signal reaches its maximum intensity during the dead time of the RFQ instrument (10 milliseconds), and remains constant over a 10-second time course (Figure 2.4). Assuming that the intensity of the 2.2 MHz peak can be fitted as a single exponential function of mixing time, a lower-limit exchange rate of 3000 s^{-1} can be calculated.

Number of protons exchanged

To quantify the dependence of the extent of exchange on ^2H_2O concentration, a range of concentrations of ^2H_2O was mixed with the enzyme, resulting in final ^2H_2O enrichments of 15% to 75% (v/v). The intensity of the 2.2 MHz deuterium signal increased as ^2H_2O concentration increased and a non-linear relationship was observed between the echo amplitude and the ^2H_2O concentration (Figure 2.5). To extrapolate to the peak height for a sample with complete deuterium substitution (a D_2O concentration of 100%), a polynomial fit of the data was carried out. The best fit of the data was obtained with a cubic polynomial, consistent with the

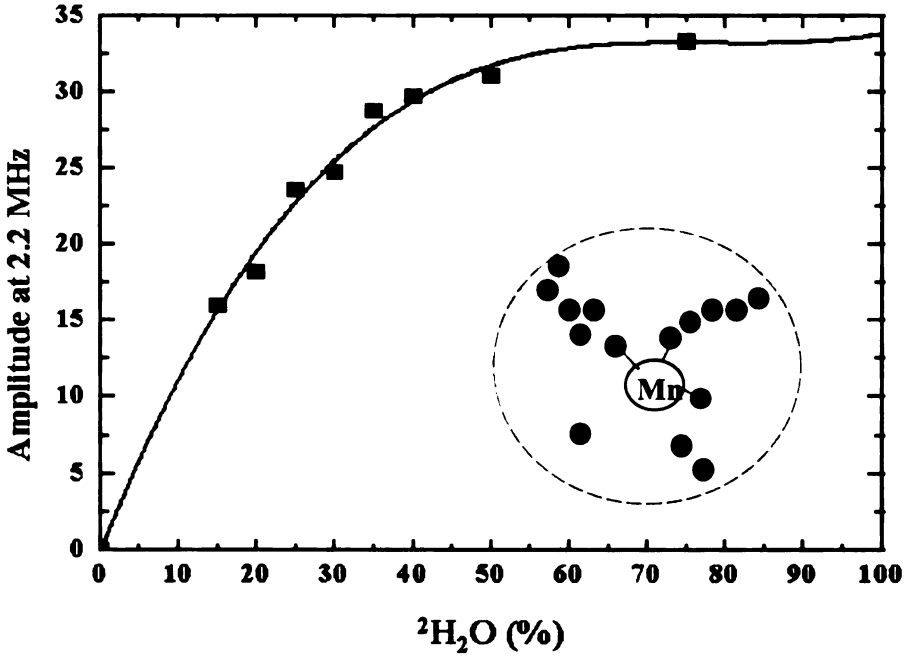

Figure 2.5: Graph of ^2H_2O dependence of 2.2 MHz peak in *R. sphaeroides* CcO. Samples were prepared by using varying levels of ^2H_2O in the mixing buffer. The 75% point was obtained using a third syringe, containing 100% deuterated buffer, which was combined with the mixture of the first two syringes. The data were fit to a cubic polynomial to extrapolate the peak height at 100% ^2H_2O. The inset represents the number of crystallographically defined waters (blue spheres) within 10 Å (dashed line) of the Mn.

theoretical calculation of Mims and Davis (Mims and Davis, 1976) for the echo modulation of a paramagnetic center with three equivalent nuclei at a certain distance.

The X-ray crystal structures of CcO indicate that three waters contribute to the ligation of the Mn/Mg (Figure 2.2). While the deuterium exchange data demonstrates proton/deuteron exchange can occur on a catalytically relevant time scale, it does not by itself indicate the number of waters/protons exchanged. To estimate the number of exchanged waters/protons manganese aquo, $Mn(H_2O)_6$, was used as a standard to compare with the maximum 2.2 MHz deuterium peak determined for CcO. A deuterated standard sample was prepared by dissolving 1 mM $MnSO_4$ in 100% ^2H_2O and adding glycerol to 40% (v/v) to ensure proper glassing of the sample. A calculation of final ^2H_2O concentration, based on molar ratios of ^2H from ^2H_2O and ^1H from the hydroxyl protons of glycerol and assuming an exchange constant between water and glycerol hydroxyl protons of approximately one, gives a final concentration of 80% ^2H_2O in the standard curve. Thus the spectrum (Figure 2.6, (5)) shows the contribution of five ^2H_2O molecules (eighty percent of the six molecules that ligate the metal) ligated directly to the Mn along with outer-sphere deuterium molecules. Since the total echo modulation is the product of each contributing nucleus, the fifth root of the spectrum gives the echo modulation of Mn by one ^2H_2O ligand plus the region containing approximately one-sixth of the outer sphere deuterons (Figure 2.6, (1)). Raising this spectrum to increasing powers (up to five) results in the spectrum of the echo modulation resulting from that number of bound ^2H_2O ligands and the associated outer-sphere contribution. This can be used to create a standard curve of FT peak height at 2.2 MHz versus the number of bound ^2H_2O ligands (Figure 2.7).

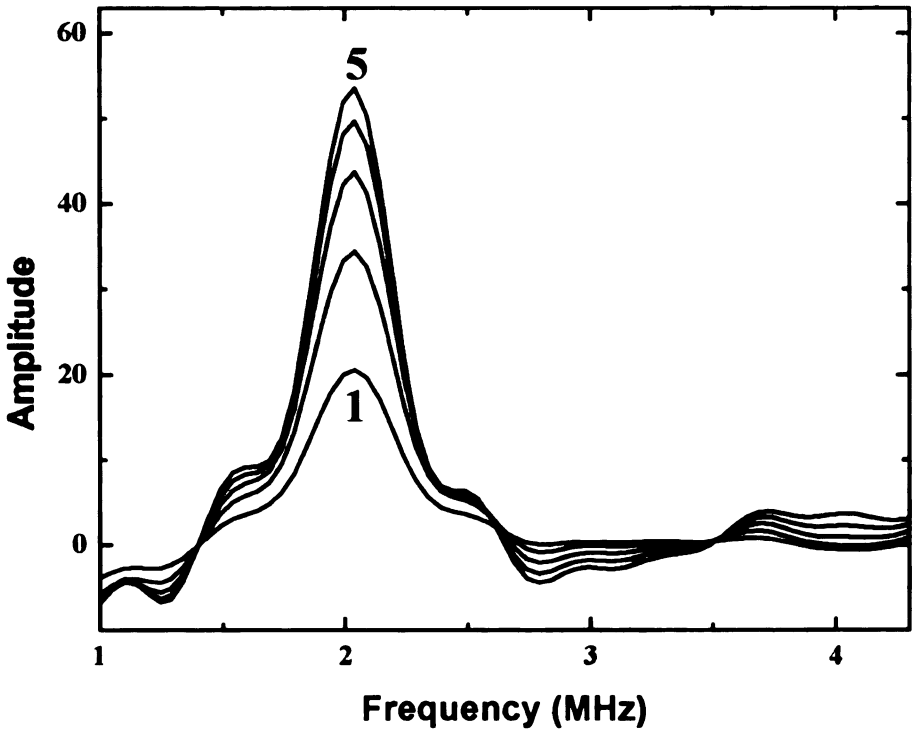

Figure 2.6: Fourier transforms of two-pulse ESEEM spectra of a standard, $Mn(H_2O)_6$, with increasing numbers of ^2H_2O bound to the Mn. The spectrum of one bound ^2H_2O (**1**) was calculated by taking the fifth root of a sample (**5**) containing 1 mM $MnSO_4$ dissolved in 80% ^2H_2O. Spectra for additional numbers of bound ^2H_2O were calculated by raising the one-bound ^2H_2O spectrum to increasing powers.

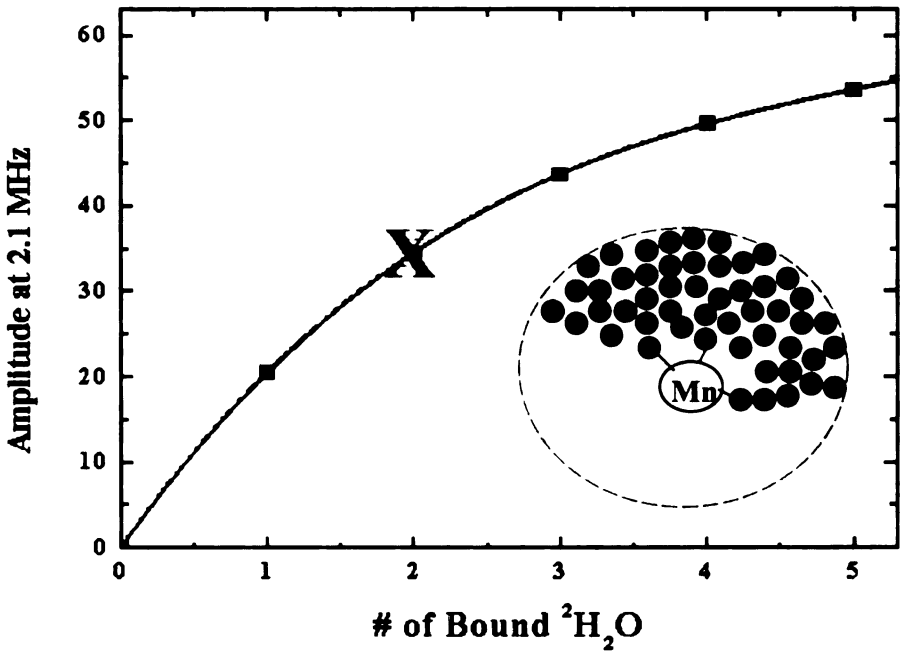

igure 2.7: Graph of ^2H_2O dependence of the 2.2 MHz peak for $Mn(H_2O)_6$. In addition to the number of bound ^2H_2O shown on the x-axis, there are also contributions from outer sphere ^2H_2O. The data were fitted to a cubic polynomial. The X on the fit indicates the extrapolated 2.2 MHz peak height of CcO in 100% ^2H_2O. While the fit suggests only two of the three Mn water ligands are exchanging, the standard has a larger number of outer sphere ^2H_2O contributing to the modulation (represented in the inset). Hence the standard is an underestimation, suggesting all three bound waters are rapidly exchanged.

Comparing the height of the extrapolated 100% ^2H_2O peak from CcO samples (Figure 2.5) to this standard curve (Figure 2.7), we get amplitude equivalent to approximately two bound ^2H_2O. However, this number is an underestimate of the waters at the Mn in the protein, because the model, $Mn(^2H_2O)_6$, has a greater number of outer-sphere ^2H_2O contributing to its modulation. The number of waters in a 10 Å radius sphere around a metal was calculated based on molarity and density of water. The number of waters in a smaller sphere of 2.3 Å radius was calculated and subtracted from the larger sphere to account for van der Waals volume of the metal. The six waters that are the direct ligands to the manganese aquo were also subtracted to yield 130 water molecules contained within a 10 Å radius sphere of the metal in solution. Thus, three bound ^2H_2O molecules in $Mn(H_2O)_6$ have an additional contribution from outer sphere waters equivalent to 65 ^2H_2O molecules (half of the total 130 waters within a 10 Å radius). Comparatively, high-resolution crystallographic analysis of bovine CcO reveals that, in addition to the three bound waters, there are only 21 water molecules within 10 Å of the Mn (S. Yoshikawa, personal communication). The much smaller contribution of outer sphere deuterons to the amplitude of the signal from the CcO Mn^{2+} site compared to the Mn standard (qualitative comparison can be seen in insets of Figures 2.5 and 2.7), leads to an underestimation of the number of waters exchanged.

Additional evidence for the underestimation provided by the standard curve used can be seen the shape of each fitting curve. Previous ESEEM studies of metal-aquo complexes have shown that the outer sphere proton/deuteron contribution to the spectrum can be approximated as a linear addition (Mims and Davis, 1976; Mims et al., 1977). In contrast, deuterons in the first coordination sphere have a large

contribution, and each additional nucleus contributes to the peak amplitude in a multiplicative fashion. Thus, the standard curve of $Mn(H_2O)$ can be divided into an exponential curve with a linear addition. In the plot of ^2H modulation amplitude versus increasing ^2H_2O concentration for the protein (Figure 2.5), the curve clearly shows asymptotic behavior, with 50% showing nearly maximal amplitude. However, the corresponding curve of the $Mn(H_2O)_6$ standard (Figure 2.7) shows a more modest rise, or less of a "saturation" behavior, indicating a substantial contribution from outer sphere deuterons. The much smaller contribution of outer sphere deuterons to the amplitude of the signal from the CcO Mn site leads to an underestimation of the waters exchanged. We cannot accurately calculate the extent of the underestimation, but clearly our data implies that more than two Mn-bound ^2H_2O molecules have exchanged by 10 milliseconds after mixing. Based on the number of crystallographically defined water ligands to the Mn site (Figure 2.2), we have an upper-limit of three coordinating water molecules, indicating the likely exchange of all three.

Proton movement through ice

Previous studies have indicated that protons can tunnel rapidly through an ice matrix with an estimated speed of $10^{-3}cm^2/V{\cdot}sec$ (Nagle and Morowitz, 1978), though other studies suggest that proton tunneling virtually stops at temperatures below 190 K (Cowin et al., 2000). In light of this controversy, if protons can tunnel in an ice matrix at low temperatures and the deuterons are moving through the frozen enzyme even after rapid freezing, this could be problematic for the interpretation of our data. This would make the time points for exchange of protons or deuterons at the Mn site irrelevant without accounting for the length of time the samples are stored

before being examined spectroscopically and their rate of movement during sample storage. To determine if such an exchange occurs in our studies, a sample was prepared by spraying a 120 μM oxidase solution and a 100% ^2H_2O solution simultaneously, but independently, into chilled isopentane. The RFQ apparatus was used, but with the mixing step bypassed, to obtain the most comparable control samples. Sample packing and storage was carried out in the same manner as the samples for time-resolution of exchange. After two weeks of storage in liquid nitrogen, an ESEEM spectrum of the sample was taken. The spectrum shows no modulation at 2.2 MHz (Figure 2.8), indicating no deuterons had access to the Mn either during the packing of the sample or during storage between sample preparation and acquisition of the spectrum.

Exchange of bulk water

The ability of bulk water to access the Mn site on a catalytically relevant timescale was tested by mixing CcO with isotopically labeled water ($H_2{}^{17}O$, 22% final enrichment in ^{17}O) using the RFQ system. The presence of isotopically labeled water, $H_2{}^{17}O$, at the Mn site was assayed by line broadening of the Mn EPR spectrum. Using samples without ^{17}O as a reference, line broadening (as evidenced by loss of resolution of the hyperfine structure) was detected to an equivalent extent in samples that had been incubated with labeled water for several minutes and RFQ samples that had only been incubated for 10 milliseconds (Figure 2.9). Additional evidence of ^{17}O presence near the Mn could be seen by ESEEM, which shows a peak at the 2.2 MHz Larmour frequency of ^{17}O (Figure 2.10). While exact quantitation is difficult, the line-broadening data suggest the exchange appears to be completed within the instrumental dead time of 10 milliseconds, as seen for deuterium exchange.

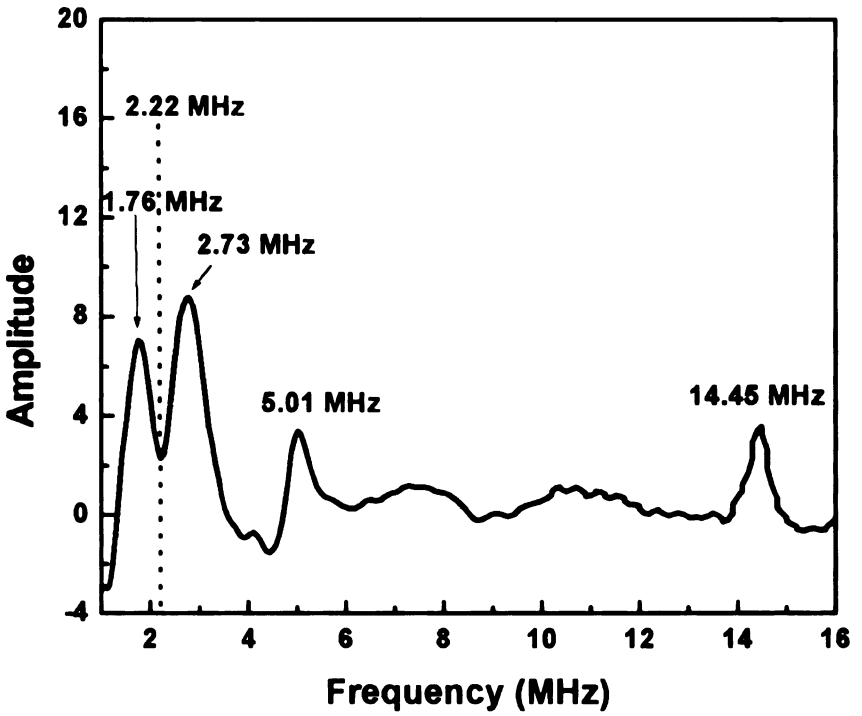

Figure 2.8: Exchangeability of protons at the Mn site at 77K. To ensure proton/deuteron exchange was not occurring in the frozen sample, CcO and 100% $^{2}H_2O$ were frozen simultaneously, but independently, in an EPR tube using the freeze-quench apparatus. The spectrum was acquired after 15 days of storage in liquid nitrogen. Peaks at 1.76, 2.73 and 5 MHz arise from ^{14}N, while the peak at 14.45 MHz is due to ^{1}H. The absence of a 2.2 MHz peak indicates no exchange is occurring in the frozen matrix.

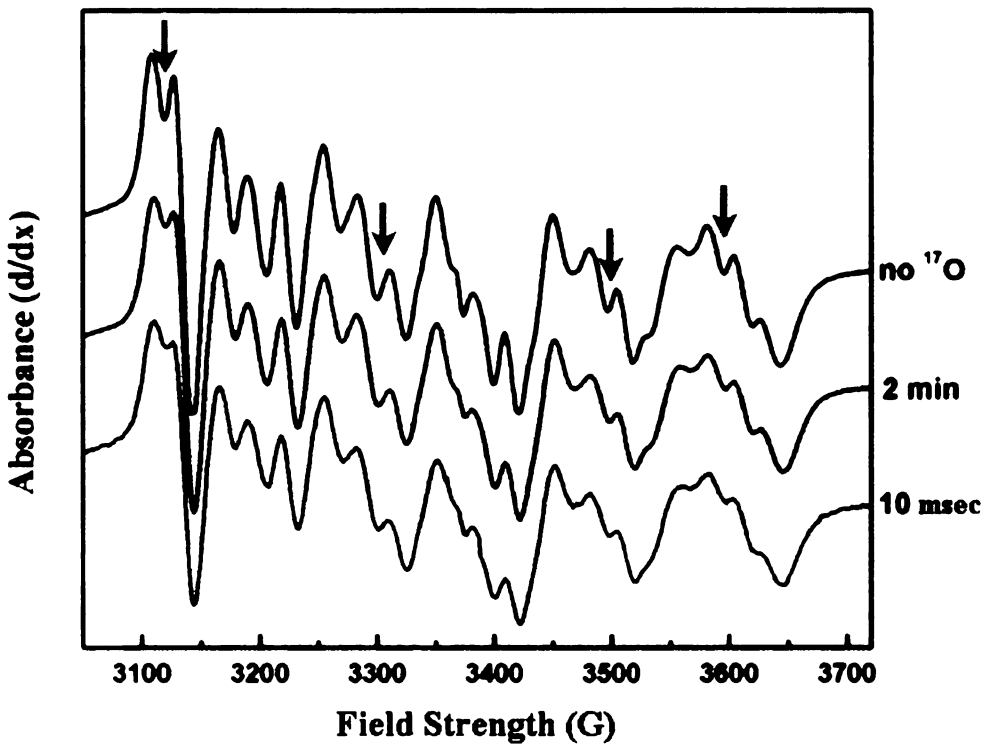

Figure 2.9: Line broadening of the Mn spectrum after mixing with $H_2{}^{17}O$. The broadening of the Mn pattern by interaction of the 5/2 nuclear spin of ^{17}O can be seen in samples incubated in 25% labeled $H_2{}^{17}O$ for two minutes (blue trace) and after 10 milliseconds of mixing with 22% $H_2{}^{17}O$ (red trace). The broadening effects compared to sample with no enrichment of ^{17}O (black trace) can best be seen where indicated by arrows. The clearest regions of line broadening are marked by red arrows and are evidenced by filling in of the peaks. The similar amounts of broadening seen in the 10 millisecond sample and the two minute sample indicate the exchange of the $H_2{}^{17}O$ occurs in less than 10 milliseconds.

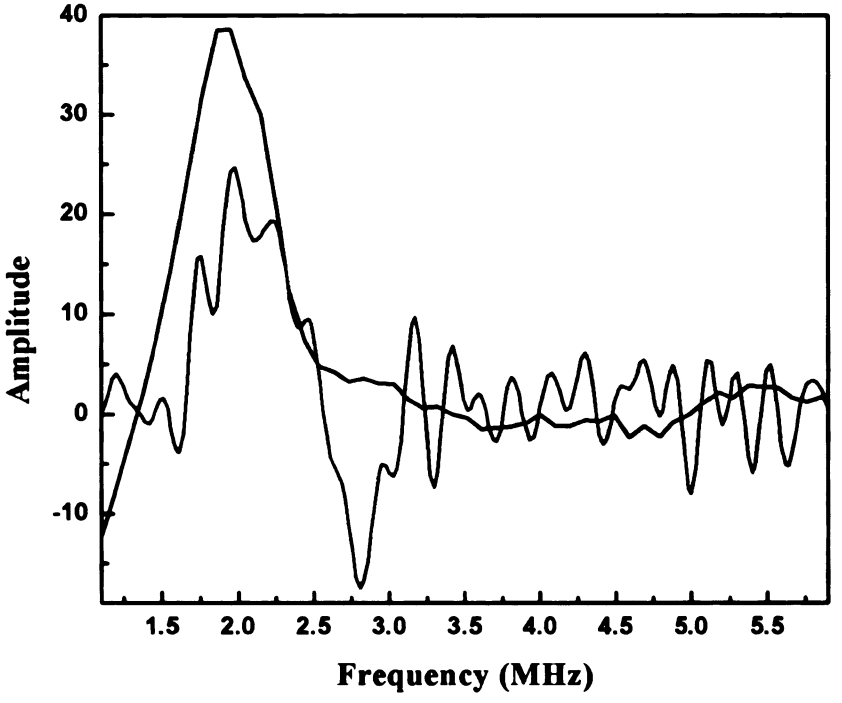

Figure 2.10: ESEEM detection of an ^{17}O matrix line. Three-pulse ESEEM data from CcO incubated with 22% $H_2{}^{17}O$ for 10 milliseconds (red trace) shows a peak at 2.2 MHz, the Larmour frequency of matrix ^{17}O at this field. $Mn(H_2O)_6$ in 25% ^{17}O-enriched water (black trace) also shows a peak at the same frequency. The large amount of noise in the CcO spectrum is due to the small sample size and low concentration.

Discussion

The routes for proton uptake in CcO are relatively well defined, but there is little evidence regarding the proton/water release pathway(s). Computer modeling and crystallographic structures indicate a large number of waters in the region above the hemes, but how rapidly these waters exchange with bulk solvent is a critical issue. The current model of Wikström and colleagues (Wikström, 2003) implies that when the protons are moved to the region above the hemes, they are already "outside", or have unhindered access to bulk solvent. Alternatively, the model of the Michel group (Michel, 1999) requires a location above the hemes where the proton can be trapped prior to release to the outside and inaccessible to bulk solvent. A third suggestion is that all the waters seen in this area above the hemes are structural waters, and no rapid exchange can occur (S. Yoshikawa, personal communication). Further complicating the search for an exit route is the possibility of multiple or ill-defined pathways, as was previously believed for the bacterial photosynthetic reaction center (Baciou and Michel, 1995; Paddock et al., 2000). Previous studies have shown the accessibility of the Mn site in CcO to $^{2}H_2O$ and $H_2{}^{17}O$ after many hours of incubation, but contained no kinetic time resolution (Haltia, 1992).

Kinetic data on the rate of water flow in proteins is difficult to obtain in complex enzymes such as CcO. The Mn ion, however, is spectrally accessible and conveniently located at the bottom of the putative water channel just above the active site and thus it is a good probe of water flow in this region. ESEEM is the technique of choice to examine the magnetic nuclei in the vicinity of the Mn ion because it can

provide information regarding nuclei weakly coupled (such as ^{1}H and ^{2}H) to the transition metal. We used an RFQ apparatus for the preparation of samples to introduce rapid time-resolution to the ESEEM experiments. Such RFQ techniques (Ballou, 1978), combined with EPR spectroscopy, have been used for studying the appearance of radical intermediates in reaction mechanisms (Padmakumar and Banerjee, 1995; Schultz et al., 1998). The use of this technique to obtain the rate of water/proton flow in a protein has not been previously reported.

We define a lower limit of 3000 s^{-1} for the rate of the water/deuterium exchange at the Mn site. When the CcO is in its resting state (fully oxidized, not turning over), the maximal proton/deuterium exchange at the Mn site occurs in less than 10 milliseconds at room temperature and at 4°C, which indicates that the protons of the water molecules in close association with the Mn are in rapid equilibrium with the bulk solvent. The deuterium exchange cannot differentiate if the accessibility determined is by the exchange of protons or if it is the entire water molecule that exchanges. The observed exchange of $H_2{}^{17}O$ demonstrate that entire water molecules are exchanging, though it cannot be clarified if individual protons also can exchange without being associated with an exchanging water molecule. The results reported here support the concept that there is a kinetically relevant route for water, and possibly individual protons, to exchange with bulk solvent to the depth of the water ligands of the Mg/Mn site.

Because of the complex hydrogen-bonding network of waters around the Mn in the protein, it is unclear where exactly water and/or protons are moving and by what routes they are accessing the Mn site. However, the methodology established

here provides a useful tool to test possible pathways by mutational analysis. The question of whether there is one pathway or whether this region is generally accessible to external solvent is an important current issue. Can subtle changes in the conformation of this region, which may occur during the oxygen chemistry at heme a_3-Cu_B, alter pK_a values and control accessibility, as in the case of bacteriorhodopsin? In bacteriorhodopsin, a proton exit route involving hydrogen-bonded water and amino acid side chains exists in the resting state but protons are not released until light induces a series of pK_a and conformational changes (Luecke et al., 1999).

Although the turnover rate of CcO activity can be as high as 2000 electrons per second (producing 1000 H_2O per second), giving a time constant of 0.5 milliseconds, the 10 millisecond and longer time range that this method can sample is suitable for measuring deuterium exchange rates at the Mn site during turnover in the 100 s^{-1} range often found in mutants, and it is ideal for determining if slow turnover of mutant forms is correlated with slowed movement of water or protons in this region. Hence, we have established a methodology combining RFQ ^2H_2O and $H_2{}^{17}O$ exchange with ESEEM for measuring the kinetics of the water flow in the exit water/proton channel, providing an assay for mutants designed to reversibly or irreversibly block it.

Chapter 3:

The Water Exit Channel

Portions of this chapter are based on data published in (Schmidt et al., 2003a).

Introduction

Cytochrome *c* oxidase (CcO) is an intrinsic membrane protein that functions as the terminal enzyme of the respiratory electron transport chain. It transfers electrons from cytochrome *c* to dioxygen, which is reduced to water. Water is generated at the buried active site at rates as high as 1000 s^{-1}. Spatial constraints, as well as the hydrophobic nature of the active site in the middle of the membrane, provide the thermodynamic driving force for water expulsion (Zheng et al., 2003). While there have been a few proposals for water exit channels (Backgren et al., 2000; Florens et al., 1999; Soulimane et al., 2000; Tsukihara et al., 1996; Zheng et al., 2003), the crystal structures do not show any clear routes from the active site (Figure 3.1). Indeed, it can be argued that no channel is necessary, since water has been shown to rapidly exchange within proteins (Garcia and Hummer, 2000; Gottschalk et al., 2001). However, the function of CcO as a proton pump suggests that access of water to random sites within the protein is not likely. CcO requires the controlled movement of electrons and protons, and therefore water, since the latter can serves as a pathway for the protons, potentially short-circuiting the pump.

ESEEM studies of $^{2}H_2O$ and $H_2{}^{17}O$ exchange at the buried Mn site described in the previous chapter indicate rapid access of water to the metal from the bulk. While this access was demonstrated to occur on a catalytically relevant time scale, it is still unclear if the product water produced at the active site reaches the Mn site preferentially over the other regions of the protein, indicative of a channel. Additionally, it has not yet been defined how the water from the bulk reaches the Mn site and if there is an explicit water pathway. In these studies, turnover of isotopically

Figure 3.1: Hydrophobic isolation of the binuclear active site from the Mn. The binuclear active site (heme a_3 in green; Cu_B in blue) is 12 Å from the Mn (magenta sphere), but is hydrophobically isolated. Once water from the active site reaches the Mn, it then has several possible routes to the bulk, including a proposed channel, which contains residues along the interface of subunit I (colored yellow) and subunit II (colored orange). The distance from the Mn to the solvent accessible surface (solid line) is 13 Å. Crystallographically defined water molecules near the Mn site are indicated as cyan spheres.

labeled substrate ($^{17}O_2$) is used to test whether there is rapid preferential access of the product water to the Mn site.

To further define the channel, a site-directed mutant protein was engineered to block the external end of a proposed water channel and was examined with respect to its ^2H_2O exchange rate. An arginine near the protein surface and at the end of a water chain that is seen in the crystal structure, R234, (Figure 3.2) was changed to a cysteine. After characterization of this mutant protein, deuterium exchange at the Mn site was measured and compared to wild-type CcO. The mutant was then labeled with the cysteine-specific fluorescent label, fluorescein maleimide, in an attempt to block the channel. Deuterium exchange was again measured and compared to the wild-type and unlabeled mutant enzymes. These studies give us the first evidence for a defined water exit pathway.

Experimental procedures

Protein purification, rapid freeze-quenching and magnetic resonance spectroscopies were carried out as described in chapter 2. For experiments in which there was catalytic turnover of the CcO, samples were mixed with 2 mM pre-reduced cytochrome *c*. Both the CcO and cytochrome c^{2+} samples were degassed and saturated with either $^{17}O_2$ or $^{16}O_2$ at room temperature. The cytochrome *c* and the CcO were mixed in the RFQ, allowing several turnovers, and frozen by spraying into chilled isopentane maintained at 140 K. An incubation time before freezing of 4 milliseconds, with the freezing process taking approximately 5 milliseconds, gives an overall reaction time of less than 10 milliseconds. Deuterium exchange at the Mn site

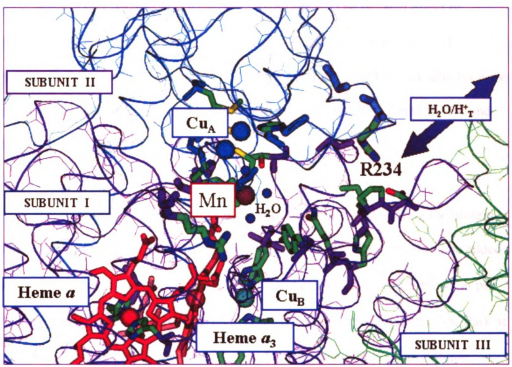

Figure 3.2: Location of R234 near the end of a possible water exit pathway. While R234 is directed towards the interior of the channel and is kept in this conformation by a salt bridge, it is near the solvent exposed surface of the protein. Its location near, but not at, the solvent exposed surface makes it ideal for examining the function of this potential channel.

during catalytic turnover was determined in an identical manner, except that the cytochrome *c* was washed into 95% deuterated buffer. The isolated effect of cytochrome *c* binding on deuterium exchange was examined using identical conditions except using cytochrome c^{3+} in 95% deuterated buffer. All samples were maintained at pH 7.9 in a buffer consisting of 100 mM HEPES, 1 mM EDTA and 0.1% lauryl maltoside.

Maximal fluorescent labeling was achieved by incubating the protein with a ten-fold excess of fluorescein maleimide (FM). Fluorescent label was added to the CcO sample, at a concentration of 50 μM and in 100 mM HEPES buffer at pH 7.9, to a final concentration of 500 μM. After two hours of incubation in the dark at room temperature, excess label was removed by two consecutive spin-column chromatography steps using a Sephadex G50-50 resin. Specific labeling of R234C was verified by SDS-PAGE. In order to prevent fluorescein degradation and ensure maximal resolution of subunits, an 18% cross-linked gel with a resolving phase buffer at pH 7.9 was used.

$^{17}O_2$ with an isotopic purity of 80% was from Isotec.

Results

Product water exit

Product water interaction with the Mn was tested by RFQ-EPR studies where catalytic turnover of the enzyme was initiated by mixing with reduced cytochrome *c* in the presence of 80% enriched $^{17}O_2$ substrate. The top trace of Figure 3.3 shows the Mn EPR spectrum for the situation where no turnover occurred: $^{17}O_2$-

saturated CcO was mixed with $^{17}O_2$-saturated buffer with no source of reducing equivalents. It is identical to the control spectrum CcO saturated in $^{16}O_2$ (Figure 3.4, top trace). However, if $^{17}O_2$-saturated CcO samples are mixed with $^{17}O_2$-saturated, reduced cytochrome *c*, using the RFQ system, and allowed to turn over for 10 milliseconds before freezing, significant broadening of the Mn EPR spectrum is clearly observed (Figure 3.3, bottom trace). The observed broadening was not caused by changes in the Cu_A reduction state due to turnover, as evidenced by identical samples saturated with $^{16}O_2$ and mixed with reduced cytochrome *c* which did not show significant broadening (Figure 3.4, bottom trace).

Catalytic turnover of the enzyme when incubated in D_2O results in a marked decrease in deuterium access from the bulk to the Mn site, to approximately half the level of exchange seen when the enzyme is not turning over (Table 3.1). This decreased exchange is not due to the binding of the substrate cytochrome *c*, as deuterium access was unaffected by the binding of oxidized cytochrome *c*. Thus, the decreased level of deuterium exchange can be directly attributed to the process of catalytic turnover.

Effects of the mutation of arginine 234 to cysteine

The mutation of an arginine to a cysteine at the subunit I/II/III intersection point (Figure 3.5) has substantial effects on CcO activity (Table 3.2). The most substantial effect is the loss of protein stability, evidenced by the loss of subunit III. However, the protein can be FPLC purified on an ion-exchange column to isolate a homogeneous fraction that still has subunit III. This fraction shows a normal UV-visible spectrum (Figure 3.6), it still has reduced maximal activity

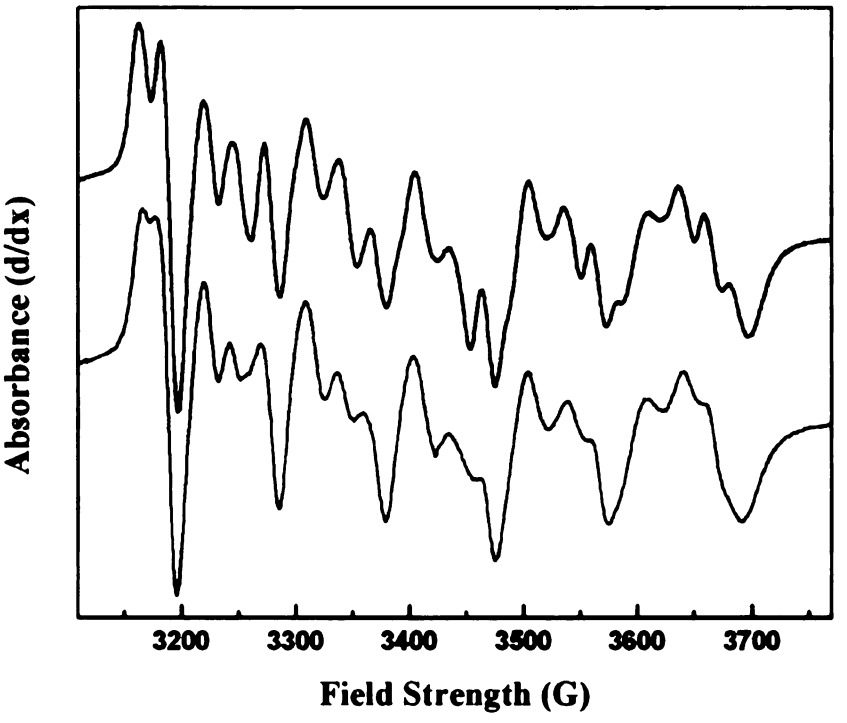

Figure 3.3: Line broadening of the Mn spectrum after turnover with $^{17}O_2$. The Mn spectrum of wild-type CcO incubated with 80% enriched $^{17}O_2$, but not yet turned over (black trace), shows no broadening, indicating no $^{17}O_2$ is bound at the metal. After less than 5 turnovers (red trace) substantial line broadening can be seen in all the fine structure of the spectrum.

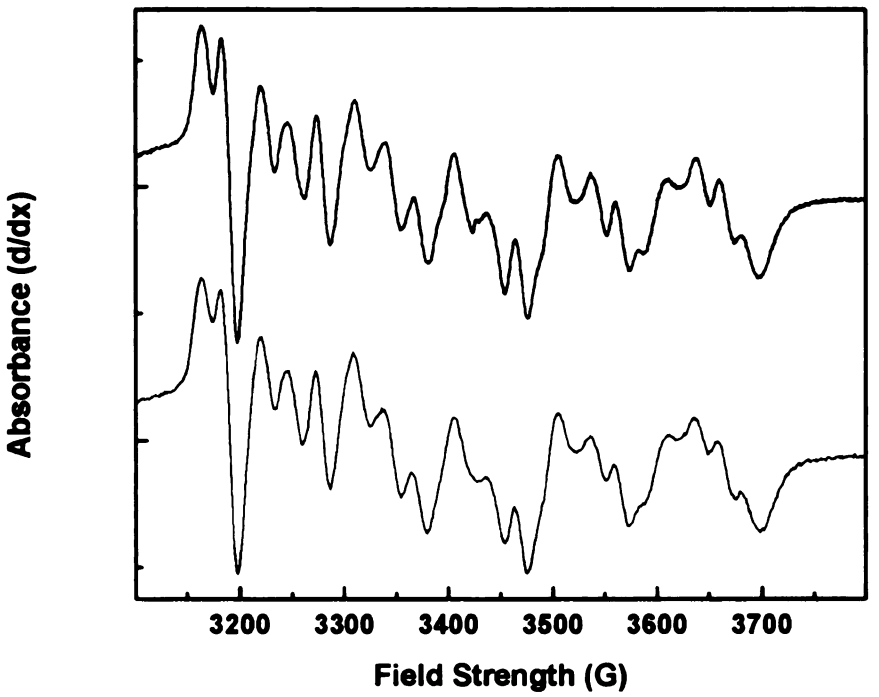

Figure 3.4: Turnover of the enzyme does not substantially effect the Mn spectrum. The potential effect of reduction of Cu_A during turnover affecting the Mn spectrum was assessed by comparison of samples saturated in $^{16}O_2$ before (black trace) and after (red trace) turnover with reduced cytochrome *c*. While a small level of broadening can be seen in some of the hyperfine features, it is not significant, especially in comparison to the broadening caused by turnover in $^{17}O_2$ (see Figure 3.3).

Table 3.1: 2.22 MHz peak amplitudes from the Fourier transform of three pulse ESEEM for samples incubated in D_2O. All points are for samples incubated in D_2O for 10 milliseconds, except where noted. Peak heights are taken from the Fourier transforms of three-pulse ESEEM spectra, as in chapter 2. There is an error of approximately 2% for each point.

	FT peak height at 2.22 MHz	**2.22 MHz peak height, relative to wild-type**
Wild-type	43	100%
FM-labeled wild-type	44	102%
Wild-type in the presence of cytochrome c^{3+}	45	105%
Wild-type in the presence of cytochrome c^{2+}	22	51%
R234C	45	105%
FM-labeled R234C	27	63%
FM-labeled R234C, 30 seconds incubation	65	150%

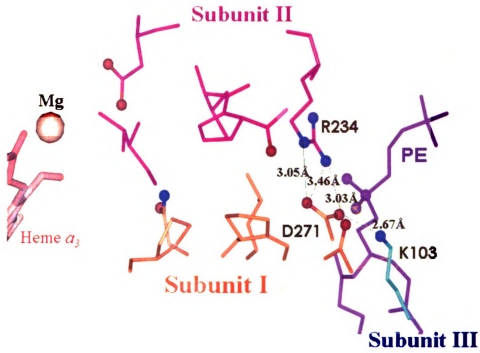

Figure 3.5: R234 is involved in the intersection of all four subunits. D271 of subunit I is salt-bridged to R234 of subunit II and K103 of subunit III, providing a crucial intersection point of the three subunits. Additionally, an essential phosphatidyl ethanolamine that binds subunit IV interacts with D271, making D271 the junction point of all three subunits. The role of R234 in this junction suggests that it is essential for proper arrangement of all four subunits. This figure is courtesy of Jun Yang.

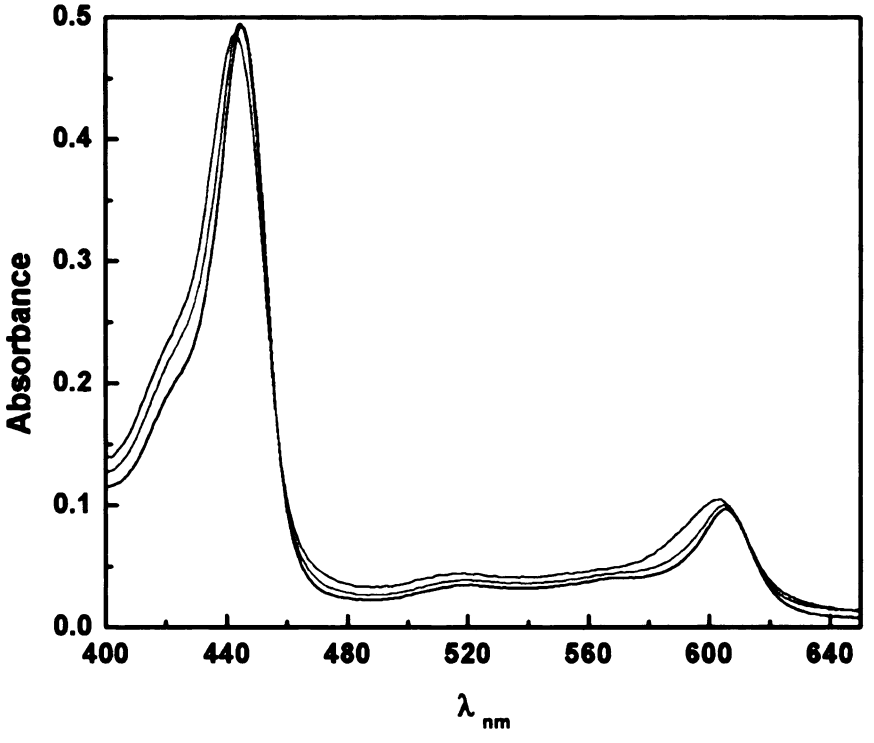

Figure 3.6: UV-visible spectrum of R234C at different stages of purification. The UV-visible spectrum of Ni-NTA purified R234C (blue trace) shows broadened and shifted peaks in the α-band (from 606 nm to 603 nm) and Soret band (from 444 nm to 442 nm) when compared to wild-type CcO (black trace). After further purification by DEAE ion-exchange chromatography, the α and Soret bands of the R234C enzyme (red trace) were very close to wild-type CcO.

Table 3.2: Activity of R234C compared to wild-type CcO. Steady-state oxygen consumption activities were measured polarographically at pH 6.5 in 50 mM HEPES. FM-labeled R234C was FPLC purified both prior to and after fluorescent labeling.

	Activity (e^-/sec/aa_3)
Wild-type	1550
FM-labeled wild-type	1500
R234C	450
R234C – FPLC purified	1000
FM-labeled R234C	600

(Table 3.2) and pumps protons at a reduced stoichiometry (Figure 3.7). A small perturbation of the Mn site can be seen by the EPR spectrum (Figure 3.8), but this does not imply a major change in the ligation geometry.

Fluorescein maleimide labeling of R234C was maximized when incubated for two hours at room temperature in the presence of a ten-fold molar excess of label. This incubation time also minimized the amount of protein degradation, which can be detected by a blue shift of the heme *a* band in the UV-visible spectrum. The amount of labeling could not be accurately measured due to several factors. The amphipathic nature of fluorescein maleimide causes it to interact with the detergent, giving a large background absorbance. Also, there is a cysteine on subunit III that also labels (Marantz et al., 1998), making it difficult to deconvolute the absorbance due to the labeling of subunit III and the absorbance due to labeling of R234C (Figure 3.9). Finally, while an extinction coefficient for the fluorescein maleimide visible absorption band has been determined, this band is pH sensitive. Possible local pH differences at the location of the label, as suggested by a 10 nm red shift in the absorbance band compared to that expected for aqueous solution (Figure 3.10), prohibit using the literature extinction coefficient at face value. If the literature value is used, different levels of labeling are calculated depending on the stage of purification, apparently getting higher as the sample gets purer.

The level of deuterium exchange at the Mn site was not affected by the R234C mutation (Table 3.1). However, when the mutant was labeled with fluorescein the level of deuterium exchange was diminished at 10 milliseconds, though complete exchange was seen after approximately 30 seconds of incubation

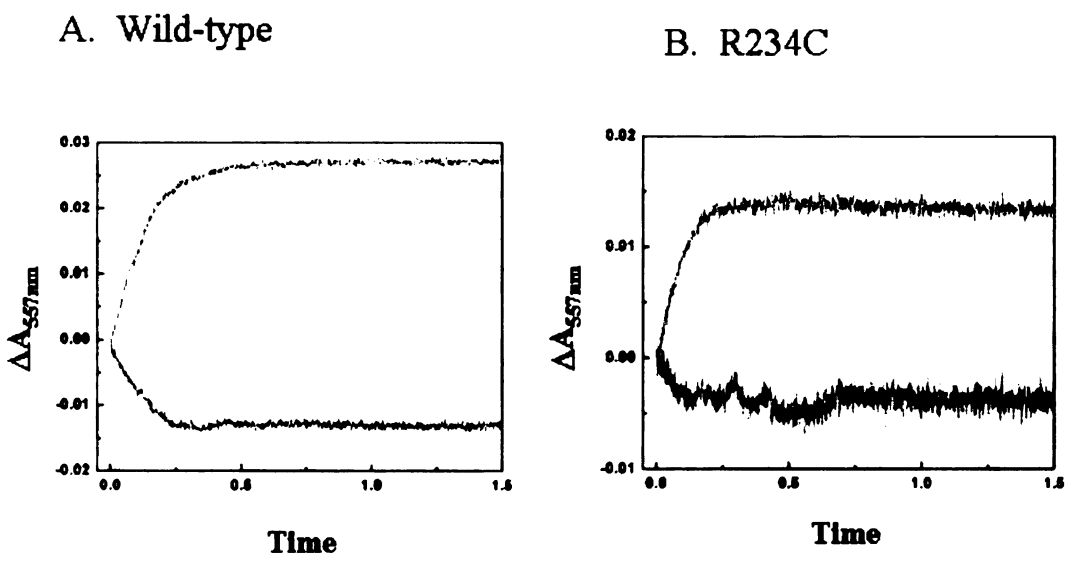

Figure 3.7: R234C retains proton pumping (B), but at a lower efficiency than wild-type CcO (A). While there was acidification of the bulk during turnover of R234C in liposome vesicles in the presence of the potassium ionophore valinomycin (B, blue trace), the alkalinization during turnover in the presence of the proton ionophore FCCP was far greater (red trace). This led to a smaller H^+/e^- stoichiometry of the R234C mutant compared to wild-type CcO.

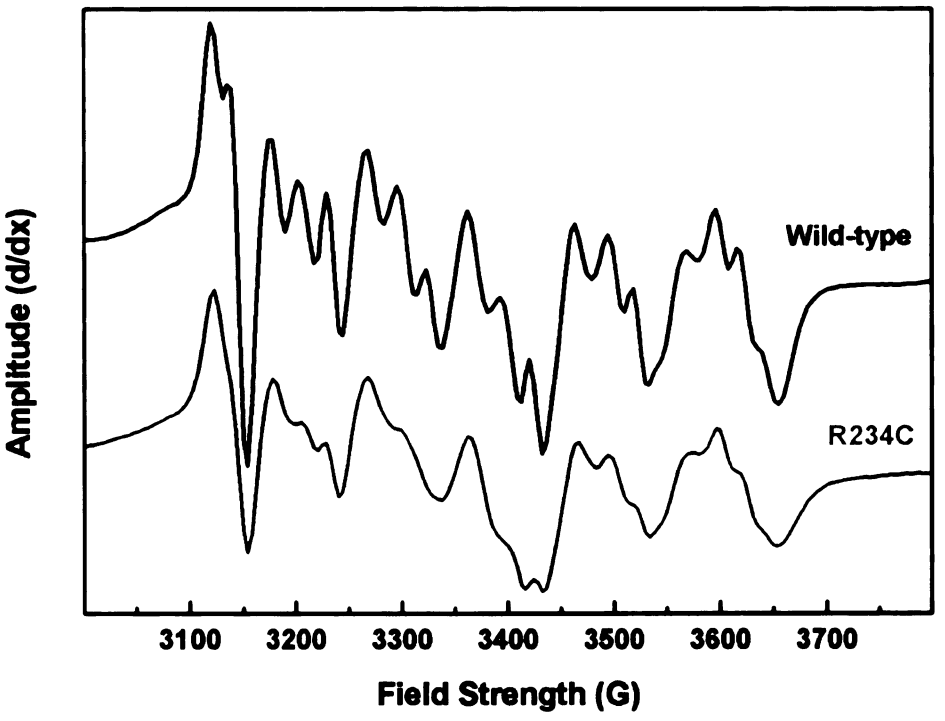

Figure 3.8: The R234C mutation has a small effect on the Mn binding site. The R234C Mn EPR spectrum (red trace) shows substantial differences from the wild-type Mn EPR spectrum (black trace) in the hyperfine structure. The overall six-line fine pattern is still found, indicating the Mn is still in a similar octahedral geometry. This indicates the R234C mutation results in a small change in the Mn ligand geometry, but the overall features of the site are undisturbed.

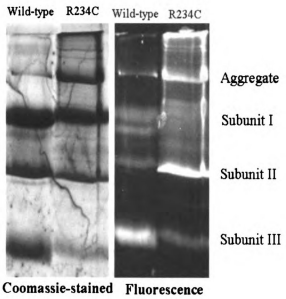

Figure 3.9: SDS-PAGE gel analysis shows labeling of subunit III in both wild-type and R324C and specific labeling of subunit II only in the R234C mutant. The only subunit that shows labeling at a level above background in the wild-type CcO is subunit III. The labeling of subunit III is still present in the R234C mutant, and a large increase in fluorescence is seen in subunit II. Coomassie blue staining of the gel shows a large decrease in subunit III in the R234C mutant, but some of this could be present as aggregates, seen in greater amounts at the top of the gel in R234C.

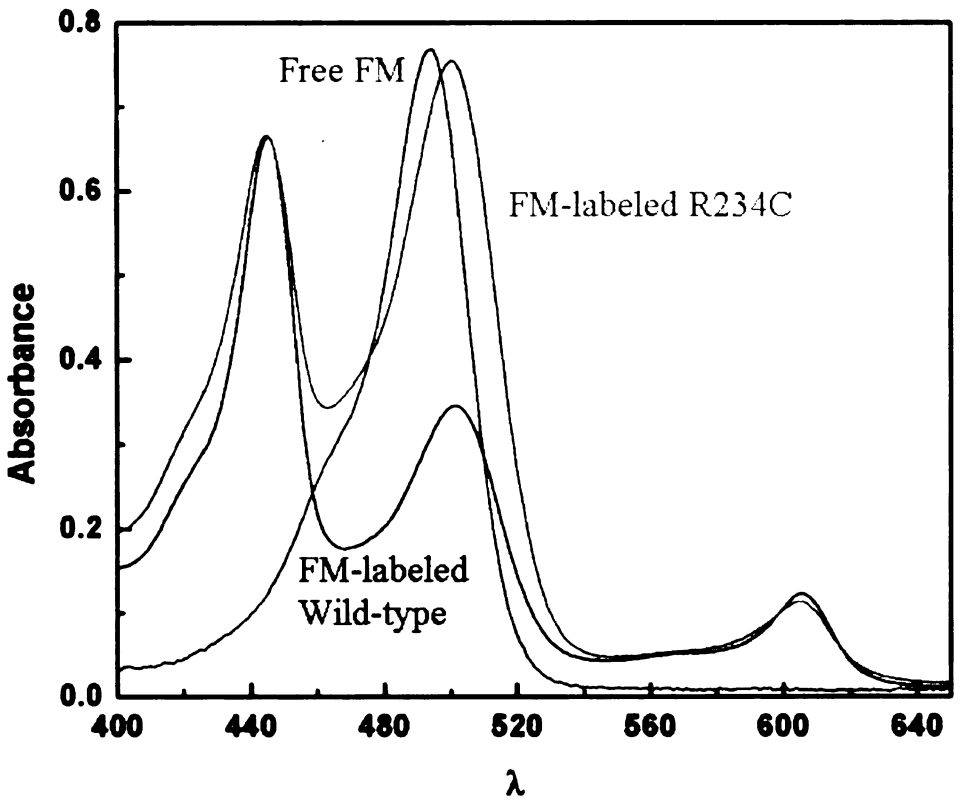

Figure 3.10: UV-visible absorbance shows a perturbation in the fluorescein maleimide peak when bound to CcO. The binding of fluorescein maleimide to CcO shifts the absorbance band of the fluorophore 10 nm to the red of the normal free fluorescein peak. This shift occurs both when bound only to subunit III in wild-type (black trace), as well as when both subunit II and III are labeled in R234C (red trace). The solution spectrum of free fluorescein maleimide is shown in green.

(Table 3.1). The slightly higher than wild-type CcO 2.2 MHz peak intensity for completely exchanged, labeled R234C indicates that there is slight perturbation of the Mn site that allows more water near the metal. The slower exchange of deuterium at the Mn site in the fluorescein labeled mutant can be attributed directly to the labeling of R234C, as fluorescent labeling of wild-type CcO, at the site on subunit III, had no effect on the exchange rate (Table 3.1).

Discussion

Product water movement from the active site

The routes for proton uptake in CcO are relatively well defined, but there is little evidence regarding the proton/water release pathway(s). The experiments described in chapter 2 have shown that the buried Mn site is accessible to proton and water exchange on a catalytically relevant timescale. While these experiments validate the idea that a water exit path could involve the Mn, they do not necessarily imply that this pathway is actually used during catalysis, nor that it is unique. To test the actual use of the proposed channel during turnover, RFQ was employed to look for isotopically-labeled product water at the Mn after turnover in $^{17}O_2$. If the $^{17}O_2$, converted to $H_2{}^{17}O$ at the active site, reaches the Mn, it should broaden the cw-EPR lineshape. Surprisingly, major broadening of the Mn spectrum was observed (Figure 3.3), indicating several water molecules bound to the metal (Bellew et al., 1996; Kofron et al., 1988).

While reduction of Cu_A has been shown to influence the Mn spectrum of

CcO (Haltia, 1992; Kaess et al., 2000), causing broadening in certain regions of the spectrum, the broadening observed when the enzyme is catalytically turned over in the presence of $^{17}O_2$ is not due to this effect but can be attributed exclusively to the presence of $H_2{}^{17}O$ at the metal site. The first evidence for this is the nature of the line broadening that is observed. The oxidation state of Cu_A only broadens certain regions of the Mn spectrum. However, the line broadening observed in the turned over samples is uniform across the spectrum, indicating it is not due to the reduction of Cu_A (Figure 3.3). The Mn spectrum of CcO turned over in the presence of $^{16}O_2$ further clarifies this issue. When treated in an identical manner, but lacking the nuclear magnetic moment that is provided by ^{17}O, CcO turned over in buffer saturated with $^{16}O_2$ and in the presence of reduced cytochrome *c* does not show significant broadening of the Mn spectrum (Figure 3.4). This clearly indicates that the line broadening observed when CcO is turned over in the presence of $^{17}O_2$ is a direct result of the presence of $H_2{}^{17}O$ at the Mn site and is not affected by turnover conditions.

It was initially a puzzle that a substantial amount of product $H_2{}^{17}O$ was observed at the Mn, since it seems in contradiction to our previous results showing rapid exchange of water with the bulk phase in the same time frame (<10 milliseconds). However, calculations indicate that the turnover of the enzyme continues until the freezing of the sample occurs. By using a CcO concentration of ~50 μM, an O_2 concentration of 1 mM (saturated at room temperature) and providing electrons from reduced cytochrome *c* at ~1 mM, the reaction was limited by reducing equivalents to 5 or fewer complete conversions of O_2 to two H_2O per CcO molecule (four electrons are required to convert one $^{17}O_2$ to two $H_2{}^{17}O$). Even if all the

cytochrome c^{2+} is oxidized, no more than 10 water molecules can be produced per CcO during the reaction time. In fact, under the conditions of this experiment, this is an upper limit for $H_2{}^{17}O$ production, due to the limited amount of reduced cytochrome *c* competing with increasing levels of oxidized cytochrome *c*, causing the rate of turnover to slow down exponentially as the reaction proceeds. Stopped-flow kinetic studies, when similarly limited by substrate electrons, suggest that only approximately two to three complete turnovers would occur within the first 10 milliseconds of the reaction (Figure 3.11), producing an average of four to six water molecules per CcO and resulting in continued availability of reducing equivalents until the end of the 10 milliseconds before freezing.

Due to the large discrepancy in the amount of labeled water produced at the active site as compared to the concentration of water in the bulk (55000:1 ratio), any labeled water that reached the bulk phase would be so dilute that diffusion back into the Mn site would be negligible. Hence any labeled water coupled to the Mn must have come directly from the active site. Given the level of broadening and the limited number of product waters produced, it is likely that most or all of the waters exit via this route. Thus the appearance of water at the Mn site in only a few turnovers argues strongly against the idea that water exits by random diffusion from the active site of CcO. It also argues against the possibility that this is one of several specific exit paths for water (Backgren et al., 2000; Zheng et al., 2003).

A defined water pathway to the surface

The results described provide strong evidence for a major water exit pathway that reaches the Mn from the heme a_3 – Cu_B site. From there, it has rapid access to

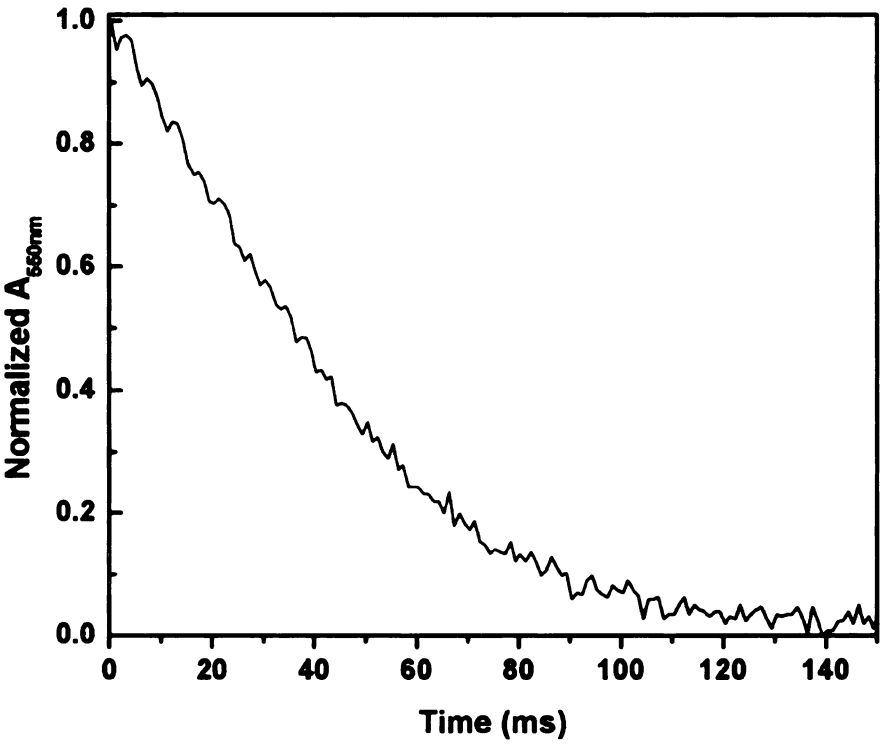

Figure 3.11: Reduction of cytochrome *c* when under electron-limiting conditions. Stopped-flow analysis of cytochrome *c* oxidation by wild-type CcO incorporated into uncontrolled vesicles, with enough reduced cytochrome *c* provided for six turnovers, indicates that it takes approximately 120 milliseconds to complete six turnovers. The reaction was observed and the number of turnovers estimated by monitoring the absorbance change at 550 nm, which is the characteristic wavelength for absorption by reduced cytochrome *c*. The concentrations of enzyme and substrate used in these experiments are substantially smaller than those used to generate freeze-quench samples of turned over enzyme (1000 fold for both substrate and enzyme), which will lead to differences in turnover rate. However, as both reactions are limited by electron donors, a similar curve is expected. Even with an initial rate of activity several fold higher than the uncontrolled vesicles, only a few turnovers can be expected in the first 10 milliseconds of reaction when turnover is limited by electron donors.

the bulk phase, but the exact pathway from Mn to the outside is not known, nor is it a foregone conclusion that a defined pathway from this site is needed. To address this issue, the rate of deuterium exchange from the bulk phase to the Mn site was monitored in a mutant CcO (R234C) specifically designed to disrupt a possible proton or water channel. R234C is near the protein surface at the interface of subunits I and II, and near the subunit I/III junction (Figure 3.5). The arginine normally forms a salt bridge with an aspartate on subunit I (D271), which also interacts with a lysine on subunit III (K103) as well as a phosphate of a phosphatidyl ethanolamine that binds subunit IV. The mutation of this arginine to a cysteine causes a disruption in the subunit I/II/III/IV interface and results in a more unstable protein that tends to lose subunit III and likely subunit IV.

This increased instability due to the mutation has made characterization of this mutant difficult. While the mutant has been shown to retain proton pumping, a proton to electron ratio of 1:1 is not readily attainable (Figure 3.7). There are several possible explanations for this decreased proton pumping efficiency. The increased instability of the mutant protein makes it likely that some fraction of the enzyme has lost subunit III by the time proton pumping can be measured. It has been shown that loss of subunit III leads to decreased proton pumping efficiency, as well as suicide inactivation of the enzyme (Bratton et al., 1999). Indeed, the R234C CcO also shows some suicide inactivation, which is sensitive to numerous environmental variables. However, decreased proton pumping efficiency would also be expected for a mutant in which there was a disruption of the proton and/or water exit channel(s) that could result in increased proton backleak. In this scenario, the gating mechanism that is required for unidirectional proton movement could be impaired or short-circuited,

allowing for protons from the exterior to be used for the reaction rather than protons from the interior.

The normal degree of access of deuterium to the Mn site in the R234C mutant indicates that there are not any large disturbances that affect the Mn site. The decreased levels of deuterium exchange observed when the introduced cysteine was covalently modified by the addition of fluorescein maleimide strongly supports the possibility that the subunit I/II interface, including the region around R234, functions as a proton or water channel. The large, hydrophobic nature of the fluorescein and partially buried nature of the R324C could result in blocking of this channel when the cysteine is modified. Indeed, a decreased level of deuterium exchange, to a level approximately 60% of the level exchanged in unlabeled protein, is seen after 10 milliseconds of incubation, though by 30 seconds the deuterium has more than fully exchanged (Table 3.1), indicating that the alteration of this region disrupts access of bulk water to the Mn site.

There are several possible reasons for the substantial amount of remaining deuterium exchange observed within 10 milliseconds. Due to the difficulties mentioned above in determining the level of fluorescein labeling, it cannot be estimated whether the amount of rapid exchange is correlated with the amount of unmodified CcO. Using the literature value for the extinction coefficient, the concentration of fluorescein maleimide in the purified samples is well below the ratio of 2:1 that one would expect if both the introduced cysteine in subunit II, as well as the existing cysteine in subunit III, were to be completely modified. Hence, it is likely that some of the enzyme in the reaction has not been labeled and should show

normal deuterium exchange. The modification of the CcO may also have caused conformational changes that allowed access to the Mn from a new route or may not have completely occluded the channel. Conformational changes are indicated by the increased 2.2 MHz peak maximum in the fluorescently labeled protein at longer times of incubation (Table 3.1). The high peak intensity indicates that there is more deuterium in the vicinity of the Mn than is seen in wild-type CcO, possibly due to the presence of a new pathway to the bulk.

An increase in the presence of deuterium around the Mn is also possible if there is further disruption of the subunit I/II/III interface, resulting in the increased loss of subunit III. The sensitivity of this region to perturbation that causes increased loss of subunit III has already been shown. Additional strain of this region caused by fluorescein modification could increase the likelihood of subunit III loss, resulting in a destabilization of the subunit I/II interface that allows for more solvent access to the Mn. This loss of subunit is suggested by the SDS-PAGE gel, which shows a diminution of the band for subunit III in the labeled R234C in comparison to wild-type CcO that has also been labeled with fluorescein maleimide (Figure 3.9). However, there are also increased levels of aggregated and polymerized forms involving subunit III, suggesting that subunit III may not be lost but is more readily disrupted under the conditions used to run the gel, a well known problem with subunit III.

While the limited decrease in deuterium exchange on the millisecond timescale allows for uncertainty regarding the uniqueness of this channel for water and/or proton exit from the enzyme, the fact that there is a decrease in the rate of

exchange implicates this area in proton and/or water transport. In conjunction with the studies using $^{17}O_2$ as substrate to produce isotopically labeled product water, we can now begin to define the water exit pathway in CcO. The presence of $H_2{}^{17}O$ at the Mn site after only a few turnovers demonstrates that product water passes this site as it exits the protein. The large degree of line broadening observed in these samples with such a limited number of waters produced strongly indicates that this is not just one of several possible exit routes, but likely the exclusive route used for water exit. The route from the Mn site to the bulk phase cannot be as definitely assigned. It may bifurcate into multiple pathways, but at least a significant fraction water exchange appears to utilize a channel involving the subunit I/II interface that ends near the subunit I/II/III/IV junction in the vicinity of R234.

Evidence for a single pathway for water exit

The limited exchange of deuterium in wild-type CcO at the Mn when the CcO is turning over suggests that this may in fact be the exclusive pathway. With a diffusion rate of approximately 10^6 cm^2/s, protons from the bulk should be able to diffuse the approximately 12 angstroms to the Mn site within picoseconds. This rate of diffusion well exceeds the microsecond to millisecond turnover rate of CcO and hence deuterium exchange from the bulk phase to the Mn site should not be affected by turnover. However, there is a clear decrease in accessibility of deuterium as the enzyme turns over (Table 3.1). This suggests that the pathway from the external bulk to the Mn site is either conformationally occluded during turnover or that deuterium flow into the protein is impeded by some other method. Conformational occlusion could likely be induced by the binding of cytochrome *c*, however this is not the case as deuterium access when oxidized cytochrome *c* is bound to the CcO is unaffected.

It is possible, though, that reduction of the different metal cofactors may induce a conformational change that occludes water and proton access to the Mn. However, it is also possible that the limitation is due to the presence of a single exit channel that is occluded by the exit of product water as the enzyme turns over. This would result in a partial decrease in rapid deuterium access, as is indeed seen, as the deuterium would have free access to diffuse to the Mn in the brief times between water production, only to be extruded again as the product water is forced out. However, it cannot be determined yet if the limited rapid access of deuterium to the Mn as the enzyme is turning over is due to a conformationally induced occlusion, the presence of a single, exclusive exit channel, or a combination of both.

Further studies are required to clarify the uniqueness of the subunit I/II interface channel, but we can now define a water exit channel as leading from the active site to the external surface of the enzyme, passing the Mn site along its route and at least one branch of which likely terminates near R234.

Chapter 4:

Regulation of the Exit Channel

Work in this chapter was done in extensive collaboration with Dr. Denise Mills, Dr. Warwick Hillier and Dr. Carrie Hiser. Portions of this chapter are based on data published in (Schmidt et al., 2003b).

Introduction

During the process of reducing molecular oxygen to water using electrons donated from cytochrome *c*, CcO pumps protons across the membrane. Extensive mutagenesis studies, along with high-resolution crystal structures, have helped define two channels for the intake of the substrate and the pumped protons. The data in the previous chapters begin to define the water exit channel, but do not necessarily define a proton exit channel. In the comparison of oxidized and fully reduced crystal structures of CcO from bovine heart (Yoshikawa et al., 1998a), the only significant change in the enzyme was seen in the region around the residue D51 (bovine numbering). Based on these data, a third proton channel, named the H-channel, was proposed for proton pumping, continuing through the entire protein from the internal side to the external side (Tsukihara et al., 1996; Yoshikawa et al., 1998a; Yoshikawa et al., 2000). Mutagenesis studies of several residues in this proposed channel were performed to test the viability of this hypothesis (Lee et al., 2000), but none of the mutants significantly affected the enzyme properties. Additionally, many of the proposed residues in this channel are not conserved between species, particularly at the external end of the channel and hence no mutations were made in this area. Previous work trying to characterize an external zinc-binding site resulted in the examination of this area as a possible zinc-binding site (Mills et al., 2002). In the present study, a mutation of an external histidine (H93 in *R. sphaeroides* numbering), which is the residue in closest alignment spatially with D51 of bovine heart enzyme, was made in order to test the role of this region in proton exit or zinc binding. A mutation was also made of a residue two helix-turns further into the enzyme (T100) to test whether the mutation might be causing a change in the activity by a superficial effect on cytochrome *c* binding.

Experimental procedures

Mutation of T100

A portion of the *R. sphaeroides coxI* gene was subcloned as a *Bam*HI fragment from the plasmid pYJ100 (Zhen et al., 1998) into pUC119. A PCR-based mutagenesis method (Horton et al., 1990) utilizing Pfu polymerase was used to mutate the codon for T100 to one encoding a leucine. All mutagenesis primers were synthesized by the Macromolecular Structure Facility in the Michigan State University Biochemistry and Molecular Biology department, and the mutated fragment was subsequently sequenced by the MSU-DNA Sequencing Facility. After mutagenesis, the *coxI* fragment was returned to its operon and then cloned into the *Hind*III site in the host plasmid pCH88 (Hiser and Ferguson-Miller, unpublished), which carries the subunit II/III operon with a His-tagged subunit II. This expression plasmid was transferred to *R. sphaeroides* strain JS100 (Shapleigh and Gennis, 1992) by biparental conjugation (Hiser et al., 2001). Mutation of the codon for H93 was performed in a similar manner by Dr. Carrie Hiser.

Spectroscopy

UV-visible spectra of enzyme fully reduced by addition of excess dithionite were recorded on a Perkin-Elmer Lamda 40P spectrophotometer after appropriate dilution into 100 mM HEPES, 1 mM EDTA, 0.1% lauryl maltoside, pH 7.9. Flow-flash spectroscopy was measured as previously described (Adelroth et al., 1995) in collaboration with Magnus Branden and Dr. Peter Brzezinski at Stockholm University.

Activity assays

Steady-state oxygen consumption activity was measured polarographically using a Gilson 5/6H oxygraph that was thermostated by using a Lauda Ecoline RE106 circulating water bath. Sample temperatures reported were measured in the sample chamber. The reaction medium contained 0.05% lauryl maltoside, 2.8 mM ascorbate, 0.55 mM TMPD and 4-10 nM CcO and the reactions were initiated by addition of horse cytochrome *c* to a concentration of 30 μM. The pH of the reaction buffer was maintained by 50 mM of an appropriate buffering salt (50 mM MES for pH 6 to 6.8, 50 mM HEPES for pH 7.0 to 8.2, and 50 mM glycylglycine for pH 8.6 and 9.0) with KCl added to maintain a constant ionic strength of 45 mM.

Determination of the K_m for cytochrome *c* was performed polarographically in a solution of 0.05% lauryl maltoside, 11 mM KCl, 2.8 mM ascorbate, 0.55 mM TMPD, 4-10 nM CcO and buffered to pH 6.5 by 50 mM MES. The reaction was initiated by the addition of horse cytochrome *c* to a final concentration ranging from 0.02 to 30 μM.

FTIR

CcO at a concentration of approximately 1 mM in a 40 mM HEPES, 1 mM EDTA and 0.1% lauryl maltoside buffer of pH 7.4 was used to record the FTIR difference spectra. Electrochemistry was performed with a custom-built optically transparent thin-layer electrochemical (OTTLE) cell designed along the lines proposed by W. Mäntele (Baymann et al., 1991; Moss et al., 1990). BaF_2 windows

were used to enhance the lower frequency cutoff region and a 10 μm gold grid was used as the working electrode (200 lines per inch; Buckbee-Mears, St Paul, MN). Before use the Au electrode-grid was cleaned in 3:1 concentrated H_2SO_4, 30% H_2O_2) and then coated with 2 mM cystamine for >2 hr. Protein electrochemistry of CcO enzyme was performed in the presence of a series of redox mediators (Hellwig et al., 1998) to accelerate the electrochemistry. These mediators were each present at 40 μM concentrations and did not interfere with spectra from the CcO enzyme. Electrochemistry was applied via a PAR 263 potentiostat (Perkin Elmer) using an Ag/AgCl aqueous reference electrode (BAS, West Lafayette, IN) and was operated under a non IR-compensated scan rate of 20 mV/s.

FTIR spectroscopy was performed in the OTTLE cell as a function of applied potential and was recorded with a Bruker Equinox 55 spectrometer using an MCT detector. The IR optics comprised a KBr beamsplitter used in conjunction with a Ge filter (OCLI L02547-9, Santa Ross, CA), which reduced spectral bandwidth. A Lake Shore 340 temperature controller and Si-diode combination (Lake Shore, Westerville, OH) maintained a homebuilt sample compartment at 10 ± 0.005°C. A stable background spectrum could be achieved after temperature equilibration of approximately 60 minutes. At this point the potentiostat could be used to electrochemically poise the CcO enzyme at a reduced or oxidized form. The oxidized and reduced spectra were an average of 800 scans. The spectra were fully reversible and each 800-scan acquisition lasted approximately 80 seconds and all spectra were collected at 4 cm^{-1} resolution. No baseline corrections were made to any of the spectra.

Protein purification and EPR spectroscopy were carried out as described in chapter 2. Fluorescein maleimide labeling was performed as described in chapter 3, except that cytochrome *c* was present at a concentration of 200 μM. The fluorescently labeled CcO was further purified by anion-exchange FPLC on a DEAE Sephadex column to remove cytochrome *c* and any remaining excess fluorescein maleimide.

Results

pH profiles of oxygen consumption activity: free enzyme and vesicles

While CcO oxygen consumption activity in wild-type enzyme increases as the pH is lowered, the oxygen consumption activity in the T100L and H93C mutants show a decrease in activity below pH 7.0, giving a local maximum of activity at around pH 6.8 (Figure 4.1). This decrease in activity of the T100L and H93C mutants was not relieved upon addition of lipid, suggesting that it is not caused by increased instability at lower pH. When the H93N mutant CcO was reconstituted into liposomes and activity was measured as a function of bulk pH on the outside of the vesicles, a similar plateau of activity at lower pH was observed. The inhibition at low pH is not as substantial in controlled vesicles, showing a plateau in activity rather than a decreased activity (Figure 4.2).

Lowered kinetic isotope effect at low temperature

Though steady-state CcO activity involves proton movements, which are generally considered to be rate limiting for the activity of CcO, the overall kinetic

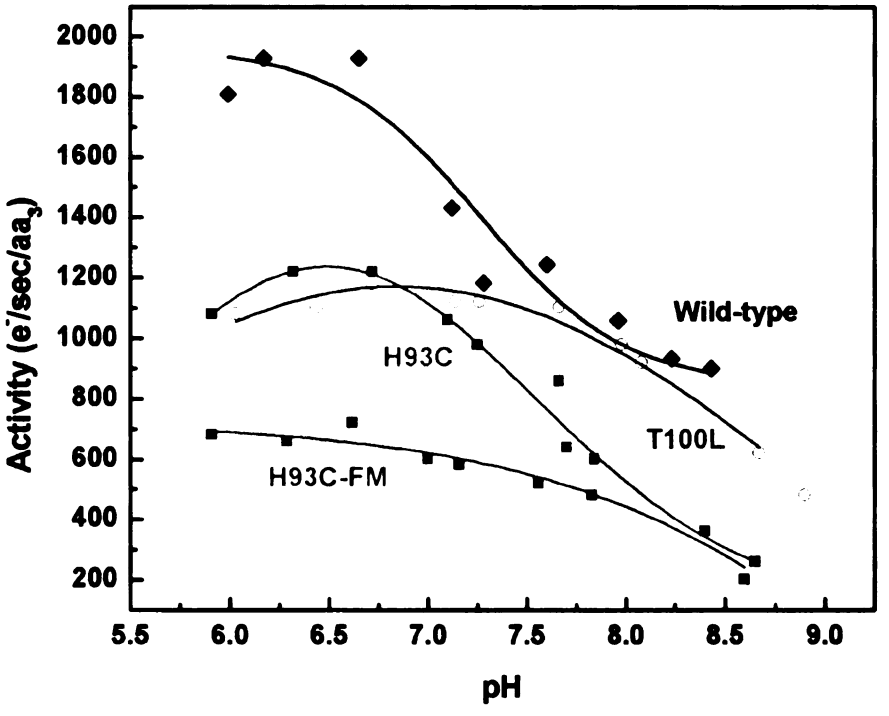

Figure 4.1: Effect of pH on catalytic activity of free enzyme. The activity of wild-type CcO (black trace) increases as the pH of the buffer is decreased. The T100L mutant (blue trace) shows similar activity to wild-type at high pH, but shows a slight decrease in activity at pH below 7.0. H93C (red trace) shows an overall lower activity. Below pH 7.0, the H93C mutant shows inhibition of activity. After binding of fluorescein maleimide to H93C (green trace), the activity is markedly inhibited across the entire pH range, but no longer has a local maximum of activity around pH 6.8. The wild-type dataset presented here is courtesy of Dr. Denise Mills.

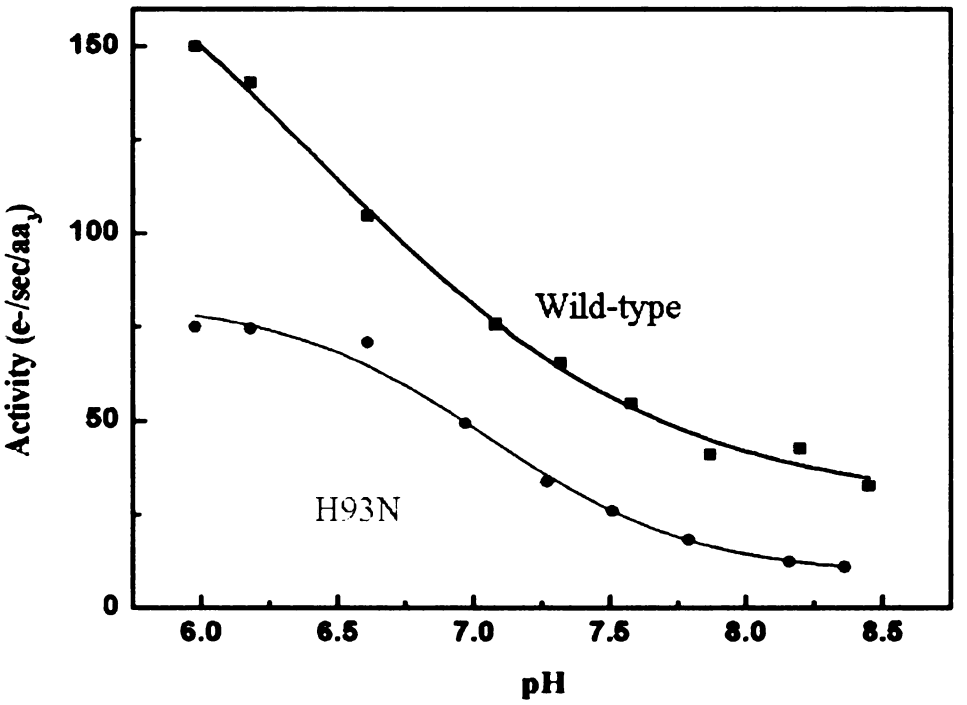

Figure 4.2: Effect of pH on catalytic activity of CcO in controlled vesicles. The oxygen consumption activity of wild-type CcO incorporated into controlled liposome vesicles increases as the pH of the buffer is lowered (black trace), much as is the case in free enzyme. In the H93N mutant, a similar increase in activity at low pH is noted (red trace), but is muted compared to wild-type CcO. The data presented in this figure are courtesy of Dr. Denise Mills.

isotope effect (KIE) is small (<3) in CcO when measured at 25 C (Figure 4.3) (Hállen and Nilsson, 1992; Karpefors et al., 2000). However, as the temperature is dropped, the KIE increases from ~1.7 at 25 C to ~8 at 4 C, suggesting that a proton movement becomes rate limiting at lower temperatures. In the T100L and H93C/N mutants, however, the increase in KIE as the temperature decreases is much less than wild-type CcO, increasing only to ~3 at 4 C. This suggests that a protonation or deprotonation event that becomes rate limiting at low temperature for the wild-type enzyme is not rate limiting in these mutants.

Oxygen consumption activity as a function of temperature

Wild-type CcO, both in normal buffer and deuterated buffer, shows a sigmoidal response of oxygen consumption activity to temperature, with increased activity at higher temperatures (Figure 4.4). The H93C/N and T100L mutants, however, both in normal buffer and deuterated buffer, show a far more linear response to temperature (Figure 4.4). The linear response of H93/N and T100L activities as temperature increases is more clearly seen in an Arrhenius plot (Figure 4.5). In wild-type CcO, a transition in the slope of the line is seen around 30 °C. A more distinct transition in the fitted line also occurs around 30 °C in deuterated buffer. In the mutants, these transitions are not clear, but rather the Arrhenius plot is best fitted with a convex curve.

UV and visible spectroscopy

UV and visible spectroscopic characterization of the mutants showed no deviation from wild-type CcO. Both wild-type and the mutants have α peaks at 606 nm and Soret peaks at 445 nm (for reduced CcO) and 424 nm (for oxidized CcO) in

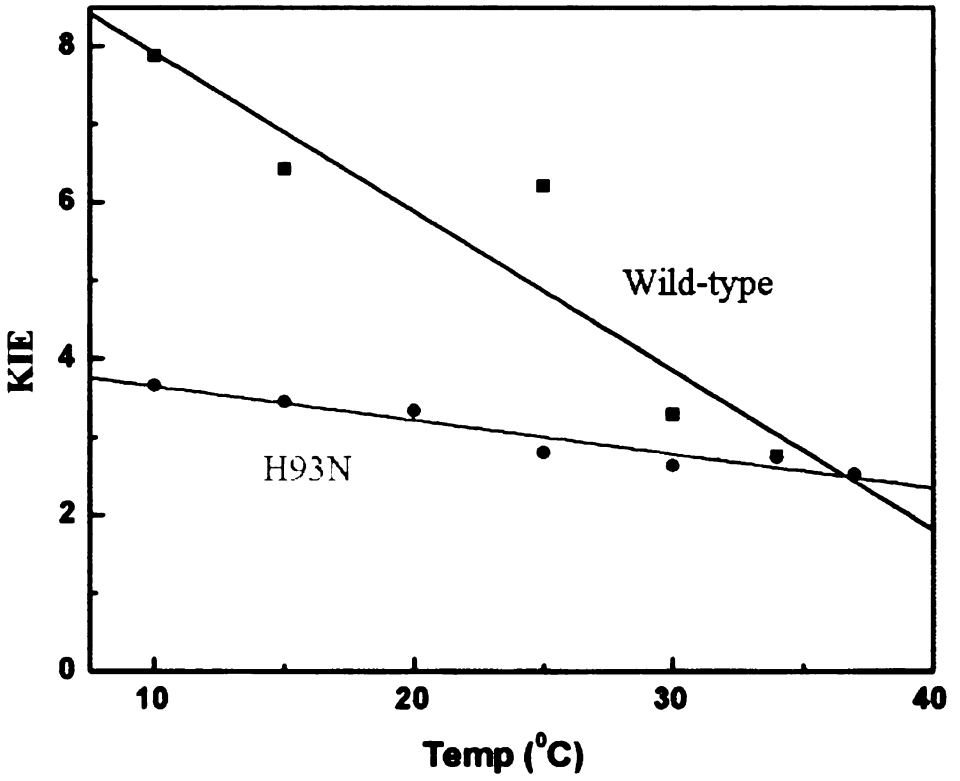

Figure 4.3: Effect of temperature on the kinetic isotope effect of steady-state CcO activity. Due to the linear response of H93N activity versus temperature in both normal and deuterated buffer, the kinetic isotope effect of steady-state activity shows only a slight increase at lower temperatures, from ~2.8 at 37 °C to ~3.9 at 10 °C (red trace). Conversely, wild-type CcO has a far more substantial steady-state kinetic isotope effect at lower temperatures, increasing from ~2.8 at 37 °C to ~8 at 10 °C (black trace). The data presented in this figure are courtesy of Dr. Denise Mills.

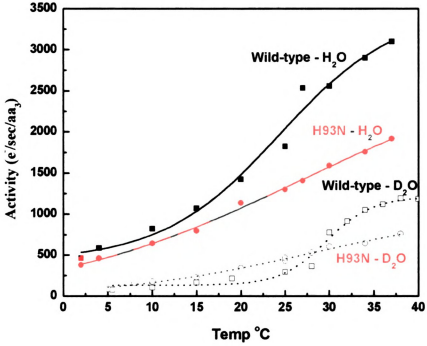

Figure 4.4: Effect of temperature on the catalytic activity of CcO. Wild-type oxidase, both in normal buffer (black trace) and deuterated buffer (dashed black trace), shows a sigmoidal response of activity to increasing temperature. H93N, however, both in normal buffer (red trace) and deuterated buffer (dashed red trace) shows a far more linear response to temperature. The data presented in this figure are courtesy of Dr. Denise Mills.

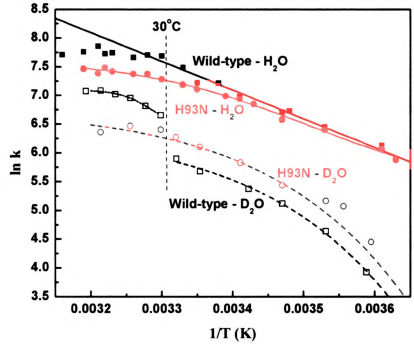

Figure 4.5: Arrhenius plots of activity versus temperature for wild-type and H93N CcO. The linear response of H93N activity as temperature increases is more clearly seen in an Arrhenius plot. In wild-type CcO (black trace), a transition is seen around 30°C (indicated by a dashed vertical line). A similar, more profound transition also occurs around 30°C in deuterated buffer (dashed black trace). In H93N, such transitions are not seen in either normal (red trace) or deuterated buffer (dashed red trace). The data presented in this figure are courtesy of Dr. Denise Mills.

their UV-visible spectra, with no additional peaks and similar half-height, full-width dimensions for the peaks. No alteration in the Cu_A site was evidenced in the 850 nm peak. EPR spectra of the mutants grown in high Mn medium reveal a normal Mg/Mn binding site, and mutant CcO samples obtained from cells grown in a high Mg medium show no alteration of the magnetic environment of the Cu_A or heme *a* sites, in agreement with the UV-vis spectrum.

Flow-flash spectroscopy

Analysis by flow-flash spectroscopy follows the reaction of fully reduced CcO with oxygen and can determine the rate of formation of each of the semi-stable intermediates of the reaction in the microseconds to milliseconds timescale (Greenwood and Gibson, 1967). The rates of formation and decay of all three intermediates, P_M, F and O, were all observed in the H93N mutant and were identical to the formation and decay rates for each intermediate in wild-type CcO.

Proton pumping

T100L, H93C/N and wild-type CcO were incorporated into lipid vesicles to analyze the proton pumping capability of the mutants. While no net acidification of the vesicle exterior is seen under controlled conditions, removing the membrane potential with the ionophore valinomycin allows protons to be pumped across the vesicular membrane, resulting in an acidification of the external bulk phase. Upon the addition of the proton ionophore FCCP, a net alkalinization of the external bulk is observed, as protons taken up from the vesicle interior for the catalytic formation of water at the CcO active site are replaced from the external bulk phase, mediated by the FCCP. The net amplitude of acidification of the external bulk during turnover

with valinomycin, measured by the pH sensitive dye phenol red (monitored as a change in absorbance at 557 nm), when compared to the amplitude of alkalinization of the external bulk during turnover with FCCP, yields an estimate of the H^+/e^- stoichiometry. Both the T100L and H93C/N mutants show unimpeded proton pumping, with a H^+/e^- ratio of ~1 as observed for wild-type CcO (Figure 4.6).

Cytochrome *c* binding

Because H93 is close to the surface of CcO (Figure 4.7) and could possibly be near the cytochrome *c* binding site (Figure 4.8), measurements of the apparent binding affinity of cytochrome *c* were performed. Steady-state oxygen consumption activity was measured for wild-type and H93N CcO as a function of cytochrome *c* concentration and plotted on a Eadie-Scatchard plot to assess effects of the mutation on the K_m for cytochrome *c*, which previous studies have shown to correlate well with the binding. When measured at pH 6.5, where the mutant CcO is inhibited compared to wild-type CcO, the H93N mutant shows two cytochrome *c* binding affinities similar to those of the wild-type CcO (Figure 4.9). Due to its location two helix-turns deeper into the enzyme than H93, the binding affinity of T100L was not measured, as it is unlikely to cause a perturbation of the binding site, particularly as the H93N/C mutants have no affect.

Zinc inhibition

Zinc is known to bind to a site on the external side of CcO and inhibit activity (Mills et al., 2002). Typical ligands for a zinc-binding site include histidines and cysteines, but can also include carboxyl groups (Holm et al., 1996; Tainer et al., 1991). Since H93 is one of the few histidine residues on the external surface of CcO,

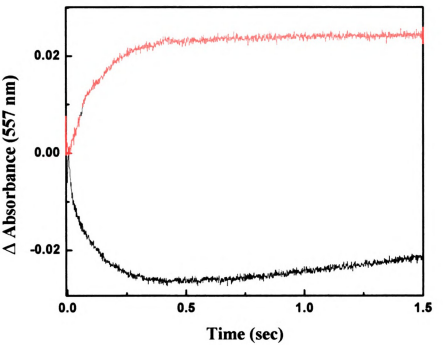

Figure 4.6: H93C shows normal proton pumping efficiency. H93 mutants, when assayed at pH 7.4, show normal proton pumping behavior. When vesicles containing the mutant are mixed with a phenol red solution with valinomycin, acidification on the outside of the vesicles is seen (blue trace). If the experiment is repeated with the uncoupler FCCP, alkalinization due to substrate proton uptake from the interior is seen to an equivalent level (red trace). Based on the amplitude of the acidification and alkalinization, the mutant has a normal pumping ratio of 1 H^+/e^-. The data presented in this figure are courtesy of Dr. Denise Mills.

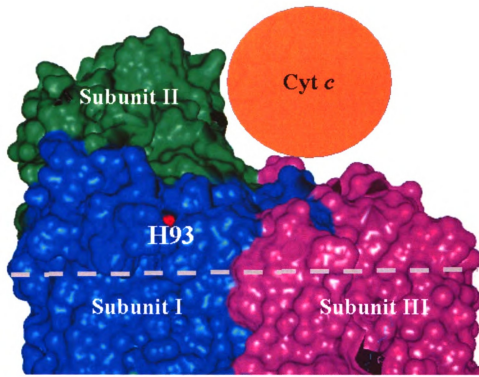

Figure 4.7: H93 is located on the solvent exposed surface. A Connolly molecular surface of *R. sphaeroides* CcO shows contribution of H93 (red color) to the molecular surface on the outside of the enzyme. It is located in subunit I (colored blue) near the interface with subunit II (colored green), but not near subunit III (colored purple). It is above the level of the hydrophobic portion of the membrane (dashed line) and approximately 12 Å away from the cytochrome *c* binding site (approximated by orange sphere).

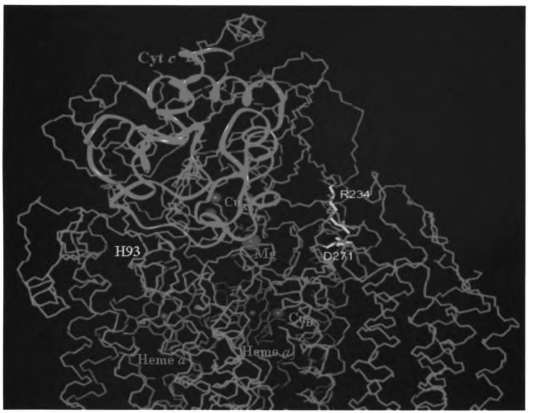

Figure 4.8: H93 resides close to the predicted cytochrome *c* docking site. The location of H93 on the solvent exposed surface and proximity to subunit II places it in a region of potential interaction with the cytochrome *c* docking site. Based on the predicted docking site, H93 is approximately 15 Å from cytochrome *c* (shown as a red ribbon).

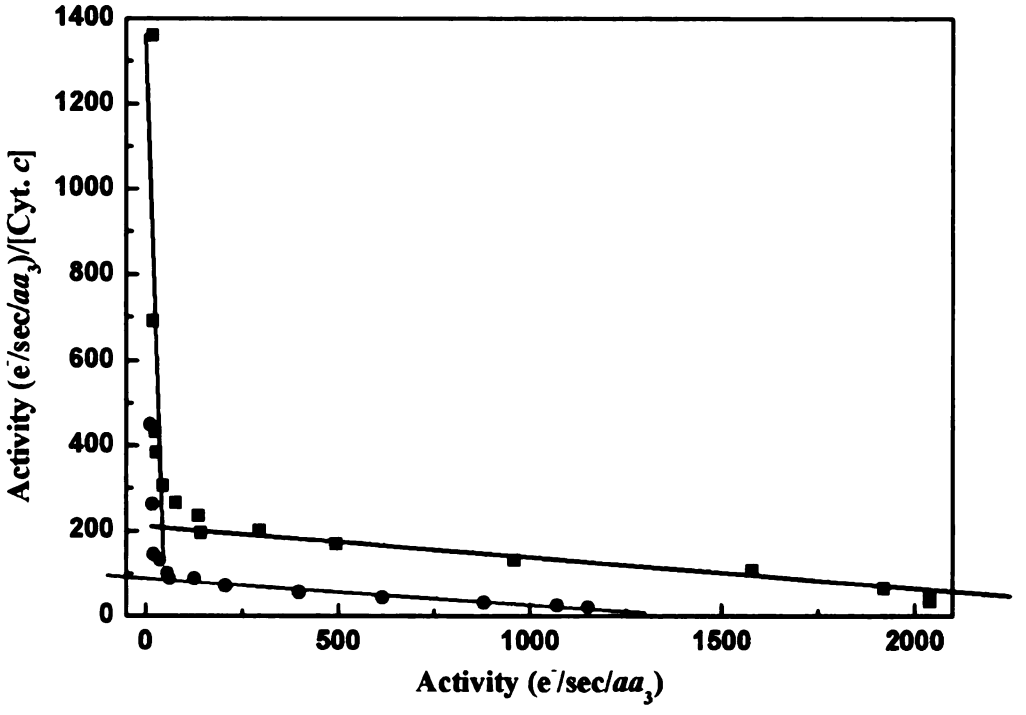

Figure 4.9: Mutation of H93 does not affect steady-state affinity for cytochrome *c*. Wild-type oxidase shows two sites for cytochrome *c* binding (black trace); one high-affinity (steep slope) and one low-affinity. At pH 6.5, where H93 mutants show significant inhibition, H93N (blue trace) shows a lower V_{max}, but both the high-affinity and the low-affinity K_m are identical to wild-type CcO. The data presented in this figure are courtesy of Dr. Denise Mills.

it is a potential target for zinc binding and therefore the mutant was examined for its ability to bind zinc. The effect of Zn^{2+} on the oxygen consumption activity of coupled vesicles was measured for wild-type and H93N CcO. Under these conditions, zinc can only bind to the outside surface of the enzyme. Zinc inhibited both the wild-type and mutant CcO to an equal extent and both with inhibition constants of 5 μM and 1 mM (Figure 4.10).

Fluorescent labeling of the cysteine mutant

The addition of a cysteine to the external surface in the H93C mutant should allow for labeling of this site by cysteine-specific fluorescent labels such as fluorescein maleimide (FM) if the residue is sufficiently exposed to the bulk phase. Although there are two cysteine residues in subunit I of wild-type CcO (assumed to be forming a disulfide bond), and two cysteine residues in subunit II (ligands to Cu_A), only subunit III (which has three cysteine residues) specifically labels with FM in wild-type CcO (Figure 4.11). In resting, oxidized H93C, the same labeling pattern is seen, with no specific labeling of the introduced cysteine (H93C) in subunit I. However, when FM labeling of the H93C mutant is carried out in the presence of cytochrome *c*, the labeling pattern is altered, with subunit I now labeling specifically. Wild-type CcO in the presence of cytochrome *c* results in the same labeling pattern as is see in the absence of cytochrome *c*, with no labeling of subunit I. FM labeling of the enzyme resulted in lowered activity overall but the shape of the curve of activity as a function of pH is closer to that observed for wild-type CcO (Figure 4.1).

Heme a_3 EPR spectrum

Though heme a_3 in its oxidized state (Fe^{3+}) is paramagnetic, and hence

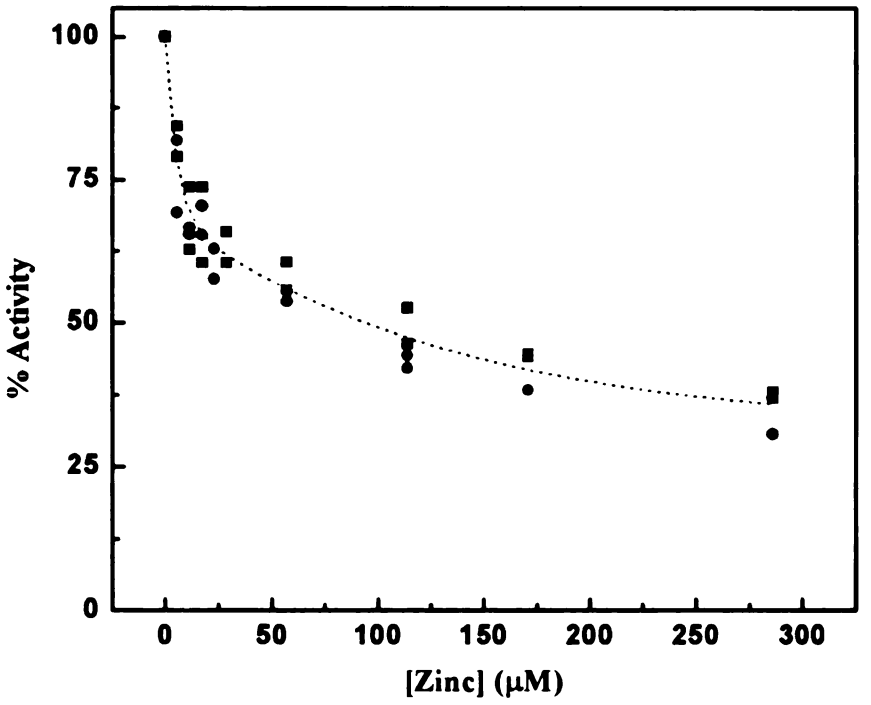

Figure 3.10: Mutation of H93 does not alter zinc inhibition. While originally investigated as a potential zinc-binding site on the enzyme exterior, both wild-type (black squares) and H93N (red circles) have similar affinity for and extent of inhibition by zinc, making the possibility of H93 being at the zinc-binding site unlikely. The best fit for both wild-type and H93N is shown as a dotted line. The exterior zinc site was specifically observed by measuring steady-state activity of coupled vesicles in the presence of zinc. Two datasets are represented for both wild-type and H93N. The data presented in this figure are courtesy of Dr. Denise Mills.

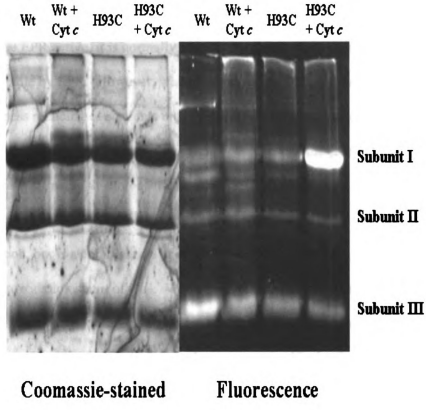

Figure 4.11: SDS-PAGE gel analysis reveals the specific labeling of H93C by fluorescein maleimide only in the presence of cytochrome *c*. In spite of the location of H93 on the molecular surface, H93C does not label with fluorescein maleimide. Labeling is only induced when cytochrome *c* is present. The additional labeling of subunit I in the presence of cytochrome *c* is not due to a change in subunit stoichiometry or protein degradation, as evidenced by Coomassie staining of the same gel. The labelling of subunit I can be attributed solely to the introduced cysteine in H93C, as subunit I does not label in either the presence or absence of cytochrome *c* for wild-type CcO.

should be EPR active, it is normally strongly magnetically coupled to Cu_B and hence undetectable by EPR. However, when CcO in solution is enzymatically turned over with excess reducing equivalents until all the oxygen is consumed and the solution becomes anaerobic, the heme a_3 EPR signal becomes visible (Figure 4.12). The mechanism allowing this to occur is unknown. The complicated splitting pattern of the spectrum is significantly different from other high-spin heme spectra and is not understood, but is a combination of at least two different species, likely indicating different oxidation states of Cu_B. When the CcO is in buffer saturated with $^{17}O_2$, the peaks in the corresponding spectrum are broadened, indicating the presence of an oxygen product attached to the heme. In a mutant that blocks the uptake of substrate protons (K362M), and hence is difficult to reduce and very slow to turn over, a different heme a_3 EPR signal is seen after anaerobiosis (Figure 4.13). This spectrum shows no ^{17}O sensitivity and is characteristic of high-spin, five-coordinate heme. The H93C/N mutant is not expected to disrupt the active site and has wild-type like activity and undisturbed reduction rates. However, when treated as above, it has a spectrum similar to the five-coordinate heme spectrum seen in K362M, and has only a small portion of the broader, ^{17}O sensitive component that is observed in wild-type CcO (Figure 4.13).

FTIR spectra of mutants

The fully reduced minus fully oxidized FTIR difference spectra of wild-type CcO have many absorption bands, most of which have not yet been definitely

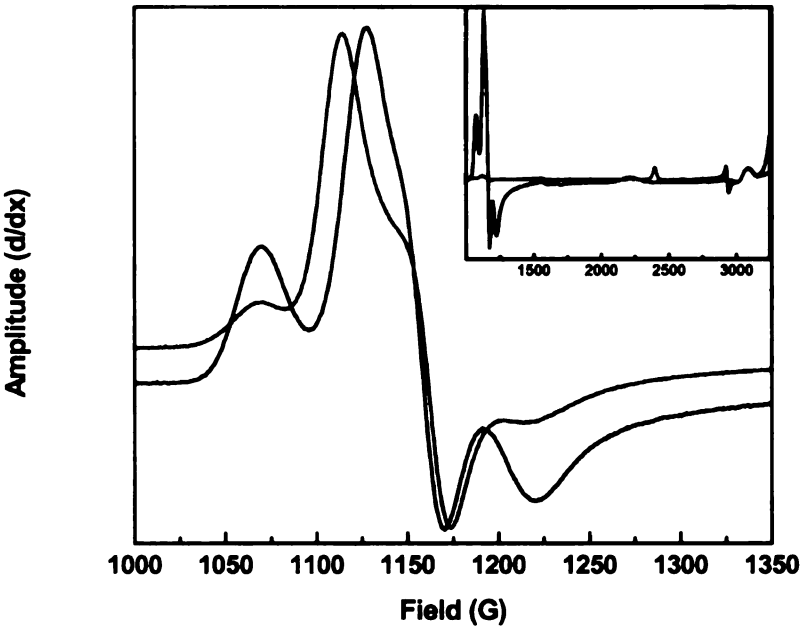

Figure 4.12: The high-spin heme a_3 EPR spectrum from wild-type CcO. When CcO is allowed to turn over in oxygenated buffer with excess reductant, a majority of heme a_3 is visible by EPR (black trace). When performed in buffer saturated with $^{17}O_2$, the resulting broadening of the signal clearly shows the presence of an oxygen ligand that is a product of turnover (blue trace). Inset: A wide scan of the sample without $^{17}O_2$, showing heme a_3 and Cu_A spectra consistent with 100% of these metals in the oxidized state but heme a completely reduced (black trace), and resting enzyme (red trace), with fully oxidized Cu_A and heme a but no heme a_3 or Cu_B observed.

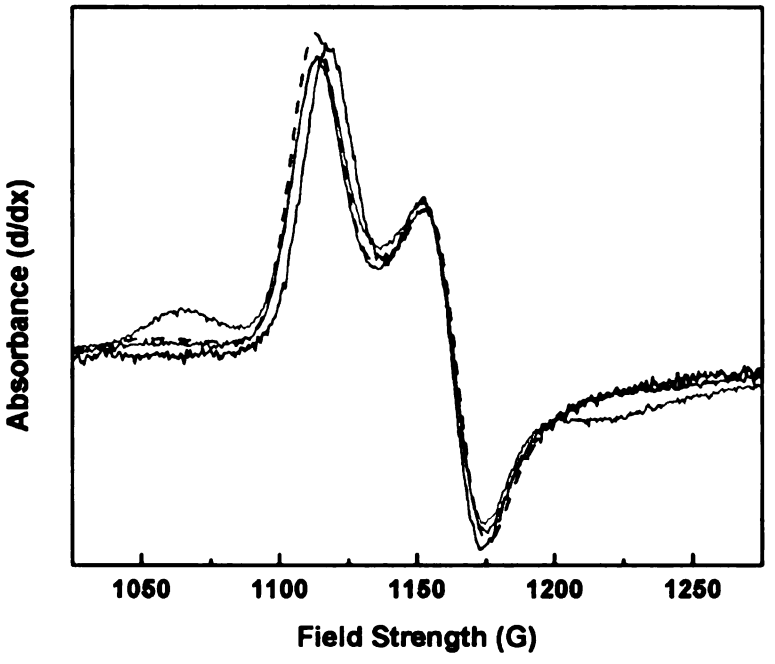

Figure 4.13: Mutations that affect the binuclear center alter the high-spin heme a_3 EPR spectrum. Mutants that inhibit reduction of the binuclear center, such as M263L (blue trace) or K362M (black trace), give a heme a_3 EPR signal different from wild-type and consistent with spectra of 5-coordinate high-spin hemes. This is supported by the lack of broadening for the M263L mutant with a heme a_3 spectrum generated in buffer saturated with $^{17}O_2$ (dashed blue trace). While turnover rates of H93 mutants (red trace) are identical to wild-type CcO at the pH used to generate the heme *a3* signal (pH 7.4), the resulting spectrum is more consistent with that seen for K362M than it is with wild-type enzyme. This suggests that this mutation has a significant effect at the binuclear center even at a pH at which activity is normal.

assigned. However, a band seen at 1104 cm^{-1} has been assigned by specific isotope labeling to belong to histidine. The H93C mutation causes a shift in the histidine mode, normally seen at 1104 cm^{-1} in wild-type CcO, to 1102 cm^{-1} (Figure 4.14). Additionally, three bands at 1090, 1082 and 1076 cm^{-1} also have a reproducibly larger amplitude in the H93C FTIR difference spectrum than is observed in the wild-type CcO FTIR difference spectrum. While the band at 1104/1102 cm^{-1} can be assigned to histidine, the other bands are not yet assigned. There are no mid-IR bands that appear to shift in the mutant CcO, but there are several that change in amplitude, with the change being significantly higher than the standard deviation between measurements of similar samples for wild-type CcO, most notably the bands at 1669, 1625 and 1613 cm^{-1} (Figure 4.15). These bands have not yet been unambiguously assigned, but are of the correct amplitude and in the correct region to arise from secondary structure.

Discussion

Proton pumping

A combination of mutational and structural studies have defined two proton uptake channels (termed the D and K pathways, based on a conserved aspartate and lysine residue in each channel, respectively), but neither mutational nor structural studies have defined an exit pathway for pumped protons. Based on studies of the high resolution crystal structure of bovine heart CcO, a third channel, termed the H channel in reference to proton pumping, was proposed (Tsukihara et al., 1996; Yoshikawa et al., 1998a; Yoshikawa et al., 2000). This channel was initially very attractive as it spans the protein and the last few residues are the only area of the

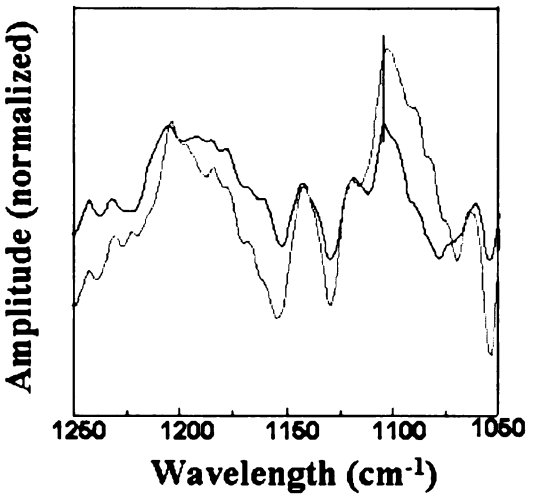

Figure 4.14: The histidine FTIR mode observed in CcO is retained in the H93C mutant but is shifted to a lower frequency. The H93C mutation causes a shift in the histidine mode, normally seen at 1104 cm^{-1} (denoted by a solid vertical line) in wild-type (black trace), to 1102 cm^{-1} (red trace). Additionally, the three bands at 1090, 1082 and 1076 cm^{-1} also show greater amplitude than seen in wild-type. While the band at 1104/1102 cm^{-1} can be assigned to histidine (but cannot be H93), the other bands are not assigned. The increased amplitude of the histidine band is likely due to some (possibly small) conformational change. The data presented in this figure are courtesy of Dr. Warwick Hillier.

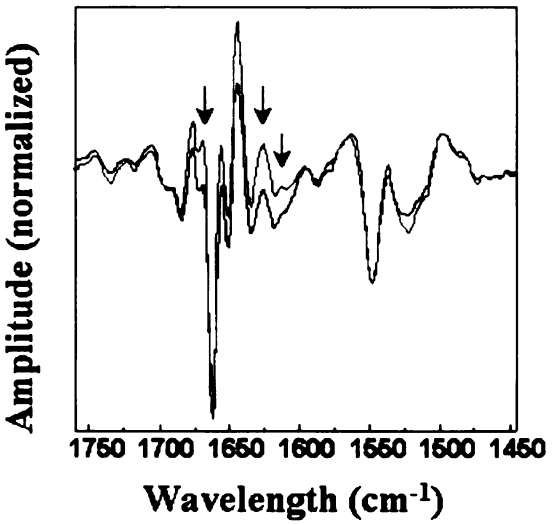

Figure 4.15: The mid-IR region of the FTIR difference spectrum shows changes in the H93C mutant that could reflect an alteration in secondary structure. While there are no mid-IR bands that appear to shift upon the mutation, there are several that increase in amplitude significantly beyond the standard deviation between measurements of similar samples. While the bands cannot yet be assigned, the modes at 1669, 1625 and 1613 cm^{-1} (black arrows) show increased amplitude in the H93C mutant (red trace) compared to wild-type (black trace). The data presented in this figure are courtesy of Dr. Warwick Hillier.

protein that differs in the oxidized and reduced crystal structures. However, the role of this channel in CcO function was rapidly dismissed by most investigators due to the lack of conservation in the bacterial CcO of a number of residues proposed to participate in the channel. In addition, several residues of the proposed channel that are conserved were mutated in bacterial CcO, resulting in unaltered activity (Lee et al., 2000). The normal activity of these mutants, as well as the lack of conserved residues through much of the channel suggested that the proposed pathway was not used for proton-pumping. The extensive conformational changes in the position of the terminal residue of this channel (D51, bovine numbering) seen between the oxidized and reduced crystal structures (Yoshikawa et al., 1998a) was also discounted, as this residue is not conserved between species. However, the cause of the redox change in this area is still to be explained. The residue in *Rhodobacter sphaeroides* that is spatially close to this position is H93, located at the top of helix II in subunit I (Figure 4.16).

Previous work on zinc inhibition at the exterior surface of CcO suggested H93 as a possible zinc binding site (Mills et al., 2002), based on its location and geometry. Zinc inhibition causes a reduction in proton backleak, although no proton backleak pathway has yet been defined. The mutation of H93 to either asparagine or cysteine did not alter the affinity for zinc, as measured by the inhibition constant, making its role in zinc binding unlikely. However, several other unique characteristics have been noted for these mutant enzymes. In wild-type CcO, activity is increased as the pH is lowered. This is due, in part, to the increased concentration of one of the substrates of the reaction that CcO catalyzes: protons. In the H93N/C mutants, however, the oxygen consumption activity does not increase any further as

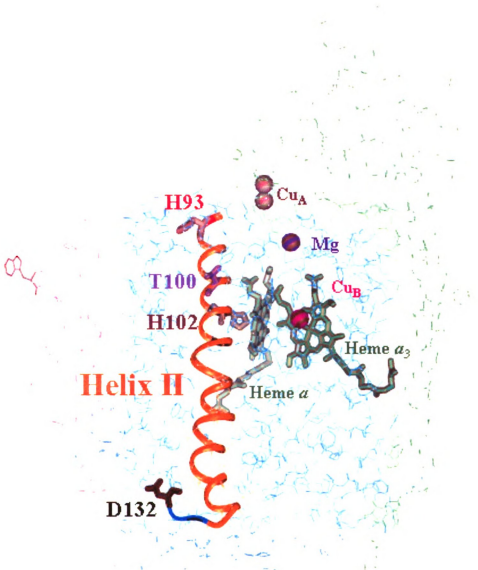

Figure 4.16: Helix II of subunit I contains H93, T100 and the heme *a* ligand, H102. H93 (in red) is on the outside of the enzyme in subunit I (in blue). It is at the top of helix II (colored orange), which also contains H102 (in gray), a ligand of the heme *a* iron, and T100 (in purple), which is two helical turns deeper into the enzyme and near the heme *a* propionate. The loop at the end of helix II (in orange) also contains D132 (in black), the beginning of the D-path proton uptake channel.

the pH drops below 7.0, suggesting that something other than protons has become rate limiting at lower pH (Figure 4.1).

Change in the rate-limiting step

Indications that the H93N/C mutations have altered the normal rate-limiting event are also indicated by changes in the kinetic isotope effect in the mutants in comparison to wild-type CcO. In processes where proton transfer is rate limiting, activity decreases dramatically when turnover is carried out in deuterated buffer due to the large relative mass difference between protons and deuterons. In these cases where proton transfer is rate limiting, the KIE can range from 4 to 10 for a single protonation event (Schowen and Schowen, 1982). When the rate-limiting step does not involve proton transfer, though, there is only a minimal perturbation in the rate of activity due to the decreased activity of D_2O, resulting in a KIE of only 1 to 2.

While a larger KIE (~8) is measured for CcO during the final step in the reaction, the F to O transition (see Figure 1.4) in the flow-flash method (Karpefors et al., 2000), the KIE for steady-state oxygen consumption activity at room temperature and across the pH range remains approximately 3 (Hállen and Nilsson, 1992). As the temperature of the reaction is lowered, however, proton transfer becomes more rate-limiting to the steady-state activity. Consequently the KIE increases to ~8 at 4 C and pH 6.5. In the H93C/N mutant, however, this increase in KIE of steady-state activity at lower temperatures is not seen. The KIE measurements at pH 6.5, where H93N/C oxygen consumption is inhibited compared to wild-type CcO oxygen consumption, do not increase above 4 in the mutant CcO (Figure 4.3).

There are two ways of producing a lower KIE: decreasing the activity in H_2O, or increasing the activity in D_2O. In the case of H93N/C, it has a higher activity than that of wild-type CcO in D_2O, resulting in the lower KIE (Figure 4.4). This is further evidence that proton transfer is no longer rate limiting in the H93N/C mutant, where the decrease in activity when changing from protonated buffer to deuterated buffer can be attributed to a general solvent effect, whereas proton transfer in wild-type CcO is rate limiting, having a decrease in activity in deuterated buffer that is beyond the limitation imposed by a general solvent effect.

The final evidence that suggests a change in a proton-associated rate-limiting step comes from Arrhenius plots of oxygen consumption rates as a function of solvent temperature. In wild-type CcO, there is a break in the linearity of the Arrhenius plot at approximately 30 °C. The break in linearity suggests a change in the rate-limiting step to a process that is not limited by thermal energy. Interestingly, this break is also seen at 27 °C in bovine heart CcO (Robinson et al., 1985), indicating that the change in rate limitation occurs at about the same physiological temperature for both species. In the H93C/N mutants, the Arrhenius plot is generally linear across the temperature range studied, with a slightly convex curvature (Figure 4.5). This suggests that there is no abrupt change in the rate limiting step in the H93N/C mutants as there is in wild-type CcO but rather that the activation energy decreases as the thermal energy increases (Truhlar and Kohen, 2001).

Conformational changes at the H93 site

The use of the H channel in proton pumping in *Rhodobacter sphaeroides* is unlikely, based on the normal proton pumping efficiency observed for these

mutants (Figure 4.6). However, structural data suggesting the region around H93 is involved in a conformational change remains of interest. Given the surface location of H93 (Figure 4.7), it was expected that the H93C mutant would label readily with the cysteine-specific fluorescent label FM. However, under oxidized, resting conditions, this site showed no specificity for labeling. Specific labeling of the introduced cysteine could only be achieved when the labeling was carried out in the presence of cytochrome *c* (Figure 4.11). Comparison with labeling of wild-type CcO in the presence of cytochrome *c* ensures that the labeling of subunit I is only at the introduced cysteine and not due a breaking of the disulfide bond found in the same region. The inability of FM to label H93C except in the presence of cytochrome *c* suggests that a conformational change is induced by the binding of the electron donor, perhaps similar to the one observed with the change in redox state of bovine CcO. This is not unreasonable, as the binding site of cytochrome *c* is in the vicinity of Cu_A and heme *a* and may in fact induce a conformation of the enzyme that is similar to that caused by the change in redox state of these centers.

Long-range effects of the H93N/C and T100L mutations

EPR evidence of long-range effects

The paramagnetic 5/2 electron spin of the high-spin heme a_3 and the 1/2 electron spin of Cu_B in oxidized CcO should make them ideal for study by EPR, but the strong magnetic coupling of these two sites, by a mechanism that is still unclear, renders them both undetectable. This coupling can be broken by the addition of a single electron that can reduce Cu_B to a diamagnetic state, resulting in an EPR-visible heme a_3 signal. This was previously noted in 1976 (Aasa et al., 1976), but the resulting high-spin heme spectrum only accounted for approximately 20% of the

heme a_3 and could not be interpreted. This high spin heme a_3 spectrum can be produced with nearly 100% yield, by adding an excess of reductant to a sample of CcO which allows the enzyme to turn over until the sample becomes anaerobic. It is still unclear why these conditions reproducibly result in an enzyme with heme a_3 and Cu_A oxidized, heme *a* reduced, and Cu_B either reduced or in a state that is no longer magnetically coupled to the nearby heme a_3 (Figure 4.12, inset), particularly with the excess amount of reductant present which should fully reduce the CcO. However, observation of this unusual spectrum provides insight into the influence of even distant mutants on the active site.

When CcO samples are treated to yield a state with an EPR visible high spin heme a_3 signal using enzyme that is saturated in $^{17}O_2$, the resulting spectrum is clearly broadened and the outer wing features are diminished. This suggests that there are at least two different components of the spectrum, as previously postulated (Aasa et al., 1976), one or more of which is ^{17}O sensitive (the outer features) and another that is ^{17}O insensitive (the center transition). The broadening also demonstrates that there is an oxygen ligand on the heme a_3. The spectrum does not resemble typical 6-coordinate high-spin hemes, though it must be 6-coordinate to have an oxygen ligand, and suggests that interaction with the surrounding protein or the nearby Cu_B gives the ligand a unique geometry. Alternatively, the unusual spectrum may be due to the presence of several species, indicating that the sample is trapped in different stages of the turnover cycle, or may arise from a spin- coupling interaction that has not been accounted for. While no definitive structural assignments can be made yet, there are a limited number of possible states that could account for this spectrum. The presence of the EPR spectrum means the heme a_3 iron must be

ferric (Fe^{3+}). Additionally, the magnetic coupling to Cu_B that is present in resting enzyme must be broken or substantially altered. The enzyme does not bind oxygen until heme a_3 is ferrous (Fe^{2+}), and at that point rapidly reacts to become a ferryl-oxo (Fe^{4+}), diamagnetic species. Therefore the oxygen ligand seen must be in the form of either a hydroxyl or a water.

The effects of the mutation of H93 are not localized to the immediate vicinity of the residue but are felt at a long distance, as evidenced by a different heme a_3 EPR signature compared to wild-type, after both have been allowed to enzymatically turn over until anaerobiosis. Other mutants give heme a_3 EPR signals different from wild-type CcO, such as K362M which blocks the substrate proton uptake channel, or M263L which alters the Cu_A redox potential and makes electron transfer always rate limiting (Figure 4.13) (Zhen et al., 2002). Both inhibit the reduction of the binuclear center. These mutants give spectra that have a lineshape typical for rhombic species and are consistent with the spectra of 5-coordinate high-spin hemes. This is supported by the lack of line broadening when the sample is generated in buffer saturated with $^{17}O_2$, indicating there is no O_2 derived oxygen ligand on the heme. While the catalytic turnover rates of the H93 mutants are identical to wild-type CcO at the pH used to generate the heme a_3 signal (pH 7.4), the resulting spectrum is more consistent with that seen for K362M and M263L than it is with wild-type CcO. This suggests that this mutation has a significant effect at the binuclear center even at a pH at which catalytic activity of the mutant CcO is identical to wild-type activity.

FTIR evidence for long-range effects

Additional evidence for the H93 mutants having long ranging effects comes from the redox-induced FTIR difference spectrum. The redox-induced FTIR difference spectrum reports on changes both in the vibrational modes of specific residues as well as overall secondary structure changes. The overall FTIR difference spectrum of H93C is very similar to the spectrum of wild-type CcO. All of the bands present in the wild-type spectrum appear to be present in the H93C spectrum, indicating that H93 itself is not among the residues that change their vibrational modes when the oxidation states of the metal cofactors are changed (Figure 4.15). This high degree of similarity in the spectra also indicates that there are no large structural changes in the overall protein structure that are caused by the mutation.

There are subtle changes, however, that suggest structural changes that may be important in causing the perturbations noted for the H93C mutant. The mode at 1104 cm^{-1} has been definitely assigned as arising from a histidine vibration, based on specific isotopic labeling of histidine with ^{15}N. There are several histidines in CcO that could undergo changes based on the redox state of the metal cofactors, most notably the histidine ligands of the metal centers themselves. H93 was also a candidate for this mode, given the different conformations of the corresponding bovine residue in the oxidized and reduced crystal structures, and the changes in accessibility to fluorescent labeling H93C in *R. sphaeroides* upon the binding of cytochrome *c*. However, the presence of this mode in the FTIR spectrum of the H93C mutant rules out this vibration as arising from H93. The shift of this mode by 2 cm^{-1} from 1104 cm^{-1} to 1102 cm^{-1}, though, implies that the residue this mode reports on is affected by the mutation. This could imply a change at the binuclear active site, indicative of the long-range effects of this mutation from the noted changes in the

heme a_3 EPR spectrum. However, there are other potential histidine residues that this mutation could affect, such as the heme *a* ligand H102. This residue is located on the same helix as H93 and T100 (helix II, Figure 4.16). Due to the direct ligation of H102 to heme *a* it is likely to be affected by the redox state of the heme and could transmit this change to H93 and T100 via a slight helical tilt or unwinding, for example. It is interesting to note that the histidine FTIR mode in bovine CcO is located at 1101 cm^{-1} instead of 1104 cm^{-1}. Assignment of this mode to H102 would be consistent with this change, as there is a significant shift in the peak position of the low-spin heme *a* EPR spectrum between bovine and bacterial CcO that has been interpreted as being caused by a difference between the hydrogen bonding of the histidine ligands of the heme.

Other changes are observed in the amide I region of the FTIR difference spectrum between H93C and wild-type CcO. This is a convoluted region of the spectrum with many overlapping modes that make assignment of the bands difficult. In addition to specific modes arising from single residues, this region also contains information regarding the secondary structure of the entire protein. While these modes cannot yet be assigned, it is likely that they are reporting on secondary structural changes. Since the bands in question are observed in both the wild-type and the H93C mutant spectra, but with different intensities, they must arise from changes that occur in both the wild-type and the mutant CcO with the only difference being the extent of the change. For such a change in peak intensity to occur for a specific mode of an individual residue, there would have to be a change either in the extinction coefficient for that mode or a change in population of that residue undergoing the change. Since the difference spectrum is taken between fully

oxidized and fully reduced CcO, it is unlikely that there is a difference in population or a change in extinction coefficient. Thus it is reasonable to assign these bands as markers of secondary structural changes, implying that there are differences between wild-type and the H93C mutant in the extent of the secondary structural changes that occur as the redox states of the metal cofactors are changed. This interpretation is also consistent with the shift in the histidine mode described above. For the H93C mutation to affect the local environment of the H102 heme ligand, the effect would likely be translated through the helix that is shared by the two residues. A slight perturbation in the helix would translate this effect between the mutation and the histidine ligand and should be observed in the amide I region of the spectrum.

Possible roles for H93 and T100 in enzyme activity

Cytochrome *c* binding

The location of H93 on the exterior surface of the enzyme raises the possibility that the effects seen are due to surface effects such as altering cytochrome *c* binding. Indeed, the proposed docking site of cytochrome *c* (Roberts and Pique, 1999) is less than 15 angstroms from H93 (Figure 4.8). However, cytochrome *c* steady-state kinetic assays demonstrate that there is no effect of this mutation on cytochrome *c* affinity (Figure 4.9). This is further corroborated by the characterization of the T100L mutation, which behaves similarly to the H93N/C mutations. T100 is two helix turns deeper into the enzyme from H93 and is not visible from the outside. Yet substitution of this residue by a leucine results in an enzyme with characteristics similar to those observed in the H93C/N mutations.

Proton pumping

The data presented here clearly indicate that while the H93 and T100 residues have important implications for the normal function of CcO, they are not directly involved in proton pumping. Proton pumping data demonstrate that this function is not impaired in the mutants, and the loss of a deuterium isotope effect and altered pH profile of oxygen consumption activity indicate that another process has become rate-limiting. The unaltered sensitivity of the mutants to inhibition by zinc also indicates that these residues are not involved in proton transfer in either the forward or backwards direction.

Redox potential of metal cofactors

The effects of these mutations can be interpreted instead as causing a change in the redox potential of either Cu_A or heme *a*. The shift of the histidine mode observed by FTIR would indicate that it is the heme a potential that has been altered. This is also supported by the T100L mutation. The location of H93 at the surface and near subunit II suggest that this residue might affect Cu_A. However, T100 is located further into the enzyme, away from any obvious connection to subunit II and the Cu_A site, but within a few angstroms of the heme a propionates. Flow-flash spectroscopy data suggest that there is no difference in the oxygen reduction process for H93N compared to wild-type CcO, implying that there is no change in redox potential of any of the metal centers. However, this method only follows the oxidation of fully reduced enzyme and does not provide any information on the consecutive reduction of each metal center as it occurs during steady state catalytic turnover. Hence this method provides little, if any, information on the redox potentials of either heme *a* or Cu_A under normal turnover conditions.

Conformational control

The effects of mutating H93 are not limited to changes in redox potential. Fluorescent labeling, FTIR and EPR indicate that this residue undergoes a change in conformation during catalysis and that mutation of this residue causes a wide-ranging conformational change. The presentation of H93C for FM labeling only when cytochrome *c* is bound to the enzyme (Figure 4.11) verifies the movement of this residue in a similar manner as was observed in the crystal structure analysis of the bovine CcO. The change in position is likely from perturbation of the helix due to heme *a* ligand changes upon redox change. This is consistent with the changes in the FTIR spectrum, which shows a perturbation of a histidine, possibly the heme *a* histidine ligand. The changes induced by mutation of H93 are not localized to the immediate region of the residue and the helix which it is on, however, as the alteration of the heme a_3 EPR spectrum indicates. When H93 is mutated, there is also an effect on the conformational changes that normally occur during a change in redox state, altering the overall behavior of CcO as seen in the changes in the amide I region of the FTIR spectrum. The lowered activity at low pH for the H93N/C and T100L mutants might suggest that the protonation of H93, or a residue in its vicinity, is important for maintaining an active enzyme. Thus, the top of helix II in subunit I may be a conformational gate that affects electron transfer, as well as global conformation that can influence the active site.

Chapter 5:

Summary and Perspectives

Scientific investigation of the redox enzyme known as cytochrome c oxidase (CcO) has a history dating more than 100 years. However, there is still no clear understanding, at a molecular level, of its mechanism of energy transduction. This is not due to lack of brilliant minds working on the problem, but rather to the complexity of its function. CcO spans the lipid bilayer and takes electrons from one side and protons from the other, catalyzing their combination with molecular oxygen at a bimetallic heme/copper site to produce two water molecules. The manner in which this enzyme controls the cleavage of the stable dioxygen bond, while minimizing the release of any toxic intermediates, has been difficult to determine because of the rapidity of the reaction. But even a good understanding of the oxygen chemistry fails to address the fundamental action of this enzyme: how is the energy released by the oxygen bond cleavage utilized in translocating protons across a membrane to create an electrochemical gradient?

The emergence of high-resolution crystal structures of mammalian (bovine heart) (Tsukihara et al., 1995) and bacterial (*Paracoccus denitrificans*) (Iwata et al., 1995) CcO in 1995 allowed for a great advance in understanding of CcO activity, but did not reveal the mechanism of how it pumps protons. Indeed, the crystal structures give little insight into the oxygen chemistry and the conformational dynamics that occur during the reaction cycle, for which additional methods of investigation are needed. Mutational studies of bacterial CcO have been instrumental in fully defining the proton uptake channels, but have not yet been able to define proton or water exit channels.

As the understanding of the oxygen chemistry and electron transfer in CcO becomes more detailed, it is essential to address the routes of proton and water exit in the protein if a comprehensive understanding of CcO function is to be obtained. Indeed, proton exit is the most fundamental question to be addressed, as proton pumping is the ultimate function of this enzyme and the unidirectional nature of the pump is likely to be regulated on the exit side rather than the intake side of the channel. Though the necessity for understanding water exit pathways in CcO is not as clear as the necessity for understanding proton exit, the high rate at which protons can transfer across a hydrogen bonded water chain, along with the possibility of substrate water providing such a chain from the active site to the protein surface, make an understanding of water exit necessary in order to understand proton pumping and its regulation.

Water and proton exit and their relationship to proton backleak

The data presented in chapters two and three illustrate the need to define the water channel. Using the non-redox active Mg/Mn site as a probe that is located approximately midway between the binuclear active site and the exterior protein surface, it is demonstrated that product water catalytically produced at the active site passes the Mg/Mn site along its exit route. From the Mg/Mn site, the product water reaches the bulk on the exterior side of the protein; our results suggest that the water exits via a single, specific channel formed by the subunit I/II interface that terminates at the protein surface near R234 on subunit II. The exit of water towards the exterior surface instead of the interior surface creates the potential for protons to travel down a transiently formed water chain from the bulk phase to the active site, driven thermodynamically by the proton gradient created by CcO and the other members of

the electron transport chain, short-circuiting the proton pumping function the enzyme is designed to carry out.

The exit of water towards the exterior surface can also provide a mechanism of control for the enzyme. Under conditions of high membrane potential, proton pumping no longer needs to occur and eventually will not be feasible as the membrane potential reaches values above the driving force provided by the oxygen cleavage reaction. Yet there are several reasons to allow continued oxygen chemistry when the membrane potential is high. First, the potential for the creation of damaging reactive oxygen species if the oxygen chemistry is halted at an intermediate step suggests that electron transfer activity should be allowed to persist in the absence of proton pumping when required. Secondly, inhibiting the oxygen chemistry would result in a build up of reducing equivalents earlier in the respiratory chain. The build up of these equivalents has been shown to be the source of the reactive oxygen species that do the most damage in the cell. A water chain from the positive exterior side of the enzyme to the active site could provide a pathway for the backleak of protons, bypassing the gating mechanism that creates the unidirectional nature of the proton pump under normal conditions, when the membrane potential reaches a sufficiently high voltage.

The backleak of protons is observed for CcO in controlled proteoliposome vesicles, particularly for CcO with mutations that hinder the uptake of pumped protons from the interior via the D-pathway. This backleak was long assumed to be through the lipid bilayer, as proton diffusion across lipid bilayers with a pH gradient has been experimentally verified, but this diffusion cannot fully

account for the rate of proton backleak that is observed (Brookes et al., 1997). However, the backleak rate is decreased in CcO inhibited with zinc, in some mutants of CcO (R481K), in different forms of CcO (bo_3), and in CcO that is missing subunit III, indicating that most backleak observed occurs through the protein. It has not been clarified if backleaked protons cross the entire protein and then are taken back up to be used as substrate or if they transfer directly to the active site where they are consumed, or both. If the protons are transferred across the entire protein before being taken up as substrate, it is unlikely that the water exit channel facilitates this movement. If they are transferred directly to the active site, though, the water channel provides a potential route for this movement.

Experiments with isotopically labeled $^{17}O_2$ described in chapter three clearly indicates the use of the defined channel in translocation of product water, but the experiments do not address the potential for proton transfer along this pathway. Tracking of oxygen labels can clarify if water can move through proton channels, but it is not possible to differentiate whether protons are transferred as a water molecule, or as isolated protons. Thus the proton exit pathway is yet to be defined. It is possible that pumped protons exit via the same pathway as the water, though this would require two distinct gating steps: one to enforce the unidirectionality necessary to pump protons against their gradient and a second to prevent short-circuiting of the pump by protons from the exterior side reaching the active site. If the gate that gives the pump its unidirectionality were located above the active site, a second gate to prevent short-circuiting would not be necessary. However, in this case a second gate would still be required to separate the pathways for pumped and substrate protons.

There are two structural features of the water exit channel that suggest it is used for water transport only and not for pumped proton exit. The first of these features is a hydrophobic narrowing that occurs midway between the Mn and the protein surface (Figure 5.1). This narrowing has many of the characteristics of the hydrophobic narrowing found in the middle of aquaporin (Murata et al., 2000) that has been suggested to impart the selectivity for water and against protons that is integral to aquaporin function. Both channels have a six angstrom carbon-carbon distance at their narrowest point, which corresponds to a three angstrom van der Waals distance that is just large enough for water to fit through. Additionally, both in CcO and in aquaporin there are a pair of hydrogen bond donors on either side of the narrowing that can interact with the oxygen of water, pointing the protons of the water towards the walls of the hydrophobic channel, preventing hydrogen bonding across the narrowing that would be required to transport protons.

The second feature suggesting that the water channel is not used as a proton exit pathway is the presence of the Mg/Mn. The reason for this non-redox active metal at a site 12 angstroms from the active site is puzzling. The line broadening of the Mn EPR spectrum due to product $H_2{}^{17}O$ water indicates that the product water exit pathway passes the Mn, and that the waters bind to the metal. While this interaction with the Mn is unlikely to substantially affect the rate of water movement, it will have a dramatic effect on proton transfer. It is well known that waters ligated to metals can be more acidic, often with a pK_a for the loss of one proton below 10 (Alba et al., 2003; Trachtman et al., 2001). This would prevent the transfer of an extra proton through any water that is ligated to the metal, as the water would not be able to accept any additional proton. The metal could also serve to limit

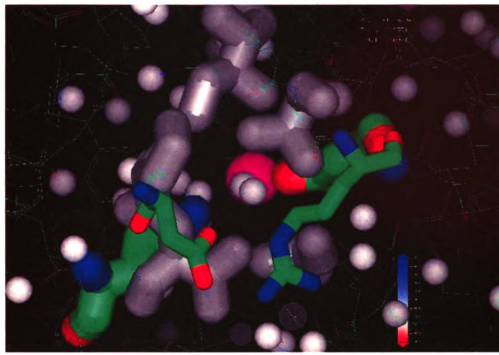

Figure 5.1: The hydrophobic constriction in the water exit channel between the Mn and the surface. The Mn at the bottom of the channel is depicted as a magenta sphere and crystallographically defined waters are shown as white spheres. The residues composing the hydrophobic narrowing are shown in gray and potential hydrogen-bond donors on either side of the constriction are shown in stick form.

proton transfer by a general electrostatic effect. The presence of a large positive charge in the low dielectric of a protein interior that would be created by a Mg/Mn buried in the protein would create a strong repulsion for protons, making it highly unlikely that proton transport would occur through a channel that bypasses the metal site.

There are several species that do not have the Mg site in their CcO (Hosler et al., 1995), which brings into question the necessity for this metal site in CcO function. This lack of conservation can be explained by the redundancy of the function proposed for this metal. The presence of the hydrophobic narrowing provides an initial barrier to proton transport though the water channel. The Mn would provide a mechanism for preventing further transport of protons that have made it past this narrowing, and due to the redundancy of this function Mn is not strictly required to prevent short-circuiting of proton pumping. Additionally, it is possible that CcO that does not have a metal at this site may have a different proton exit pathway and/or a less well controlled activity (Mills and Ferguson-Miller, 2002). No proton exit channel has clearly been defined in any species and there is a limited number of species for which the crystal structure of CcO has been determined, so there is not enough evidence to suggest that the proton exit pathway is strictly conserved across different species.

It can thus be proposed that the water channel is used only for water exit under normal conditions. Under high membrane potential conditions, it is possible that the high thermodynamic driving force on protons from the exterior could be enough to overcome these barriers to proton translocation through a subtle

conformational change and the low level of proton backleak experimentally verified can be supported through this channel.

Regulation of CcO

With the definition of a water exit channel that excludes proton translocation, the issue of a proton exit route still needs to be addressed. Of the enzymes known to pump protons, only one, bacteriorhodopsin, has an entire pathway for proton translocation been defined. The definition of the pathway in BR was obtained through a combination of mutational studies along with high-resolution crystal structures of the enzyme in most of its intermediate states. In CcO there is an abundance of mutational data, but intermediate states have not been successfully crystallized. The mechanism of proton pumping and proton transfer against a gradient, as it is currently understood in other proteins (see chapter one), indicates that the complete proton pathway is often not present in the resting state of the enzyme. Certain parts of the path form transiently to allow proton movement and then rapidly disassemble again. This appears to be the primary mechanism that allows for unidirectional transport against a gradient.

There is currently no explicitly defined proposal for proton exit in CcO, but the H93N/C and T100L mutants begin to give us insight into conformational changes that occur in the enzyme during catalytic turnover that may regulate the presence of a proton exit channel. While the primary effect on activity that is observed when these residues are mutated can be attributed to an alteration in the heme *a* redox potential, they also provide evidence for conformational change that has the potential for significantly affecting all the processes of CcO function.

The FTIR and fluorescent labeling of H93C indicate that this residue is buried when the enzyme is in the resting state and becomes exposed to solvent when cytochrome *c* binds to the enzyme. This conformational switch may be translated through helix II of subunit I to the histidine ligand of heme *a*, H102, which alters the redox potential of the heme, or vice versa. This helical movement also has the potential of affecting proton movement in the enzyme. The loop at the bottom of helix II contains D132, the entry point to the D path proton channel (Figure 5.2). Additionally, several residues that are part of the D pathway are found on helix II. Though all movements need only be very small, the overall effect would be a change across the helix.

The conformational changes associated with H93 are not necessarily localized to helix II. The disruption of the high-spin heme a_3 EPR spectrum suggests mutation of this enzyme also affects the binuclear active site. A similarly altered high-spin heme a_3 spectrum is observed for the mutation M263L that nominally has only a local affect on the Cu_A redox potential, but nevertheless results in a heme a_3/Cu_B site that is hard to reduce. The heme a_3 spectra of these two mutants also resemble the spectrum obtained for K362M, which causes an alteration in substrate proton uptake and also affects the heme a_3 reducibility. To account for the behavior of these mutants, it appears necessary to invoke a long-distance conformational effect. A mechanism that could account for the mutation of H93 affecting substrate proton uptake would involve an interaction of H127 on helix II with H300 on helix VI. H300 is one residue away from S299, a residue known to be part of the K pathway for substrate protons. If it is assumed that mutation of H93 can cause a

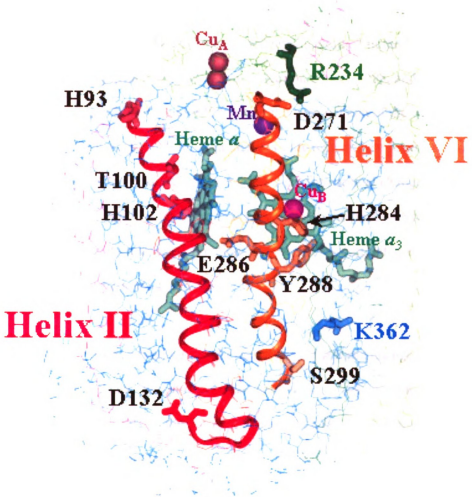

Figure 5.2: Helices II and VI of subunit I contain many of the critical residues identified for CcO function. Helix II, shown in red, contains the residues H93 and T100, as well as the heme *a* ligand H102. The entry to the D path, D132, is located on the turn between helices II and III. Helix VI, shown in orange, contains several critical residues, including D271, H284, E286, Y288 and S299. K362, in the K path, is shown in blue and R234 of subunit II, which interacts through a salt bridge with D271, is shown in dark green.

conformational change that is translated across helix II, the alteration of the other end of helix II can lead to a change in S299 and the K pathway.

If mutation of H93 affects the K pathway, this can also have much further reaching effects, as S299 and H300 are on helix VI, which contains many residues critical for CcO function (Figure 5.2). Among the residues found on this helix are a ligand of CuB, H284, the most buried residue defined in the D pathway, E286, the tyrosine implicated as a redox active electron donor, Y288, and an asparate that salt bridges with R234 of subunit II and is at the terminal end of the water exit channel, D271. Thus, between helix II and helix VI are many of the residues critical for CcO function. As there has been shown to be a conformational change in helix II that can translate the length of the helix and can potentially interact with helix VI, all the important, seemingly individual functions of CcO can be correlated and controlled through small conformational changes.

Cytochrome *c* binding could effect a conformational change that is felt through helix II to regulate the redox potential of heme *a*, as well as proton uptake though the D pathway. Indeed, there is data that suggests that the binding of induces a conformational change in the enzyme (Michel and Bosshard, 1989; Sampson and Alleyne, 2001). This change in helix II could also be translated to helix VI, which could control proton uptake in the K pathway, regulate the redox potential of Cu_B, and control water exit at the exterior side of the protein (Figure 5.2). It is possible that this can also function in the other direction, with the binding of cytochrome *c* affecting the water channel by causing a change in the subunit I/II interface, which could affect helix VI, which in turn could affect helix II.

Thus there is reason to suggest that the long range conformational changes that occur during the catalytic cycle of CcO have the potential of regulating and correlating all aspects of CcO function. A function that this model does not currently incorporate is the proton exit channel and the gating mechanism responsible for unidirectional proton translocation against the gradient, as the location of these two functions is not yet defined. However, proton exit and directional gating would also likely be controlled by the same small conformational changes responsible for controlling and correlating the other functions carried out by CcO and thus they should be located near either helix II or helix VI.

While the pathway for proton exit has not been defined, this new model provides a framework for investigation of possible pathways, as well as describes a comprehensive mechanism for the interdependence of the distinct functions of proton translocation, electron transfer, and water exit. Further mutational studies, along with reexamination of mutants that have already been made, should allow for testing of this model.

Careful analysis of proton backleak in the mutants of the proposed water channel, including R234C, should provide insight into the role of this region in water and proton movement. Due to the possibility of two aspects of this channel in preventing proton transfer, double mutations that result in the loss of the Mn site as well as disturb the hydrophobic narrowing might be required to adequately determine if protons can move through this channel.

Testing the interaction between helices II and VI and their role in regulation in many aspects of CcO function would require the design of several double mutations. Mutation of the two histidine residues proposed to provide the linkage between the two helices (H127 and H300) could provide information on the ability of conformational changes in these helices to be translated to each other. This double mutation has recently been made and full characterization of it should prove insightful. The connection between the top and bottom of each of these helices also needs to be addressed for this model to be verified. This could be most easily addressed by the double mutation of D132A/H93C. If there is connection across the length of helix II, the mutation of D132A should have an effect on the conformational change H93 undergoes, which could be monitored by the labeling of H93C in the double mutation.

While the issues of proton exit and regulation of proton movement still remain, the work documented here provides an initial understanding of these issues, as well as provides a testable hypothesis for further examination of proton pathways and their regulation in CcO.

Appendix

Publications:

L. Florens, B. Schmidt, J. McCracken, S. Ferguson-Miller (2001) "Fast Deuterium Access to the Buried Magnesium/Manganese Site in Cytochrome *c* Oxidase" *Biochemistry* **40**, 7491-7497.

Y.J. Zhen, B. Schmidt, U.G. Kang, W. Antholine, S. Ferguson-Miller (2002) "Mutants of the Cu_A Site in Cytochrome *c* Oxidase of *Rhodobacter sphaeroides*: I. Spectral and Functional Properties" *Biochemistry* **41**, 2288-2297.

D.A. Mills, B. Schmidt, C. Hiser, E. Westley, S. Ferguson-Miller (2002) "Membrane Potential-Controlled Inhibition of Cytochrome *c* Oxidase by Zinc" *J. Biol. Chem.* **277**, 14894-14901.

J.D. Artz, B. Schmidt, J. L. McCracken, M.A. Marletta (2002) "Effects of Nitroglycerin on Soluble Guanylate Cyclase: Implications for Nitrate Tolerance" *J. Biol. Chem.* **277**, 18253-18256.

B. Schmidt, J. McCracken, S. Ferguson-Miller (2003) "A Discrete Water Exit Pawthay in the Membrane Protein Cytochrome *c* Oxidase" *Proc. Natl. Acad. Sci. USA*, in press.

B. Schmidt, W. Hillier, J. McCracken, S. Ferguson-Miller (2003) "The use of stable isotopes and spectroscopy to investigate the energy transducing protein cytochrome *c* oxidase" *Biophys. Biochim. Acta*, in press.

Published Abstracts:

B. Schmidt, L. Florens, L. Qin, J. McCracken, S. Ferguson-Miller (2002) "In Search of Water and Proton Exit Routes in Cytochrome *c* Oxidase" *Biophys. J.* **82**, 1391.

D.A. Mills, B. Schmidt, C. Hiser, A. Pawate, R. Gennis, S. Ferguson-Miller (2002) "Membrane Potential-Controlled Inhibition of Cytochrome *c* Oxidase by Zinc" *Biophys. J.* **82**, 1392.

W. Hiller, B. Schmidt, S. Haymond, D. Mills, G. T. Babcock, S. Ferguson-Miller (2002) "FTIR Difference Spectra of Cytochrome *c* Oxidase Reveal a Coupling of Histidine in the Reduction Cycle" *Biophys. Biochem. Acta* **12**, 88.

B. Schmidt, L. Florens, L. Qin, J. McCracken, S. Ferguson-Miller (2002) *Biophys. Biochem. Acta* **12**, 104.

References

Aasa, R., Albracht, S. P. J., Falk, K.-E., Lanne, B. and Vanngard, T. (1976) EPR Signals from Cytochrome *c* Oxidase. *Biochim. Biophys. Acta* **422**: 260-272.

Abrahams, J. P., Leslie, A. G. W., Lutter, R. and Walker, J. E. (1994) Structure at 2.8 Å Resolution of F_1-ATPase from Bovine Heart Mitochondria. *Nature* **370**: 621-628.

Adelroth, P., Brzezinski, P. and Malmstrom, B. G. (1995) Internal electron transfer in cytochrome *c* oxidase from *Rhodobacter sphaeroides*. *Biochemistry* **34**: 2844-2849.

Adelroth, P., Sigurdson, H., Hallen, S. and Brzezinski, P. (1996) Kinetic coupling between electron and proton transfer in cytochrome c oxidase: simultaneous measurements of conductance and absorbance changes. *Proc. Natl. Acad. Sci. USA* **93**: 12292-12297.

Adelroth, P., Gennis, R. B. and Brzezinski, P. (1998) Role of the pathway through K(I-362) in proton transfer in cytochrome c oxidase from *R. sphaeroides*. *Biochemistry* **37**: 2470-2476.

Alba, M. D., Becerro, A. I., Castro, M. A., Perdigon, A. C. and Trillo, J. M. (2003) Inherent acidity of aqua metal ions in solids: An assay in layered aluminosilicates. *J Phys Chem B* **107**: 3996-4001.

Antonini, G., Malatesta, F., Sarti, P. and Brunori, M. (1993) Proton pumping by cytochrome oxidase as studied by time-resolved stopped-flow spectrophotometry. *Proc. Natl. Acad. Sci. USA* **90**: 5949-5953.

Axelrod, H., Abresch, E., Paddock, M., Okamura, M. and Feher, G. (2000) Determination of the Binding Sites of the Proton Transfer Inhibitors Cd^{2+} and Zn^{2+} in Bacterial Reaction Centers. *Proc. Natl. Acad. Sci. USA* **97**: 1542-1547.

Babcock, G. T. and Callahan, P. M. (1983) Redox-Linked Hydrogen Bond Strength Changes in Cytochrome *a*: Implications for a Cytochrome Oxidase Proton Pump. *Biochemistry* **22**: 2314-2319.

Baciou, L. and Michel, H. (1995) Interruption of the water chain in the reaction center from *Rhodobacter sphaeroides* reduces the rates of the proton uptake and of the second electron transfer to Q_B. *Biochemistry* **34**: 7967-7972.

Backgren, C., Hummer, G., Wikstrom, M. and Puustinen, A. (2000) Proton translocation by cytochrome c oxidase can take place without the conserved glutamic acid in subunit I. *Biochemistry* **39**: 7863-7867.

Ballou, D. P. (1978) Freeze-quench and chemical-quench techniques. *Methods Enzymol.* **54**: 85-93.

Baymann, F., Moss, D. A. and Mantele, W. (1991) An Electrochemical Assay for the Characterization of Redox Proteins from Biological Electron-Transfer Chains. *Anal. Biochem.* **199**: 269-274.

Behr, J., Hellwig, P., Mantele, W. and Michel, H. (1998) Redox dependent changes at

the heme propionates in cytochrome c oxidase from *Paracoccus denitrificans*: direct evidence from FTIR difference spectroscopy in combination with heme propionate 13C labeling. *Biochemistry* **37**: 7400-7406.

Beinert, H., Griffiths, D., E, Wharton, D. C. and Sands, R. H. (1962) Properties of the copper associated with cytochrome c oxidase as studied by Paramagnetic Resonance Spectroscopy. *J. Biol. Chem.* **237**: 2337-2345.

Bellew, B. F., Halkides, C. J., Gerfen, G. J., Griffin, R. G. and Singel, D. J. (1996) High frequency (139.5 GHz) electron paramagnetic resonance characterization of Mn(II)-H2(17)O interactions in GDP and GTP forms of p21 ras. *Biochemistry* **35**: 12186-12193.

Bottcher, B., Scheide, D., Hesterberg, M., Nagel-Steger, L. and Friedrich, T. (2002) A novel, enzymatically active conformation of the *Escherichia coli* NADH:ubiquinone oxidoreductase (complex I). *J. Biol. Chem.* **277**: 17970-17977.

Branden, M., Sigurdson, H., Namslauer, A., Gennis, R., Adelroth, P. and Brzezinski, P. (2001) On the role of the K-proton transfer pathway in cytochrome c oxidase. *Proc. Natl. Acad. Sci. USA* **98**: 5013-5018.

Bratton, M., Pressler, M. and Hosler, J. (1999) Suicide inactivation of cytochrome c oxidase: Catalytic turnover in the absence of subunit III alters the active site. *Biochemistry* **38**: 16236-16245.

Brookes, P. S., Hulbert, A. J. and Brand, M. D. (1997) The proton permeability of liposomes made from mitochondrial inner membrane phospholipids: no effect of fatty acid composition. *Bba-Biomembranes* **1330**: 157-164.

Bushnell, G. W., Louie, G. V. and Brayer, G. D. (1990) High-resolution three-dimensional structure of horse heart cytochrome *c*. *J. Mol. Biol.* **214**: 585-595.

Butt, H. J., Fendler, K., Bamberg, E., Tittor, J. and Oesterhelt, D. (1989) Aspartic Acids 96 and 85 Play a Central Role in the Function of Bacteriorhodopsin as a Proton Pump. *EMBO J.* **8**: 1657-1663.

Capitanio, N., Capitanio, G., Demarinis, D. A., De Nitto, E., Massari, S. and Papa, S. (1996) Factors affecting the H+/e- stoichiometry in mitochondrial cytochrome c oxidase: influence of the rate of electron flow and transmembrane delta pH. *Biochemistry* **35**: 10800-10806.

Capitanio, N., Capitanio, G., Minuto, M., De Nitto, E., Palese, L. L., Nicholls, P. and Papa, S. (2000) Coupling of electron transfer with proton transfer at heme a and Cu(A) (redox Bohr effects) in cytochrome c oxidase. Studies with the carbon monoxide inhibited enzyme. *Biochemistry* **39**: 6373-6379.

Chen, Y. R., Gunther, M. R. and Mason, R. P. (1999) An electron spin resonance spin-trapping investigation of the free radicals formed by the reaction of mitochondrial cytochrome c oxidase with H2O2. *J. Biol. Chem.* **274**: 3308-3314.

Cherny, V. and Decoursey, T. (1999) pH-dependent inhibition of voltage-gated H+ currents in rat alveolar epithelial cells by Zn^{2+} and other divalent cations. *J. Gen. Physiol.* **114**: 819-838.

Cowin, J. P., Tsekouras, A. A., Iedema, M. J., Wu, K. and Ellison, G. B. (2000) Immobility of protons in ice from 30 to 190 K. *Nature* **398**: 405-407.

Das, T. K., Tomson, F. L., Gennis, R. B., Gordon, M. and Rousseau, D. L. (2001) pH-dependent structural changes at the Heme-Copper binuclear center of cytochrome c oxidase. *Biophys. J.* **80**: 2039-2045.

De Godoy, C. M. and Cukierman, S. (2001) Modulation of proton transfer in the water wire of dioxolane-linked gramicidin channels by lipid membranes. *Biophys. J.* **81**: 1430-1438.

De Groot, B. L. and Grabmuller, H. (2001) Water permeation across biological membranes: mechanism and dynamics of aquaporin-1 and GlpF. *Science* **294**: 2353-2357.

De Grotthuss, C. J. T. (1806) Sur la decomposition de l'eau et des corps qu'elle tient en dissolution a l'aide de l'electricite galvanique. *Ann. Chim. (Paris)* **LVIII**: 54-74.

De Jong, A. M. and Albracht, S. P. (1994) Ubisemiquinones as obligatory intermediates in the electron transfer from NADH to ubiquinone. *Eur. J. Biochem.* **222**: 975-982.

Dellago, C., Naor, M. M. and Hummer, G. (2003) Proton transport through water-filled carbon nanotubes. *Phys. Rev. Lett.* **90**: 105902.

Dikanov, S. A., Shubin, A. A. and Parmon, V. N. (1981) Modulation effects in the electron spin echo resulting from hyperfine interaction with a nucleus of an arbitrary spin. *J. Magn. Reson.* **42**: 474-487.

Dwyer, J. J., Gittis, A. G., Karp, D. A., Lattman, E. E., Spencer, D. S., Stites, W. E. and Garcia-Moreno, E. B. (2000) High apparent dielectric constants in the interior of a protein reflect water penetration. *Biophys. J.* **79**: 1610-1620.

Ermler, U., Fritzsch, G., Buchanan, S. K. and Michel, H. (1994) Structure of the Photosynthetic Reaction Centre from *Rhodobacter sphaeroides* at 2.65 Å Resolution: Cofactors and Protein-Cofactor Interactions. *Structure* **2**: 925-936.

Espe, M. P., Hosler, J. P., Ferguson-Miller, S., Babcock, G. T. and Mccracken, J. (1995) A Continuous Wave and Pulsed EPR Characterization of the Mn^{2+} Binding Site in *Rhodobacter sphaeroides* Cytochrome *c* Oxidase. *Biochemistry* **34**: 7593-7602.

Ferguson-Miller, S. and Babcock, G. (1996) Heme/Copper Terminal Oxidases. *Chem. Rev.* **96**: 2889-2907.

Fetter, J. R., Qian, J., Shapleigh, J., Thomas, J. W., García-Horsman, J. A., Schmidt,

E., Hosler, J., Babcock, G. T., Gennis, R. B. and Ferguson-Miller, S. (1995) Possible Proton Relay Pathways in Cytochrome *c* Oxidase. *Proc. Natl. Acad. Sci. USA* **92**: 1604-1608.

Fillingame, R. H., Angevine, C. M. and Dmitriev, O. Y. (2002) Coupling proton movements to c-ring rotation in F(1)F(o) ATP synthase: aqueous access channels and helix rotations at the a-c interface. *Biochim. Biophys. Acta* **1555**: 29-36.

Florens, L., Schmidt, B., Mccracken, J. and Ferguson-Miller, S. (2001) Fast deuterium access to the buried magnesium/manganese site in cytochrome c oxidase. *Biochemistry* **40**: 7491-7497.

Follman, K., Arnold, S., Ferguson-Miller, S. and Kadenbach, B. (1998) Cytochrome c Oxidase from Eucaryotes but not from Procaryotes is Allosterically Inhibited by ATP. *Biochem. Mol. Biol. Internatl.* **45**: 1047-1055.

Friedrich, T. and Scheide, D. (2000) The respiratory complex I of bacteria, archaea and eukarya and its module common with membrane-bound multisubunit hydrogenases. *FEBS Lett.* **479**: 1-5.

Friedrich, T. (2001) Complex I: a chimaera of a redox and conformation-driven proton pump? *J. Bioenerg. Biomembr.* **33**: 169-177.

Fu, D., Libson, A., Miercke, L. J., Weitzman, C., Nollert, P., Krucinski, J. and Stroud, R. M. (2000) Structure of a glycerol-conducting channel and the basis for its selectivity. *Science* **290**: 481-486.

Gamgee, A. (1899) On the absorption of the extreme violet and ultra-violet rays of the spectrum by haemoglobin, and its compounds and certain of its derivatives. *Proc. R. Soc. London, B* **59**: 505-528.

Garcia, A. E. and Hummer, G. (2000) Water penetration and escape in proteins. *Proteins* **38**: 261-272.

Girvin, M. E., Rastogi, V. K., Abildgaard, F., Markley, J. L. and Fillingame, R. H. (1998) Solution structure of the transmembrane H+-transporting subunit c of the F1F0 ATP synthase. *Biochemistry* **37**: 8817-8824.

Gottschalk, M., Dencher, N. A. and Halle, B. (2001) Microsecond exchange of internal water molecules in bacteriorhodopsin. *J. Mol. Biol.* **311**: 605-621.

Greenwood, C. and Gibson, Q. H. (1967) The Reaction of Reduced Cytochrome *c* Oxidase with Oxygen. *J. Biol. Chem.* **242**: 1782-1787.

Gupta, S., Warne, A., Saraste, M. and Mazumdar, S. (2001) pH-induced conformational transition in the soluble CuA domain of *Paracoccus denitrificans* cytochrome oxidase. *Biochemistry* **40**: 6180-6189.

Hállen, S. and Nilsson, T. (1992) Proton Transfer During the Reaction Between Fully Reduced Cytochrome Oxidase and Dioxygen: pH and Deuterium Isotope Effects.

Biochemistry **31**: 11853-11859.

Haltia, T. (1992) Reduction of Cu_A Induces a Conformational Change in Cytochrome *c* Oxidase from *Paracoccus denitrificans*. *Biochim. Biophys. Acta* **1098**: 343-350.

Han, S., Ching, Y.-C. and Rousseau, D. L. (1990a) Ferryl and Hydroxy Intermediates in the Reaction of Oxygen with Reduced Cytochrome *c* Oxidase. *Nature* **348**: 89-90.

Han, S., Ching, Y.-C. and Rousseau, D. L. (1990b) Time Evolution of the Intermedciates Formed in the Reaction of Oxygen with Mixed-Valence Cytochrome *c* Oxidase. *J. Am. Chem. Soc.* **112**: 9445-9551.

Hartzell, C. R. and Beinert, H. (1974) Components of cytochrome *c* oxidase detectable by EPR spectroscopy. *Biochim. Biophys. Acta* **368**: 318-338.

Hellwig, P., Behr, J., Ostermeier, C., Richter, O. M., Pfitzner, U., Odenwald, A., Ludwig, B., Michel, H. and Mantele, W. (1998) Involvement of glutamic acid 278 in the redox reaction of the cytochrome c oxidase from *Paracoccus denitrificans* investigated by FTIR spectroscopy. *Biochemistry* **37**: 7390-7399.

Hellwig, P., Gryzbek, S., Behr, J., Ludwig, B., Michel, H. and Mantele, W. (1999) Electrochemical and ultraviolet/visible/infrared spectroscopic analysis of heme a and a3 redox reactions in the cytochrome c oxidase from *Paracoccus denitrificans*: Separation of heme a and a3 contributions and assignment of vibrational modes. *Biochemistry* **38**: 1685-1694.

Hiser, C., Mills, D. A., Schall, M. and Ferguson-Miller, S. (2001) C-terminal truncation and histidine-tagging of cytochrome c oxidase subunit II reveals the native processing site, shows involvemet of the C-terminus in cytochrome c binding, and improves the assay for proton pumping. *Biochemistry* **40**: 1606-1615.

Holm, R. H., Kennepohl, P. and Solomon, E. I. (1996) Structural and Functional Aspects of Metal Sites in Biology. *Chem. Rev.* **96**: 2239-2314.

Horton, R. M., Cai, Z., Ho, S. N. and Pease, L. R. (1990) Gene Splicing by Overlap Extension: Tailor-Made Genes Using the Polymerase Chain Reaction. *Biotechniques* **8**: 528-535.

Hosler, J. P., Fetter, J., Tecklenburg, M. M. J., Espe, M., Lerma, C. and Ferguson-Miller, S. (1992) Cytochrome aa_3 of *Rhodobacter sphaeroides* as a Model for Mitochondrial Cytochrome *c* Oxidase. *J. Biol. Chem.* **267**: 24264-24272.

Hosler, J. P., Espe, M. P., Zhen, Y., Babcock, G. T. and Ferguson-Miller, S. (1995) Analysis of Site-Directed Mutants Locates a Non-Redox-Active Metal near the Active Site of Cytochrome *c* Oxidase of *Rhodobacter sphaeroides*. *Biochemistry* **34**: 7586-7592.

Israilev, S., Crofts, A. R., Berry, E. A. and Schulten, K. (1999) Steered molecular dynamics simulation of the Rieske subunit motion in the cytochrome bc1 complex. *Biophys. J.* **77**: 1753-1768.

Iverson, T. M., Luna-Chavez, C., Cecchini, G. and Rees, D. C. (1999) Structure of the *Escherichia coli* fumarate reductase respiratory complex. *Science* **284**: 1961-1966.

Iwaki, M., Puustinen, A., Wikstrom, M. and Rich, P. R. (2003) ATR-FTIR Spectroscopy of the P(M) and F Intermediates of Bovine and *Paraccocus denitrificans* Cytochrome c Oxidase. *Biochemistry* **42**: 8809-8817.

Iwata, S., Ostermeier, C., Ludwig, B. and Michel, H. (1995) Structure at 2.8 Å resolution of cytochrome c oxidase from *Paracoccus denitrificans*. *Nature* **376**: 660-669.

Iwata, S., Lee, J. W., Okada, K., Lee, J. K., Iwata, M., Rasmussen, B., Link, T. A., Ramaswamy, S. and Jap, B. K. (1998) Complete structure of the 11-subunit bovine mitochondrial cytochrome bc1 complex. *Science* **281**: 64-71.

Jackson, J. B. (2003) Proton translocation by transhydrogenase. *FEBS Lett.* **545**: 18-24.

Jones, P. C. and Fillingame, R. H. (1998) Genetic fusions of subunit c in the F0 sector of H+-transporting ATP synthase. Functional dimers and trimers and determination of stoichiometry by cross-linking analysis. *J. Biol. Chem.* **273**: 29701-29705.

Kaess, H., Macmillan, F., Ludwig, B. and Prisner, T. (2000) Investigation of the Mn binding site in cytochrome c oxidase from *Paracoccus denitrificans* by high-frequency EPR. *J. Chem. Phys.* **104**: 5362-5371.

Karpefors, M., Adelroth, P., Zhen, Y., Ferguson-Miller, S. and Brzezinski, P. (1998) Proton uptake controls electron transfer in cytochrome c oxidase. *Proc. Natl. Acad. Sci. USA* **95**: 13606-13611.

Karpefors, M., Adelroth, P. and Brzezinski, P. (2000) The onset of the deuterium isotope effect in cytochrome c oxidase. *Biochemistry* **39**: 5045-5050.

Keilin, D. (1925) On cytochrome, a respiratory pigement, common to animals, yeast and higher plants. *Proc. R. Soc. Lond. B. Biol. Sci.* **98**: 312-339.

Keilin, D. (1938) Cytochrome oxidase. *Proc. R. Soc. Lond. B. Biol. Sci.* **125**: 171-186.

Keilin, D. and Hartree, E. F. (1939) Cytochrome and cytochrome oxidase. *Proc. R. Soc. Lond. B. Biol. Sci.* **127**: 167-191.

Kitagawa, T. (2000) Structures of reaction intermediates of bovine cytochrome c oxidase probed by time-resolved vibrational spectroscopy. *J. Inorg. Biochem.* **82**: 9-18.

Kofron, J. L., Ash, D. E. and Reed, G. H. (1988) Coordination of manganous ion at the active site of pyruvate, phosphate dikinase: the complex of oxalate with the phosphorylated enzyme. *Biochemistry* **27**: 4781-4787.

Konstantinov, A. A., Siletsky, S., Mitchell, D., Kaulen, A. and Gennis, R. (1997) The Roles of the Two Proton Input Channels in Cytochrome c Oxidase from *Rhodobacter sphaeroides* Probed by the Effects of Site-directed Mutations on Time-resolved Electrogenic Intraprotein Proton Transfer. *Proc. Natl. Acad. Sci (USA)* **94**: 9085-9090.

Kornblatt, J. A. (1998) The water channel of cytochrome c oxidase: inferences from inhibitor studies. *Biophys. J.* **75**: 3127-3134.

Krishtalik, L. I. (2000) The mechanism of the proton transfer: an outline. *Biochim. Biophys. Acta* **1458**: 6-27.

Kroneck, P. M. H., Antholine, W. A., Riester, J. and Zumft, W. G. (1989) The Nature of the Cupric Site in Nitrous Oxide Reductase and of Cu_A in Cytochrome *c* Oxidase. *FEBS Lett.* **248**: 212-213.

Kroneck, P. M. H., Antholine, W. E., Kastrau, D. H. W., Buse, G., Steffens, G. C. M. and Zumft, W. G. (1990) Multifrequency EPR Evidence for a Bimetallic Center at the Cu_A Site in Cytochchrome *c* Oxidase. *FEBS Lett.* **268**: 274-276.

Lee, A., Kirichenko, A., Vygodina, T., Siletsky, S. A., Das, T. K., Rousseau, D. L., Gennis, R. and Konstantinov, A. A. (2002) Ca(2+)-binding site in *Rhodobacter sphaeroides* cytochrome C oxidase. *Biochemistry* **41**: 8886-8898.

Lee, H.-M., Das, T., Rousseau, D., Mills, D., Ferguson-Miller, S. and Gennis, R. (2000) Mutations in the Putative H-Channel in the Cytochrome c Oxidase from *Rhodobacter sphaeroides* Show That This Channel Is Not Important for Proton Conduction But Reveal Modulation of the Properties of Heme *a*. *Biochemistry* **39**: 2989-2996.

Ludwig, B., Bender, E., Arnold, S., Huttemann, M., Lee, I. and Kadenbach, B. (2001) Cytochrome C oxidase and the regulation of oxidative phosphorylation. *Chembiochem* **2**: 392-403.

Luecke, H., Schobert, B., Richter, H.-T., Cartailler, J.-P. and Lanyi, J. K. (1999) Structural Changes in Bacteriorhodopsin During Ion Transport at 2 Angstrom Resolution. *Science* **286**: 255-260.

Macmillan, F., Kannt, A., Behr, J., Prisner, T. and Michel, H. (1999) Direct evidence for a tyrosine radical in the reaction of cytochrome c oxidase with hydrogen peroxide. *Biochemistry* **38**: 9179-9184.

Macmunn, C. A. (1886) Researches on myohaematin and the histohaematins. *Philos. Trans. R. Soc. Lond. B. Biol. Sci.* **177**: 267-298.

Marantz, Y., Nachliel, E., Aagaard, A., Brzezinski, P. and Gutman, M. (1998) The Proton Collecting Function of the Inner Surface of Cytochrome *c* Oxidase from *Rhodobacter sphaeroides*. *Proc. Natl. Acad. Sci. USA* **95**: 8590-8595.

Martinez, S. E., Huang, D., Ponomarev, M., Cramer, W. A. and Smith, J. L. (1996)

The heme redox center of chlorplast cytochrome f is linked to a buried five-water chain. *Protein Science* **5**: 1081.

Mccracken, J., Shin, D.-H. and Dye, J. L. (1992) Pulsed EPR studies of polycrystalline cesium hexamethyl hexacyclen sodide. *Appl. Magn. Reson.* **3**: 305-316.

Michel, B. and Bosshard, H. R. (1989) Oxidation of cytochrome c by cytochrome c oxidase: spectroscopic binding studies and steady-state kinetics support a conformational transition mechanism. *Biochemistry* **28**: 244-252.

Michel, H. (1998) The Mechanism of Proton Pumping by Cytochrome *c* Oxidase. *Proc. Natl. Acad. Sci. USA* **95**: 12819-12824.

Michel, H. (1999) Cytochrome c Oxidase: Catalytic Cycle and Mechanisms of Proton Pumping--A Discussion. *Biochemistry* **38**: 15129-15140.

Miller, L. M. and Chance, M. R. (1994) Probing Conformational Changes upon Photolysis: FTIR Studies of the Low Temperature Liganded and Photoproduct States of Oxy- and Carbomonoxymyoglobin. *Journal of the American Chemistry Society* **116**: 9662-9669.

Mills, D. A., Florens, L., Hiser, C., Qian, J. and Ferguson-Miller, S. (2000) Where is "outside" in cytochrome c oxidase and how and when do protons get there? *Biochim. Biophys. Acta* **1458**: 180-187.

Mills, D. A., Schmidt, B., Hiser, C., Westley, E. and Ferguson-Miller, S. (2002) Membrane Potential-controlled Inhibition of Cytochrome *c* Oxidase. *J. Biol. Chem.* **277**: 14894.

Mills, D. A. and Ferguson-Miller, S. (2002) Influence of structure, pH and membrane potential on proton movement in cytochrome *c* oxidase. *Biochim. Biophys. Acta* **1555**: 96-100.

Mills, D. A. and Ferguson-Miller, S. (2003) Understanding the mechanism of proton movement linked to oxygen reduction in cytochrome c oxidase: lessons from other proteins. *FEBS Lett.* **545**: 47-51.

Mims, W. B. and Davis, J. L. (1976) Proton modulation of the electron spin echo envelope in an neodymium(3+):aquo glass. *J. Chem. Phys.* **64**: 4836-4846.

Mims, W. B., Peisach, J. and Davis, J. L. (1977) Nuclear modulation of the electron spin echo envelope in glassy materials. *J. Chem. Phys.* **64**: 5536-5550.

Mims, W. B. (1984) Elimination of the Dead-Time Artifact in Electron Spin-Echo Envelope Spectra. *J. Magn. Reson.* **59**: 291-306.

Mims, W. B., Davis, J. L. and Peisach, J. (1984) The accessibility of type I copper(II) centers in laccase, azurin, and stellacyanin to exchangeable hydrogen and ambient water. *Biophys. J.* **45**: 755-766.

Mitchell, D. M. and Gennis, R. B. (1995) Rapid Purification of Wildtype and Mutant Cytochrome *c* Oxidase from *Rhodobacter sphaeroides* by Ni^{2+}-NTA Affinity Chromatography. *FEBS Lett.* **368**: 148-150.

Mitchell, P. and Moyle, J. (1965) Stoichiometry of proton translocation through the respiratory chain and adenosine triphosphatase systems of rat liver mitochondria. *Nature* **208**: 147-151.

Mogi, T., Stern, L. H., Marti, T., Chao, B. H. and Khorana, H. G. (1988) Aspartic Acid Substitutions Affect Proton Translocation by Bacteriorhodopsin. *Proc. Natl. Acad. Sci. USA* **85**: 4148-4152.

Moody, A. J. and Rich, P. R. (1990) The Effect of pH on Redox Titrations of Haem *a* in Cyanide-Liganded Cytochrome-*c* Oxidase: Experimental and Modelling Studies. *Biochim. Biophys. Acta* **1015**: 205-215.

Moody, A. J., Von Germar, F., Mantele, W. and Rich, P. R. (1995) Rapid-scan FTIR spectroscopic studies on the photolysis and recombination of the cyanide adduct of fully reduced bovine cytochrome c oxidase. *Biochem. Soc. Trans.* **23**: 521S.

Moody, M. F., Jones, P. T., Carver, J. A., Boyd, J. and Campbell, I. D. (1987) 1H nuclear magnetic resonance studies of an integral membrane protein: subunit c of the F1F0 ATP synthase. *J. Mol. Biol.* **193**: 759-774.

Moss, D., Nabedryk, E., Breton, J. and Mantele, W. (1990) Redox-Linked Conformational-Changes in Proteins Detected by a Combination of Infrared-Spectroscopy and Protein Electrochemistry - Evaluation of the Technique with Cytochrome-C. *Eur. J. Biochem.* **187**: 565-572.

Mulkidjanian, A. Y. (1999) Conformationally controlled pK-switching in membrane proteins: one more mechanism specific to the enzyme catalysis? *FEBS Lett.* **463**: 199-204.

Murata, K., Mitsuoka, K., Hiral, T., Walz, T., Agre, P., Heymann, J. B., Engel, A. and Fujiyoshi, Y. (2000) Structural Determinants of Water Permeation Through Aquaporin-1. *Nature* **407**: 599-605.

Nagle, J. F. and Morowitz, H. J. (1978) Molecular Mechanisms for Proton Transport in Membranes. *Proc. Natl. Acad. Sci. USA* **75**: 298-302.

Nishimura, K., Kim, S., Zhang, L. and Cross, T. A. (2002) The closed state of a H+ channel helical bundle combining precise orientational and distance restraints from solid state NMR. *Biochemistry* **41**: 13170-13177.

Noji, H., Yasuda, R., Yoshida, M. and Kinosita, K., Jr. (1997) Direct observation of the rotation of F1-ATPase. *Nature* **386**: 299-302.

Nyquist, R. M., Heitbrink, D., Bolwien, C., Wells, T. A., Gennis, R. B. and Heberle, J. (2001) Perfusion-induced redox differences in cytochrome c oxidase: ATR/FT-IR spectroscopy. *FEBS Lett.* **505**: 63-67.

Nyquist, R. M., Heitbrink, D., Bolwien, C., Gennis, R. B. and Heberle, J. (2003) Direct observation of protonation reactions during the catalytic cycle of cytochrome c oxidase. *Proc. Natl. Acad. Sci. USA* **100**: 8715-8720.

Okun, J. G., Lummen, P. and Brandt, U. (1999) Three classes of inhibitors share a common binding domain in mitochondrial complex I (NADH:ubiquinone oxidoreductase). *J. Biol. Chem.* **274**: 2625-2630.

Onsager, L. (1969) The Motion of Ions: Principles and Concepts. *Science* **166**: 1359-1364.

Oprea, T. I., Hummer, G. and Garcia, A. E. (1997) Identification of a functional water channel in cytochrome P450 enzymes. *Proc. Natl. Acad. Sci. USA* **94**: 2133-2138.

Ostermeier, C., Harrenga, A., Ermler, U. and Michel, H. (1997) Structure at 2.7 Å resolution of the *Paracoccus denitrificans* two-subunit cytochrome c oxidase complexed with an antibody Fv fragment. *Proc. Natl. Acad. Sci. USA* **94**: 10547-10553.

Paddock, M., Graige, M., Feher, G. and Okamura, M. (1999) Identification of the proton pathway in bacterial reaction centers: Inhibition of proton transfer by binding of Zn^{2+} or Cd^{2+}. *Proc. Natl. Acad. Sci. (USA)* **96**: 6183-6188.

Paddock, M. L., Rongey, S. H., Feher, G. and Okamura, M. Y. (1989) Pathway of proton transfer in bacterial reaction centers: replacement of glutamic acid 212 in the L subunit by glutamine inhibits quinone (secondary acceptor) turnover. *Proc. Natl. Acad. Sci. USA* **86**: 6602-6606.

Paddock, M. L., Mcpherson, P. H., Feher, G. and Okamura, M. Y. (1990) Pathway of Proton Transfer in Bacterial Reaction Centers: Replacement of Serine-L-223 by Alanine Inhibits Electron and Proton Transfers Associated with Reduction of Quinone to Dihydroquinone. *Proc. Natl. Acad. Sci. USA* **87**: 6803-6807.

Paddock, M. L., Rongey, S. H., Mcpherson, P. H., Juth, A., Feher, G. and Okamura, M. Y. (1994) Pathway of Proton Transfer in Bacterial Reaction Centers: Role of Aspartate-L213 in Proton Transfers Associated with Reduction of Quinone to Dihydroquinone. *Biochemistry* **33**: 734-745.

Paddock, M. L., Feher, G. and Okamura, M. Y. (2000) Identification of the proton pathway in bacterial reaction centers: replacement of Asp-M17 and Asp-L210 with Ans reduces the proton transfer rate in the presence of Cd(2+). *Proc. Natl. Acad. Sci. USA* **97**: 1548-1533.

Paddock, M. L., Adelroth, P., Chang, C., Abresch, E. C., Feher, G. and Okamura, M. Y. (2001) Identification of the proton pathway in bacterial reaction centers: cooperation between Asp-M17 and Asp-L210 facilitates proton transfer to the secondary quinone (QB). *Biochemistry* **40**: 6893-6902.

Padmakumar, R. and Banerjee, R. (1995) Evidence from electron paramagnetic resonance spectroscopy of the participation of radical intermediates in the reaction

catalyzed by methylmalonyl-coenzyme A mutase. *J. Biol. Chem.* **270**: 9295-9300.

Palsdottir, H., Lojero, C. G., Trumpower, B. L. and Hunte, C. (2003) Structure of the yeast cytochrome *bc1* complex with a hydroxyquinone anion Qo site inhibitor bound. *J. Biol. Chem.* **In press**:

Panke, O., Gumbiowski, K., Junge, W. and Engelbrecht, S. (2000) F-ATPase: specific observation of the rotating c subunit oligomer of EF(o)EF(1). *FEBS Lett.* **472**: 34-38.

Papa, S., Capitanio, N. and Villani, G. (1998) A cooperative model for protonmotive heme-copper oxidases. The role of heme a in the proton pump of cytochrome c oxidase. *FEBS Lett.* **439**: 1-8.

Pecoraro, C., Gennis, R. B., Vygodina, T. V. and Konstantinov, A. A. (2001) Role of the K-channel in the pH-dependence of the reaction of cytochrome c oxidase with hydrogen peroxide. *Biochemistry* **40**: 9695-9708.

Pomes, R. and Roux, B. (1998) Free energy profiles for H+ conduction along hydrogen-bonded chains of water molecules. *Biophys. J.* **75**: 33-40.

Pomes, R. and Roux, B. (2002) Molecular mechanism of H+ conduction in the single-file water chain of the gramicidin channel. *Biophys. J.* **82**: 2304-2316.

Ponamarev, M. V. and Cramer, W. A. (1998) Perturbation of the internal water chain in cytochrome f of oxygenic photosynthesis: loss of the concerted reduction of cytochromes f and b6. *Biochemistry* **37**: 17199-17208.

Proshlyakov, D. A., Ogura, T., Shinzawa-Itoh, K., Yoshikawa, S., Appelman, E. H. and Kitagawa, T. (1994) Selective Resonance Raman Observation of the "607 nm" Form Generated in the Reaction of Oxidized Cytochrome *c* Oxidase with Hydrogen Peroxide. *J. Biol. Chem.* **269**: 29385-29388.

Proshlyakov, D. A., Ogura, T., Shinzawa-Itoh, K., Yoshikawa, S. and Kitagawa, T. (1996) Resonance Raman/absorption characterization of the oxo intermediates of cytochrome c oxidase generated in its reaction with hydrogen peroxide: pH and H2O2 concentration dependence. *Biochemistry* **35**: 8580-8586.

Proshlyakov, D. A., Pressler, M. A. and Babcock, G. T. (1998) Dioxygen activation and bond cleavage by mixed-valence cytochrome c oxidase. *Proc. Natl. Acad. Sci. USA* **95**: 8020-8025.

Proshlyakov, D. A., Pressler, M. A., Demaso, C., Leykam, J. F., Dewitt, D. L. and Babcock, G. T. (2000) Oxygen activation and reduction in respiration: involvement of redox-active tyrosine 244. *Science* **290**: 1588-1591.

Puustinen, A. and Wikstrom, M. (1999) Proton exit from the heme-copper oxidase of Escherichia coli. *Proc. Natl. Acad. Sci. USA* **96**: 35-37.

Ragan, C. I., Widger, W. R. and King, T. E. (1974) Pyridine nucleotide

transhydrogenase activity of soluble cardiac NADH dehydrogenase and particulate NADH-ubiquinone reductase. *Biochem. Biophys. Res. Commun.* **60**: 894-900.

Rich, P. R., Rigby, S. E. and Heathcote, P. (2002) Radicals associated with the catalytic intermediates of bovine cytochrome c oxidase. *Biochim. Biophys. Acta* **1554**: 137-146.

Richter, H. T., Brown, L. S., Needleman, R. and Lanyi, J. K. (1996a) A linkage of the pKa's of asp-85 and glu-204 forms part of the reprotonation switch of bacteriorhodopsin. *Biochemistry* **35**: 4054-4062.

Richter, H. T., Needleman, R., Kandori, H., Maeda, A. and Lanyi, J. K. (1996b) Relationship of retinal configuration and internal proton transfer at the end of the bacteriorhodopsin photocycle. *Biochemistry* **35**: 15461-15466.

Rigby, S. E., Junemann, S., Rich, P. R. and Heathcote, P. (2000) Reaction of bovine cytochrome c oxidase with hydrogen peroxide produces a tryptophan cation radical and a porphyrin cation radical. *Biochemistry* **39**: 5921-5928.

Roberts, A. G., Bowman, M. K. and Kramer, D. M. (2002) Certain metal ions are inhibitors of cytochrome b6f complex 'Rieske' iron-sulfur protein domain movements. *Biochemistry* **41**: 4070-4079.

Roberts, V. A. and Pique, M. E. (1999) Definition of the interaction domain for cytochrome c on cytochrome c oxidase: III. Calculation of the docked complex. *J. Biol. Chem.*

Robinson, N., Neumann, J. and Wiginton, D. (1985) Influence of detergent polar and apolar structure upon the temperature dependence of beef heart cytochrome c oxidase activity. *Biochemistry* **24**: 6298-6304.

Rodrigues, D. J. and Jackson, J. B. (2002) A conformational change in the isolated NADP(H)-binding component (dIII) of transhydrogenase induced by low pH: a reflection of events during proton translocation by the complete enzyme? *Biochim. Biophys. Acta* **1555**: 8-13.

Roux, B. and Karplus, M. (1994) Molecular dynamics simulations of the gramicidin channel. *Annu. Rev. Biophys. Biomol. Struct.* **23**: 731-761.

Rowan, L. G., Hahn, E. L. and Mims, W. B. (1965) Electron-spin-echo envelope modulation. *Phys. Rev. A* **137**: 61-71.

Sagnella, D. E. and Voth, G. A. (1996) Structure and dynamics of hydronium in the ion channel gramicidin A. *Biophys. J.* **70**: 2043-2051.

Sampogna, R. V. and Honig, B. (1996) Electrostatic coupling between retinal isomerization and the ionization state of Glu-204: a general mechanism for proton release in bacteriorhodopsin. *Biophys. J.* **71**: 1165-1171.

Sampson, V. and Alleyne, T. (2001) Cytochrome c/cytochrome c oxidase interaction.

Direct structural evidence for conformational changes during enzyme turnover. *Eur. J. Biochem.* **268**: 6534-6544.

Sands, R. H. and Beinert, H. (1959) The function of copper in cytochrome oxidase. *Biochem. Biophys. Res. Commun.* **1**: 175-178.

Schiffer, C. A. and Van Gunsteren, W. F. (1999) Accessibility and order of water sites in and around proteins: A crystallographic time-averaging study. *Proteins* **36**: 501-511.

Schmidt, B., Mccracken, J. and Ferguson-Miller, S. (2003a) A discrete water exit pathway in the membrane protein cytochrome *c* oxidase. *Proc. Natl. Acad. Sci. USA* ***In press***:

Schmidt, B., Hillier, W., Mccracken, J. and Ferguson-Miller, S. (2003b) The use of stable isotopes and spectroscopy to investigate the energy transducing protein cytochrome *c* oxidase. *Biochim. Biophys. Acta* ***In press***:

Schowen, K. B. and Schowen, R. L. (1982) Solvent isotope effects of enzyme systems. *Methods Enzymol.* **87**: 551-606.

Schultz, B. E., Edmondson, D. E. and Chan, S. I. (1998) Reaction of *Escherichia coli* cytochrome bo3 with substoichiometric ubiquinol-2: a freeze-quench electron paramagnetic resonance investigation. *Biochemistry* **37**: 4160-4168.

Shapleigh, J. P. and Gennis, R. B. (1992) Cloning, Sequencing, and Deletion from the Chromosome of the Gene Encoding Subunit I of the aa_3-type cytochrome *c* oxidase of *Rhodobacter sphaeroides*. *Mol. Microbiol.* **6**: 635-642.

Silverman, D. N. (2000) Marcus rate theory applied to enzymatic proton transfer. *Biochim. Biophys. Acta* **1458**: 88-103.

Smondyrev, A. M. and Voth, G. A. (2002) Molecular dynamics simulation of proton transport through the influenza A virus M2 channel. *Biophys. J.* **83**: 1987-1996.

Soret, J. L. (1878) Recherches sur l'absorption des rayons ultra-violets par diverses substances. *Arch. Sci. Physiq. Nat.* **61**: 322-359.

Soulimane, T., Buse, G., Bourenkov, G. P., Bartunik, H. D., Huber, R. and Than, M. E. (2000) Structure and mechanism of the aberrant ba(3)-cytochrome c oxidase from thermus thermophilus. *EMBO J.* **19**: 1766-1776.

Steuber, J. (2001) The Na+-translocating NADH:quinone oxidoreductase (NDH I) from Klebsiella pneumoniae and Escherichia coli: implications for the mechanism of redox-driven cation translocation by complex I. *J. Bioenerg. Biomembr.* **33**: 179-186.

Stock, D., Leslie, A. G. W. and Walker, J. E. (1999) Molecular architecture of the rotary motor in ATP synthase. *Science* **286**: 1700-1705.

Svensson-Ek, M., Abramson, J., Larsson, G., Tornoth, S., Brzezinski, P. and Iwata, S.

(2002) The X-ray crystal structures of wild-type and EQ(I-286) mutant cytochrome c oxidases from *Rhodobacter sphaeroides*. *J. Mol. Biol.* **321**: 329-339.

Szundi, I., Cappuccio, J. A., Borovok, N., Kotlyar, A. B. and Einarsdottir, O. (2001a) Photoinduced electron transfer in the cytochrome c/cytochrome c oxidase complex using thiouredopyrenetrisulfonate-labeled cytochrome c. Optical multichannel detection. *Biochemistry* **40**: 2186-2193.

Szundi, I., Liao, G. L. and Einarsdottir, O. (2001b) Near-infrared time-resolved optical absorption studies of the reaction of fully reduced cytochrome c oxidase with dioxygen. *Biochemistry* **40**: 2332-2339.

Tainer, J. A., Roberts, V. A. and Getzoff, E. D. (1991) Metal-binding sites in proteins. *Curr. Opin. Biotechnol.* **2**: 582-591.

Takahashi, E. and Wraight, C. A. (1990) A Crucial Role for Asp^{L213} in the Proton Transfer Pathway to the Secondary Quinone of Reaction Centers from *Rhodobacter sphaeroides*. *Biochim. Biophys. Acta* **1020**: 107-111.

Tang, Y., Zaitseva, F., Lamb, R. A. and Pinto, L. H. (2002) The gate of the influenza virus M2 proton channel is formed by a single tryptophan residue. *J. Biol. Chem.* **277**: 39880-39886.

Thomas, J. W., Puustinen, A., Alben, J. O., Gennis, R. B. and Wikstrom, M. (1993) Substitution of asparagine for aspartate-135 in subunit I of the cytochrome bo ubiquinol oxidase of Escherichia coli eliminates proton-pumping activity. *Biochemistry* **32**: 10923-10928.

Trachtman, M., Markham, G. D., Glusker, J. P., George, P. and Bock, C. W. (2001) Interactions of metal ions with water: ab initio molecular orbital studies of structure, vibrational frequencies, charge distributions, bonding enthalpies, and deprotonation enthalpies. 2. Monohydroxides. *Inorg. Chem.* **40**: 4230-4241.

Truhlar, D. and Kohen, A. (2001) Convex Arrhenius plots and their interpretation. *Proc. Natl. Acad. Sci. USA* **98**: 848-851.

Tsai, A. L., Berka, V., Kulmacz, R. J., Wu, G. and Palmer, G. (1998) An improved sample packing device for rapid freeze-trap electron paramagnetic resonance spectroscopy kinetic measurements. *Anal. Biochem.* **264**: 165-171.

Tsukihara, T., Aoyama, H., Yamashita, E., Tomizaki, T., Yamaguchi, H., Shinzawa-Itoh, K., Nakashima, R., Yaono, R. and Yoshikawa, S. (1995) Structure of Metal Sites of Oxidized Bovine Heart cytochrome c Oxidase at 2.8 Å. *Science* **269**: 1069-1074.

Tsukihara, T., Aoyama, H., Yamashita, E., Tomizaki, T., Yamaguchi, H., Shinzawa-Itoh, K., Nakashima, R., Yaono, R. and Yoshikawa, S. (1996) The Whole Structure of the 13-Subunit Oxidized Cytochrome c Oxidase at 2.8 Å. *Science* **272**: 1136-1144.

Unger, V. M., Hargrave, P. A., Baldwin, J. M. and Schertler, G. F. (1997)

Arrangement of rhodopsin transmembrane alpha-helices. *Nature* **389**: 203-206.

Van Eps, N., Szundi, I. and Einarsdottir, O. (2003) pH dependence of the reduction of dioxygen to water by cytochrome c oxidase. 1. The P(R) state is a pH-dependent mixture of three intermediates, A, P, and F. *Biochemistry* **42**: 5065-5073.

Wang, C., Lamb, R. A. and Pinto, L. H. (1995a) Activation of the M2 ion channel of influenza virus: a role for the transmembrane domain histidine residue. *Biophys. J.* **69**: 1363-1371.

Wang, J., Takahashi, S., Hosler, J. P., Mitchell, D. M., Ferguson-Miller, S., Gennis, R. B. and Rousseau, D. L. (1995b) Two conformations of the catalytic site in the aa3-type cytochrome c oxidase from *Rhodobacter sphaeroides*. *Biochemistry* **34**: 9819-9825.

Wikström, M. (2003) Water-gated mechanism of proton translocation by cytochrome *c* oxidase. *Biochim. Biophys. Acta submitted.*

Xia, D., Yu, C.-A., Kim, H., Xia, J.-Z., Kachurin, A. M., Zhang, L., Yu, L. and Deisenhofer, J. (1997) Crystal Structure of the Cytochrome *bc1* Complex from Bovine Heart Mitochondria. *Sciecne* **277**: 60-66.

Yoshikawa, S., Shinzawa-Itoh, K., Nakashima, R., Yaono, R., Yamashita, E., Inoue, N., Yao, M., Fei, M. J., Libeu, C. P., Mizushima, T., Yamaguchi, H., Tomizaki, T. and Tsukihara, T. (1998a) Redox-coupled crystal structural changes in bovine heart cytochrome c oxidase. *Science* **280**: 1723-1729.

Yoshikawa, S., Shinzawa-Itoh, K. and Tsukihara, T. (1998b) Crystal structure of bovine heart cytochrome c oxidase at 2.8 A resolution. *J. Bioenerg. Biomembr.* **30**: 7-14.

Yoshikawa, S., Shinzawa-Itoh, K. and Tsukihara, T. (2000) X-ray structure and the reaction mechanism of bovine heart cytochrome *c* oxidase. *J. Inorg. Biochem.* **82**: 1-7.

Yu, C. H., Cukierman, S. and Pomes, R. (2003) Theoretical study of the structure and dynamic fluctuations of dioxolane-linked gramicidin channels. *Biophys. J.* **84**: 816-831.

Zaslavsky, D. and Gennis, R. (1998) Substitution of Lysine-362 in a Putative Proton-Conducting Channel in the Cytochrome *c* Oxidase from *Rhodobacter sphaeroides* Blocks Turnover with O_2 but Not with H_2O_2. *Biochemistry* **37**: 3062-3067.

Zaslavsky, D. and Gennis, R. B. (2000) Proton pumping by cytochrome oxidase: progress, problems and postulates. *Biochim. Biophys. Acta* **1458**: 164-179.

Zhang, Y. and Fillingame, R. H. (1995) Changing the Ion Binding Specificity of the *Escherichia coli* H^+- Transporting ATP Synthase by Directed Mutagenesis of Subunit *c*. *J. Biol. Chem.* **270**: 87-93.

Zhang, Z., Huang, L., Shulmeister, V. M., Chi, Y. I., Kim, K. K., Hung, L. W., Crofts, A. R., Berry, E. A. and Kim, S. H. (1998) Electron transfer by domain movement in cytochrome bc1. *Nature* **392**: 677-684.

Zhen, Y., Qian, J., Follmann, K., Hosler, J., Hayward, T., Nilsson, T. and Ferguson-Miller, S. (1998) Overexpression and purification of cytochrome *c* oxidase from *Rhodobacter sphaeroides*. *Protein Expr. Purif.* **13**: 326-336.

Zhen, Y., Schmidt, B., Kang, U. G., Antholine, W. and Ferguson-Miller, S. (2002) Mutants of the CuA site in cytochrome c oxidase of *Rhodobacter sphaeroides*: I. Spectral and functional properties. *Biochemistry* **41**: 2288-2297.

Zheng, X., Medvedev, D. M., Swanson, J. and Stuchebrukhov, A. A. (2003) Computer simulation of water in cytochrome c oxidase. *Biochim. Biophys. Acta* **1557**: 99-107.

Zhu, F., Tajkhorshid, E. and Schulten, K. (2001) Molecular dynamics study of aquaporin-1 water channel in a lipid bilayer. *FEBS Lett.* **504**: 212-218.